# Load Balancing using Potential Functions for Hierarchical Topologies

**Gy. Molnárka, N. Varjasi**

**Széchenyi István University**
**Dept. of Machine Design and Mechanics**
**Dept. of Information Sciences**

Abstract: In this paper we consider a new approach to load balancing for parallel systems. Today's parallel computers use multiprocessors and multi-core architectures. There are big differences between homogeneous and heterogeneous parallel architectures. The new model for balancing tree topologies is based on the "amortization potential method" for homogeneous systems. Based on the our proposed model a notion can be introduced: the "goodness of the hierarchical topology", which can be characterized by potential functions. In this paper we give some examples for these potential functions, and we propose the usefulness of the model with computer experiments.

*Keywords:* *Parallel computing, cluster, distributed system, load balance, amortization potential*

## 1. Introduction

The aim of parallel programming is to break a large problem into several small components and to solve it with a concurrent system of processors. There are two main factors that play an important role in a parallel system. The first one is the amount of arithmetic calculations and the second is the communication cost between the processors and/or computational nodes. Every efficient algorithm for a given parallel system must divide evenly the computational work according to the performance capability of the system. On the other hand, communication cost must be minimal. These aspects and needs usually contradict each other. The art of parallel programming is to find a golden mean between these demands for the given parallel system.

One possible way to compromise is using the "goodness of the hierarchical topology" and its potential function.

On general systems of parallel computing the role of the computing nodes can be different. The simplest model for a parallel system is when every computing node has the

same property and same role and none of them shows special behavior. The simplest parallel algorithms (for example atomic problems) could be realized with ring, hypercube or butterfly (model) topology. These topologies are effective in the case of small number of processor since the costs of communication are grow exponentially, and these topologies can only work efficiently in homogeneous systems.

Sleator [13] and Tarjan [14] examined the balancing of binary trees and give their classical analysis. Tarjan proposes the notion of the potential function as a tool for characterizing the balancing property of binary trees. Duff [6] gives a detailed analysis of parallel algorithms for linear systems of equations. In his work he focuses on the network arrangements in order to increase the efficiency of algorithms. Becciani et al. [2] define a special tree model for the N-body problem, and describe the necessity of network balancing during simulation. Lin [10] make a "load-skewing" task assignment model to minimize the delay of the cluster. He prepares a communicational model of the network burst, and the concurrent communicational conflicts and gives a good description of them. Yero [16] investigates the load balance of large master-slave systems on heterogeneous clusters. Schliephake [12] has recently developed a new design and prototype of a runtime system for parallel numerical simulations on large-scale systems.

In the following we suggest a tool for the analysis of the load balancing problem for hierarchical topology.

## 2. Hierarchical topology

In the case of a heterogeneous multiprocessor environment a hierarchical model can be defined. In a hierarchical model for a multiprocessor environment the processors are organized into a tree-like structure. The structure allows representing connections using parent-child relationships: each parent (master) can have many children (slaves or workers), but each child has only one parent.

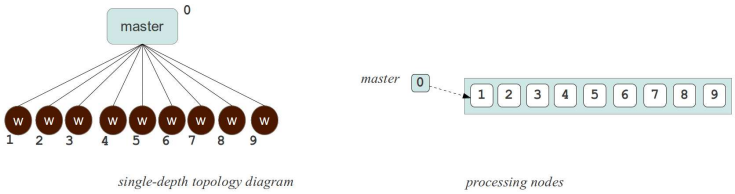


Figure 1: Single-depth hierarchical topology and its vector representation

The single-depth hierarchy is the simplest way to describe a master-slave model [16].

(See Fig. 2.) In this model the master processor has unidirectional control over other processors.

The role of the master is to divide the problem into distinct pieces, to allocate them to the corresponding slaves and finally to summarize the received results from workers. The sub-tasks are solved by the slaves.

Advantages of this system are:

- the simple hierarchy,
- the possibility to use various communication model (continuous and/or asynchronous),
- and the independence of the slave nodes, the easily convertible model.

The simplest representation of the model is a vector with the number of the nodes, where the master's number is 0 and slaves are pointed to $1, 2, \ldots, p-1$, where $p$ is the total number of processors.

Disadvantages of the hierarchical topology are:

- the division of the problem must be appropriate for the slaves,
- the work of the master node has a different role: to record the status of sub-tasks and it is restricted to the control of slaves
- therefore the overall efficiency can decrease [10].

Based on the principles of parallelism, (Amhdahl's, Gustaffson's law) [1] [7] the network cannot be extended effectively. By increasing the number of processors the execution time cannot be reduced beyond a certain level in this hierarchical model. The presence of the master may cause the degradation of efficiency (one less processor performs the actual work). This effect can be avoided by increasing the number of workers [4].

However, the capacity of the communication channels is limited and the number of the workers is limited also. The delay of communication service may cause starvation on worker nodes, and at the same time the master may continuously be overloaded. Such kind of systems are only effective, when the algorithmic execution time is greater than the communication time between the processors.

In the case of larger number of processors in a cluster let us examine two- or higher-level hierarchical models. These models are based on the general n-branched tree structure (see Fig. 2.). The multi-level hierarchical model serves for the load balancing of communicational channels. Between the master and slave levels one or more sub-master layer can be inserted. Communication tasks are divided between the master, sub-master and worker nodes.

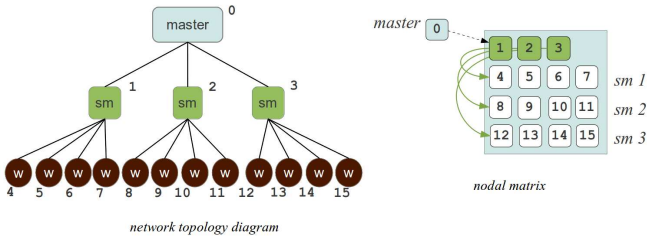


Figure 2: Tree topology and nodal matrix representation

Advantages of this topology are the better load balance and potentially lower communication costs [6]. We have to remark, that the division of the algorithms or tasks is more complicated for multi-level topologies. In the case of atomic tasks, only a small group of workers can be reached by a sub-master node [3]. By using sub-masters the overhead cost increases because of the lower number of slave processors. Such kind of topology is effective only for a large number of processors [16].

The hierarchy can be described by n-branched tree hierarchy or nodal matrix data structure (see on the right hand side of Fig. 2.).

The topology of the hierarchy [12] can be specified with the following methods:

- randomly,
- with a fixed model (in advance we define all details of the hierarchy),
- by searching the most balanced structure (this method needs a given potential function).

In the following we give the definition for the potential function definition.

## 3. Load balancing in homogeneous hierarchical topology

For the homogeneous topology we can define a model which is based on the results of earlier works [13], [14], [9], [5]. We use the description of binary or multiple search tree systems given by the above authors and we adopt them to the parallel computational systems with tree structures. In these papers the main result was that the optimal searching method could be realized by a balanced tree. One of the measures of the balance property of a binary tree can be described by the amortization potential function [5]. For the notation of the amortization function $\Phi$ was introduced. In the following we use the same notation, $\Phi : T \to [0,1]$, where $T$ is the set of tree network topologies.

For parallel computational systems with tree structures the potential function can be extended in a way that the potential function describes the "strength" of the topology. The greater value of the potential function indicates a shorter execution time.

### 3.1. The possible form of the potential function

$$\Phi = \frac{p-1}{p};\ \Phi : N \to [0,1] \tag{1}$$

where $p$ is the number of all processors (master and slaves). This potential function describes the master-slave relationship well, but does not describe the higher-level tree topologies because it does not contain information about the sub structure and the balancing property of the topology.

Let us see some generalization of the potential function (1) for the case of multi-level model.

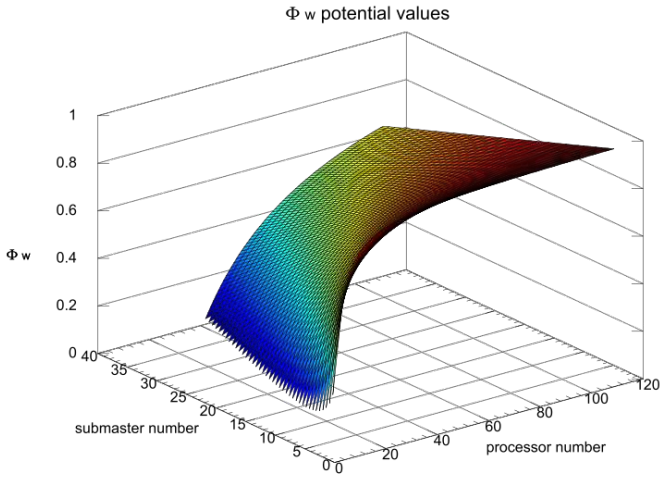


Figure 3: Potential values $\Phi_W(p,p_{sm})$

Let $\Phi_W$ be a worker potential value of the hierarchical tree topology

$$\Phi_W = \frac{p_w}{p};\ \Phi_W(p,p_w) : N \times N \to [0,1] \tag{2}$$

where $p$ is the number of processors, $p_{sm}$ is the number of sub-masters and $p_w = p - p_{sm} - 1$ is the number of worker processors. For the real hierarchical tree topology must hold that $p \geq p_w$ and $p_w \geq p_{sm}$ (see Fig. 3.1.).

The function defined by (2) describes the ratio between the worker, master and sub-master processors well, but does not give a good description about the finer details of the topology. It does not take into account how many workers are connected to a sub-master node and if the parallel communication is balanced or unbalanced.

To get a further generalization let us introduce the following $\Delta x$ correction term:

$$\Delta x = \max_{i \in \{0,1,\ldots,p_{sm}\}} (sm(i)) - \min_{i \in \{0,1,\ldots,p_{sm}\}} (sm(i)), \tag{3}$$

where $sm(i)$ is the number of children of $i$-th sub-master node of the hierarchy. The $\Delta x$ value gives the maximal difference in the number of the children of sub-masters for the whole tree.

Let us introduce the following quantity:

$$p_{avg} = \frac{\sum_{i \in \{0,1,\ldots,p_{sm}\}} (sm(i))}{p_{sm}} \tag{4}$$

where $p_{avg}$ is the average breadth of the sub-trees on the whole tree structure.

By using (3) and (4) we can define a new potential function, which describes the inhomogeneity of the tree structure:

$$\Phi_L = \frac{p_{sm} \cdot p_{avg} - \Delta x}{p_w};\ \Phi_L : N^3 \times R \to [-1,1] \tag{5}$$

The above defined $\Phi_W$ and $\Phi_L$ functions characterize the property of the tree from two different points of view. Therefore a new potential function that contains both functions could describe the balancing property of the tree structure more adequately.

### 3.2. Potential values for homogeneous network

Let $\Phi_T$ be the potential value of the whole topology

$$\Phi_T = \zeta \Phi_L + (1 - \zeta)\Phi_W;\ \zeta, \Phi_T \in R[0,1], \tag{6}$$

where $\Phi_L$ and $\Phi_W$ are defined above (2), (5) and $\zeta$ is an empirical balancing value. The graph of the potential function $\Phi_T$ (see Fig. 3.2.) shows that the maximum value is attained when the tree structure is well balanced. Therefore the potential function $\Phi_T$ can be used as an indicator of the balance of the tree structure.

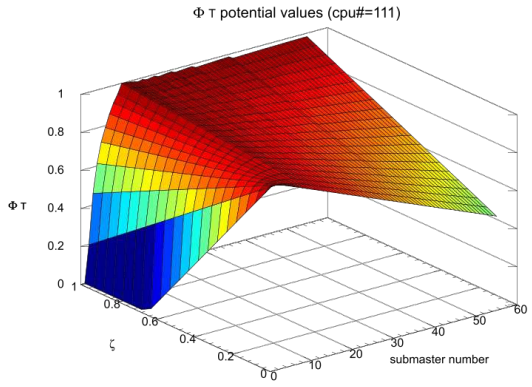


Figure 4: Potential values $\Phi_T(\zeta,p_{sm})$ with $p = 111$ nodes

Observation: For parallel cluster systems with homogeneous networks the same parallel algorithm can have different run times depending on different tree structures. Our proposed $\Phi_T$ potential function can characterize the different tree structures so that larger $\Phi_T$ value indicates shorter run time value.

More precisely: in case of the same numbers of processors the running time is shorter at a great value of $\Phi_T$.

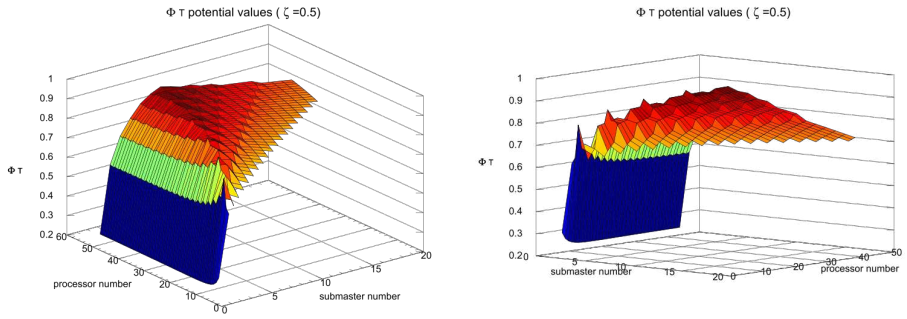


Figure 5: Potential values $\Phi_T(p,p_{sm})$ with $\zeta = 0.5$

These observations can be justified with run-time tests and computer analysis. We give some examples later in section 4.

Remark: The above formula (6) is a special potential function for homogeneous systems, but it works for heterogeneous systems as well.

For the generalization of the above proposed $\Phi_T$ potential function the general nodal matrix representation of graphs can be used. This approach could be used to define the proposed potential function for heterogeneous systems, but this approach is more sophisticated than the method we gave.

Possible methods for generalization are:

– take the difference between processor powers into consideration,

– take the communication costs between processors into consideration (speed of communication channels).

Such generalization would be very useful because the advantages of a good potential function are:

First: by using potential functions a good qualification of parallel computer network topologies can be done without benchmark tests.

Second: in the designing process of new parallel computing topologies it gives useful information. Before executing a long run-time task a "quick" test can be made to optimize the topology for a given hardware. Such experiments have been made and on the Fig. 5. shows that this idea works in practice as well.

Consequence: with the potential function (6) a well scalable hierarchy can be built.

## 4. Case-study for using the potential function

Let us examine some practical examples [8] [15] [11], where a simple balanced-unbalanced model can be characterized well with the potential function:

Let us see a two-level hierarchy and use $p = 13{,}16$ or 17 processors with different topologies, so that the potential function values will be different too. In the case of balanced trees like Fig. 4. and Fig. 4. $\Phi_T = 0.8021$ and $\Phi_T = 0.8446$. These values are better than the unbalanced case Fig. 4. with $\Phi_T = 0.5684$.

The computer tests were done by performing atomic tasks. Every worker executed the Miller–Rabin prime tests. In this case the algorithmic cost was always much higher than the communication costs (in this case our model is adequate).

Our potential function method must work for higher numbers of processors that we gave in examples Fig. 4, 4, 4.

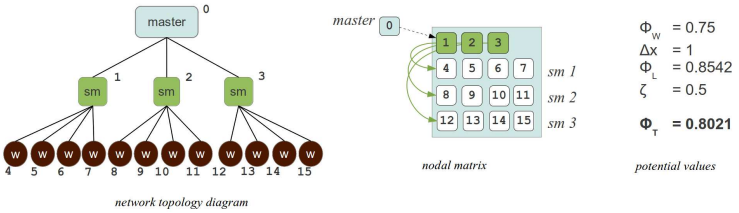


Figure 6: Load balanced topology $p = 16$, $p_{sm} = 3$

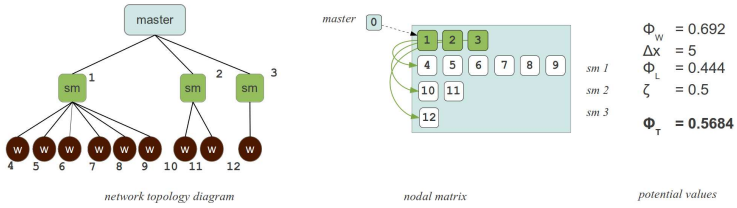


Figure 7: Unbalanced topology $p = 13$, $p_{sm} = 3$

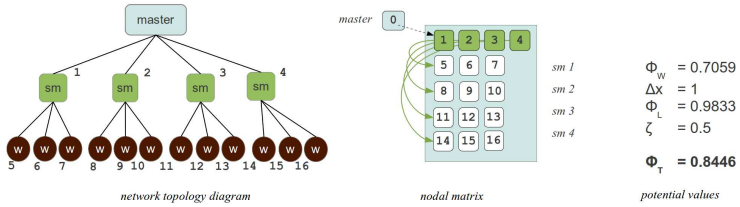


Figure 8: Balanced topology $p = 17$, $p_{sm} = 4$

On Fig. 4. we demonstrate the results of tests made on a *HP Blade c3000* system. The processor number was $p = 73$ with different sub-master number from $sm = 2$ up to $sm = 36$. in these tests we used as uniformly distributed workers as possible because the total number of possible topologies is huge (inhomogeneity was between the sub-master and worker processor numbers). With the relatively small sample the test results shows very good accordance between the expectations and computational results.

Even though this experiment does not prove the idea that our potential function is the

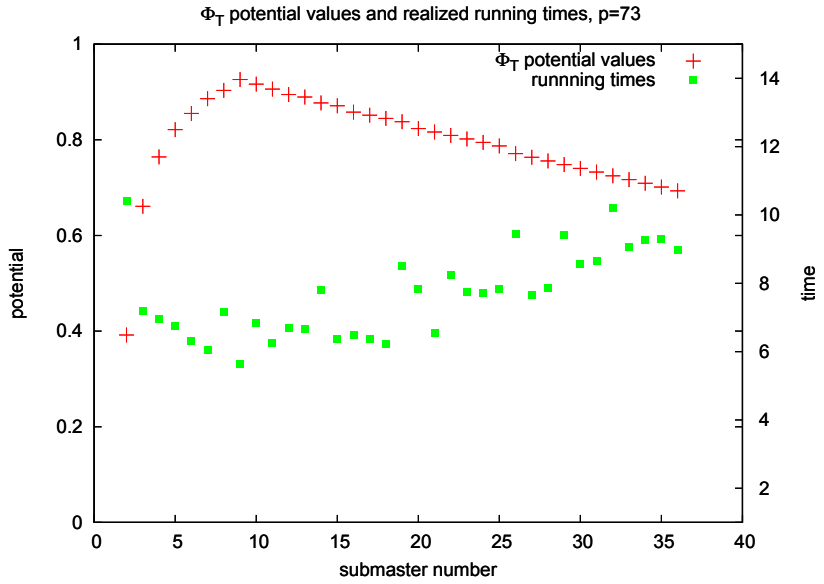


Figure 9: Topology potential values and the computer test results $p = 73$, $p_{sm} = 2..36$ , $\zeta = 0.5$

appropriate indicator of the goodness of parallel network systems, but it validates it's usefulness. Therefore further research in this field is promising. The two main directions seem to be beneficial to realize more precise results: to perform further computer experiments and to formulate a more general potential function for inhomogeneous parallel computer systems.

## Acknowledgements

This work was supported by TÁMOP-4.2.2-08/1/2008-0021 and by GOP-1.1.2-07/1-2008-0003 projects.

## References

[1] G. M. Amdahl: *Validity of the single-processor approach to achieving large scale computing capabilities*, in Proceedings of AFIPS Conference, 1967.

[2] U. Becciani, R. Ansaloni, V. Antonuccio-Delogu, G. Erbacci, M. Gambera, A. Pagliaro *A parallel tree code for large N-body simulation: dynamic load balance and data distribution on a CRAY T3D system* Computer Physics Communications 106., 1997. pp. 105–113

[3] Y. Chen, Y. Deng: *A detailed analysis of communication load balance on BlueGene supercomputer*, Computer Physics Communications 180., 2009. pp. 1251–1258

[4] X. H. Sun, Y. Chen: *Reevaluating Amdahl's law in the multicore era* J. Parallel Distrib Comput. 70., 2010. pp. 183–188

[5] T. H. Cormen, Ch. Leiserson, R. Rivest: *Algoritmusok* Műszaki Könyvkiadó, Budapest, 2001. ISBN 963-16-3029-3

[6] I. S. Duff, H. A. van der Vorst: *Developments and trends in the parallel solution of linear systems*, Parallel Computing 25., 1999. pp. 1931–1970

[7] J. L. Gustafson: *Reevaluating Amdahl's law*, in Communications of ACM, 1988.

[8] G. Kanti: *Hierarchikus szervezésű párhuzamos programozási modellek MPI rendszerben*, Széchenyi István Egyetem Győr, 2011. p.63

[9] Z. Király: *Adatstruktúrák*, ELTE, 2011. p.92; http://www.cs.elte.hu/ kiraly/Adatstrukturak.pdf

[10] W.-M. Lin, W. Xie: *Load-skewing task assignment to minimize communication conflicts on network of workstations*, Parallel Computing 26., 2000. pp. 179–197

[11] G. Molnárka, N. Varjasi: *A simultaneous solution for general linear equations on a ring or hierarchical cluster*, Acta Technica Jaurinensis Vol. 3. No. 1., 2010. pp. 65–73

[12] M. Schliephake, X. Aguilar, E. Laure: *Design and Implementation of a Runtime System for Parallel Numerical Simulations on Large-Scale Clusters* Procedia Computer Science 4, 2011. pp. 2105–2114

[13] D.D.Sleator, R. E. Tarjan *Self-Adjusting Binary Search Trees* Journal of the Association for Computing Machinery. Vol. 32, No. 3., 1985. pp. 652–686

[14] R. E. Tarjan *Amortized Computational Complexity* SIAM Journal on Algebraic and Discrete Methods, Vol. 6. No. 2. 1985. pp. 306–317

[15] N. Varjasi: *Parallel Algorithm for linear equations with different network topologies*, Proceedings of International e-Conference on Computer Science (IeCCS) 2006 in Lecture Series on Computer and Computational Sciences, Brill Academic Publishers, 2007. pp. 502–505, ISBN 978-90-04-15592-3

[16] E. J. H. Yero, M. A. A Henriques: *Speedup and scalability analysis of Master-Slave applications on large heterogeneous clusters*, Journal of Parallel and Distributed Computing 67. 2007. pp. 1155–1167

# The Entropy of a Natural Number

**N. Minculete[1], C. Pozna[2,3]**

**[1]Departament of REI, University Dimitrie Cantemir of Braşov, Romania,**
**e-mail: minculeten@yahoo.com**
**[2]Department of Automation, Transilvania University of Brasov, Brasov, Romania**
**[3]Department of Informatics, Széchenyi István University, Győr, Hungary,**
**e-mail:pozna@sze.hu**

Abstract: The aim of this paper is to introduce the concept of the entropy of a natural number. This new concept is the synthesis of the entropy and of the prime numbers concepts. The natural number structure is represented by its factorization in prime numbers. The entropy gives us the possibility to analyze the order of this structure. Using the natural number entropy concept has reviled interesting results concerning the internal structure of a natural number.

*Keywords: Shannon's entropy, prime numbers, natural numbers*

## 1. Introduction

Present paper proposes an original idea which corroborates two important concepts: the entropy and the natural numbers.

The entropy is defined, in information theory like a measure of uncertainty. For this reason it is associated with a random variable. The most acknowledged way to define the entropy is the Shannon entropy. The idea (inspired from thermodynamics) is to measure the uncertainty associated with the mentioned random variable. Thereby the Shannon entropy is the expected value of the information contained in a message [5]. The specific realization of the random variable is defined like message. The entropy is the minimum descriptive complexity of a random variable

A natural number is called a prime number if it is greater than 1 and has exact two divisors, one and the number itself. The fundamental theorem of arithmetic states that each natural number can be written as a product of prime numbers in a unique way. For this reason the primes can be considered the basic elements on which are constructed the natural numbers.

Each natural number can be expressed like a product of prime number (of basic elements). These prime numbers are prime factors of the number. Each prim number can have a certain multiplicity. The multiplicity of prime relative to a natural number is the largest exponent for which this prime divides the natural number.

If for a natural number we consider that a prime factor can be meet (found) with the frequency of its multiplicity we can define the relative frequency of the prime factor like the ratio between its multiplicity and the sum of the prim factors multiplicity.

The concept of relative frequency is related to the concept of probability. This gives us the possibility to define the entropy of a natural number.

Let $n = p_1^{a_1} p_2^{a_2} ... p_r^{a_r} > 1$ be a positive integer number, where $p_i$ are the prime factors of the natural number and $a_i$ is the multiplicity of the factor $p_i$.

If $\Omega(n) = a_1 + a_2 + ... + a_r$ is total number of prime factors of *n*, then we can define the probabilities $p(a_i) = \frac{a_i}{\Omega(n)}$, for every $i \in \{1, 2, ..., r\}$, so, we associate to *n* the random variable $X(n) = \{p(a_1), p(a_2), ..., p(a_r)\}$, where $\sum_{i=1}^{r} p(a_i) = 1$.

In section 2 we introduce the natural numbers entropy concept definition and we present several initial analyses of this concept. Section 3 will continue this analysis for special cases of natural numbers the *k* – free and the *k* – full numbers. In Section 4 we have analyzed the exponential divisors of a natural number from the point of view of the distance between two random variables. Conclusions will end the paper.

## 2. The definition and analysis of the natural number entropy

In this section we define the natural number entropy and based on this definition we analyze this concept from mathematical point of view. The mentioned analysis is focused in reveling particular values of entropy and in boundaries finding.

**Definition 1.** *The entropy of a positive integer number* $n = p_1^{a_1} p_2^{a_2} ... p_r^{a_r} > 1$ is given by

$$H(n) = -\sum_{i=1}^{r} p(a_i) \log p(a_i). \tag{1}$$

Since $0 \log 0 = 0$, by convention, we take $H(1) = 0$.

Relation (1) can be written in following way

$$H(n) = \log \Omega(n) - \frac{1}{\Omega(n)} \sum_{i=1}^{r} a_i \log a_i. \tag{2}$$

For example, if $n = 2 \cdot 3^2 \cdot 5^3$, then the entropy of *n* is

$$H(n) = \log 6 - \frac{1}{6}(2 \log 2 + 3 \log 3) = \frac{1}{6} \log \frac{6^6}{2^2 3^3} = \frac{1}{6} \log 2 \cdot 6^3 \approx 1.011.$$

**Remark 1.** From the previous definitions we can obtain the following results:

If $n = p^a$, then $H\left(p^a\right) = 0$.

If $n = p_1 p_2 ... p_r$, we obtain $H(n) = \log \omega(n)$, where $\omega(n)$ is the number of distinct prime factors of n;

If $n = \left(p_1 p_2 ... p_r\right)^k$, then $H(n) = \log \omega(n)$.

**Theorem 2.** For all $n \geq 2$, there we have:

$$0 \leq H(n) \leq \log \omega(n). \tag{3}$$

Proof. From (1), we have $H(n) = -\sum_{i=1}^{r} p(a_i) \log p(a_i)$, with $\sum_{i=1}^{r} p(a_i) = 1$, but $p(a_i) \log p(a_i) \leq 0$, therefore, we deduce $H(n) = -\sum_{i=1}^{r} p(a_i) \log p(a_i) \geq 0$. We consider the function $f : [1, \infty) \to R$, defined by $f(x) = x \log x$. But $f''(x) = \frac{1}{x} > 0$, which means that the function *f* is convex. Therefore, if we apply Jensen's inequality for the function *f*, then we deduce the inequality

$$\sum_{i=1}^{r} a_i \log a_i \geq r \frac{\sum_{i=1}^{r} a_i}{r} \log \frac{\sum_{i=1}^{r} a_i}{r} = \Omega(n) \log \frac{\Omega(n)}{\omega(n)}. \tag{4}$$

Combining relations (2) and (4), we find that $H(n) \leq \log \omega(n)$. Thus, the proof of theorem is complete.

**Theorem 3.** For all $n \geq 3$, we have:

$$0 \leq H(n) \leq \log \log n - \log \log \log n + \log c_1, \tag{5}$$

where $c_1 = 1.38402...$.

Proof. In [3], G. Robin proved that $\omega(n) \leq \frac{\log n}{\log \log n} c_1$, for all $n \geq 3$. Using this relation and relation (3), we obtain the relation desired.

We observe that the entropy of a positive integer number n is minimum (i.e. 0) when n is a prime number or a power of prime number, and the entropy is maximum (i.e. $\log \omega(n)$), when n is square-free or a square-free to power k, where $k \geq 2$.

## 3. Applications of the entropy for different types of the positive integer numbers

This section continues the analysis of natural number entropy considering special cases like *k* – free, *k* – full numbers or Mersenne number.

Using the concept of natural number entropy we have the following results:

For $n = p^a q^b$ and $m = p^b q^a$, we have $H(n) = H(m)$. This remark implies the following result: if $n = p_1^{a_1} p_2^{a_2} \ldots p_r^{a_r}$ and $m = p_1^{a_{\sigma(1)}} p_2^{a_{\sigma(2)}} \ldots p_r^{a_{\sigma(r)}}$, then $H(n) = H(m)$, where $\sigma \in S_r$, and $S_r$ is the symmetric group of degree r.

If $n$ is a number $k$-free (see [4]), so $n = p_1^{a_1} p_2^{a_2} \ldots p_r^{a_r}$, with $a_i \le k-1$, where $k \ge 2$, then using relation (2), we find that

$$\log \omega(n) \ge H(n) \ge \log \Omega(n) - \frac{\omega(n)}{\Omega(n)}(k-1)\log(k-1). \tag{6}$$

If $n$ is a number $k$-full (see [4]), so $n = p_1^{a_1} p_2^{a_2} \ldots p_r^{a_r}$, with $a_i \ge k$, where $k \ge 2$, then using relation (2), we find that

$$0 \le H(n) \le \log \Omega(n) - \frac{\omega(n)}{\Omega(n)} k \log k. \tag{7}$$

For a number 2-full, which is called and powerfull (see [4]), applying relation (7), we get the inequality

$$0 \le H(n) \le \log \Omega(n) - \frac{2\omega(n)\log 2}{\Omega(n)}. \tag{8}$$

We note by $\sigma(n)$ the sum of the positive divisors of $n$. From [4], if we have $\sigma(n) = 2n$, then, we say that $n$ is a perfect number. Theorem Euler-Euclid (see [2]) show that every perfect number has the form $n_k = 2^k\left(2^{k+1}-1\right)$, where $2^{k+1}-1$ is a prime number and $k \ge 1$. Hence, we have $H(n) = \frac{k}{k+1}\log\frac{k+1}{k}$. Applying Lagrange's Theorem for the function $f(x) = \log x$ on $[k, k+1]$, we deduce the relation

$$\frac{1}{k+1} < \log(k+1) - \log k < \frac{1}{k},$$

which implies the inequality

$$k\log\left(\frac{k+1}{k}\right) < 1 < (k+1)\log\left(\frac{k+1}{k}\right).$$

Therefore, we obtain

$$\frac{1}{k+1} - \frac{1}{(k+1)^2} < H(n) < \frac{1}{k+1}. \tag{9}$$

It is known that the Mersenne numbers form is $2^k-1$, then if $m_k=2^k-1$ is a prime, is called a prime Mersenne number. According with [2, 4] is not known if there are an infinity of this type numbers of number, but if we assume that there are an infinity then there are an infinity of perfect numbers $(n_k)_{k\geq 1}$, and using relation (9), we deduce the following result.

$$\lim_{k\to\infty} H(n_k)=0 \text{ and } \lim_{k\to\infty} kH(n_k)=1. \tag{10}$$

## 4. Kullback-leibler distance between two positive integer numbers

The entropy concept is used in several developments like the distance between two random variables or like the relative information between two distributions. Considering this developments it was very attractive to used them for the natural numbers entropy.

In [1] the relative entropy or (Kullback-Leibler distance) between two random variables $\mathbf{p}=\{p_1,p_2,...,p_r\}$ and $\mathbf{q}=\{q_1,q_2,...,q_r\}$ was introduced in the following way:

$$\mathrm{D}(\mathbf{p}\|\mathbf{q})=\sum_{i=1}^{r} p_i \log\frac{p_i}{q_i}. \tag{11}$$

We consider two positive integer numbers $n=p_1^{a_1}p_2^{a_2}...p_r^{a_r}$ and $m=q_1^{b_1}q_2^{b_2}...q_r^{b_r}$. From here, we define the probabilities $p(a_i)=\dfrac{a_i}{\Omega(n)}$ and $q(b_i)=\dfrac{b_i}{\Omega(m)}$, for every $i\in\{1,2,...,r\}$, so, we associate to $n$ and $m$ the random variables $X(n)=\{p(a_1),p(a_2),...,p(a_r)\}$ and $X(m)=\{q(b_1),q(b_2),...,q(b_r)\}$, where $\sum_{i=1}^{r}p(a_i)=1$ and $\sum_{i=1}^{r}q(b_i)=1$.

Similar with Kullback-Leibler distance between two random variables, we define the Kullback-Leibler distance between two positive integer numbers.

**Definition 2.** The Kullback-Leibler distance between two positive integer number $n$ and $m$ with $\omega(n)=\omega(m)$ and factorization thus $n=p_1^{a_1}p_2^{a_2}...p_r^{a_r}$ and $m=q_1^{b_1}q_2^{b_2}...q_r^{b_r}$ is given as

$$\mathrm{D}(n\|m)=\sum_{i=1}^{r} p(a_i)\log\frac{p(a_i)}{q(b_i)}. \tag{12}$$

Relation (12) can be written in following way

$$\mathrm{D}(n\|m)=\log\frac{\Omega(m)}{\Omega(n)}+\frac{1}{\Omega(n)}\sum_{i=1}^{r} a_i\log\frac{a_i}{b_i}. \tag{13}$$

For example, if $n=2\cdot 3^2\cdot 5^3$ and $m=3\cdot 5^2\cdot 7^4$, then the entropy relative of $n$ and $m$ is

$$D(n||m)=\log\frac{7}{6}+\frac{1}{2}\log\frac{3}{4}\approx 0.0103.$$

**Remark 2.** It is easy to see that $D(n||m)\neq D(m||n)$.

In [**6**], M. V. Subbarao was introduced the notion of exponential divisor. So if , we have a number $n=p_1^{a_1}p_2^{a_2}...p_r^{a_r}>1$, then the number $d=\prod_{i=1}^{r}p_i^{b_i}$, with $b_i\mid a_i$, for all $i=\overline{1,r}$, is called exponential divisor (or e-divisor). We note $d\mid_{(e)} n$. In this case, because $\omega(n)=\omega(d)$, we deduce

$$D(n||d)=\log\frac{\Omega(d)}{\Omega(n)}+\frac{1}{\Omega(n)}\sum_{i=1}^{r}a_i\log\frac{a_i}{b_i}. \tag{14}$$

For $\gamma(n)=p_1p_2...p_r$ which is the lowest divisor of *n*, we calculate the relative entropy between *n* and $\gamma(n)$ and we obtain

$$D(n||\gamma(n))=\log\frac{\omega(n)}{\Omega(n)}+\frac{1}{\Omega(n)}\sum_{i=1}^{r}a_i\log a_i. \tag{15}$$

From (14) and (15), we deduce the difference

$$D(n||d)-D(n||\gamma(n))=\log\frac{\Omega(d)}{\omega(n)}+\frac{1}{\Omega(n)}\sum_{i=1}^{r}a_i\log b_i\geq 0. \tag{16}$$

Therefore, we have the inequality $D(n||d)\geq D(n||\gamma(n))$.

## 5. Conclusions

Present work proposes a new concept the entropy of natural numbers. This concept is a synthesis of the concept of entropy, used for a random variable and the concept of prime number. The significance of the entropy from information point of view is the expected value of the information contained in a message. On the other site the prime factors of a natural number can be considered the generators of this number. Using these interpretations we consider the entropy of a natural number like the measure of order of this number structure. We will remember that a prime number entropy is zero which is the minimum entropy i.e. has the meaning of maximum order. At contrary a natural number with more than one factor, which have the multiplicity of one, have the maximum entropy (whit maximum disorder meaning).The concept of natural numbers entropy is very attractive and we hope that it will lead to benefits in several fields like information theory, numerical theory etc.

## References

[1] T. Cover, J. Thomas: *Elements of information theory*, Wiley-Interscience, New Jersey, 2006.

[2] M. Nathanson: *Elementary Methods in Number Theory*, Springer, New York, 2006.

[3] G. Robin: *Estimation de la fonction de Tchebychef* $\theta$ *sur le k-ième nombre premier et grandes valeurs de la fonction* $\omega(n)$ *nombre de diviseurs premiers de n*, Acta Arith. 42, 1983, pp. 367-389.

[4] J. Sándor, D. S. Mitrinović, B. Crstici: *Handbook of Number Theory I*, Springer, 1995.

[5] C. Shannon: *A Mathematical Theory of Communication*, The Bell System Technical Journal,Vol. 27, July, October, 1948, pp. 379-423, 623-656.

[6] M. V. Subbarao: *On some arithmetic convolutions in: The Theory of Arithmetic Functions, Lecture Notes in Mathematics*, New York, Springer-Verlag, 1972.

# Real-time Program Models Used in Tiny Embedded Systems

**J. Kopják[1], J. Kovács[2]**

**[1]Óbuda University/Kandó Kálmán Faculty of Electrical Engineering, Budapest**
**[2]Széchenyi István University/Faculty of Engineering Sciences, Győr**
**e-mail: kopjak.jozsef@kvk.uni-obuda.hu, kovacs@sze.hu**

Abstract: The paper present and compare some real-time control program models used by programmers programming in tiny embedded systems, microcontrollers. The paper does not demonstrate all programming models, only the most important variations based on writer's opinion. The writer tried to show the advantages and disadvantages of each programming models discussed in article. The paper begins with traditional models like sequential model, cooperative multitasking and continues with an alternative cooperative multitasking method, timed cooperative model and finish with event-driven model.

*Keywords: cooperative multitasking, timed cooperative model, event-driven model, real-time*

## 1. Introduction

The improvement of microcontrollers using in embedded systems is very strong. Some performances of microcontrollers are on same level like in personal computers. The improvement of eight and sixteen bit controllers does not stop too. The controllers have more and more peripheries. The tasks of microcontrollers do not stop on control functions. Microcontrollers with cheep price have small cpu core with small ram size and with rich number of peripheries. With rich number of peripheries is possible to satiate user demands like LCD control, sensor-less BLDC fan motor control, lots of type of serial communication with eight bit controllers too. To resolve these new problems programmers needs to have new program modelling knowledge.

## 2. Real-time systems

Non real-time system are usually using in office technologies. In non real-time systems incoming events followed each other in time in a same priority level are not served in a queue followed each other. In these systems are known the average of processing time of events, but we do not know the maximum time of answer of occurred event.

Real-time control is very important in solutions using in industrial and medical environment. Every event has own priority in real-time system. Consecutively becoming events in a same priority level are served in one after the other. The maximum of answer time of incoming event is known and defined.

A critical aspect of real-time systems is how time itself is handled. The design of a real-time system must identify the timing requirements of the system and ensure that the system performance is both correct and timely. The three types of time constraints on computation are: hard, soft, firm [1].

## 3. Sequential programming model

Sequential programming models are used in industrial solutions usually. Sequential programming model is named linear programming model too. These programs are composed from four software component: initialization, reading status of the inputs, calculation or processing, refreshing values of the outputs. Figure 1 illustrates the simplified flow chart of program based on sequential programming model.

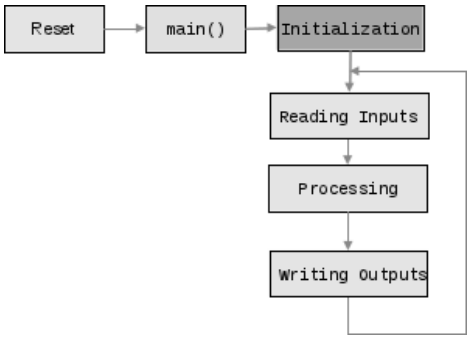


*Figure 1: Simplified flow chart of program based on sequential programming model*

The advantage of sequential programming model is the design of program is very similar to classical logical circuit design method. Simultaneously (in time) reading of all inputs and writing of all outputs exclude the hazard known in logical circuits.

The disadvantage of the model is the source code contains lots of if-else control structures and therefore is incomprehensible case of writing complex programs. Other disadvantage of the model is the poor utilization of processor. The program always recalculate the values of outputs, regardless of there is any change on inputs. The program based on this model is always running, therefore uses all CPU time. The reaction time of program depends on the program complexity due to constant recalculations.

## 4. Cooperative multitasking

In cooperative multitasking the tasks are working together with each other. The tasks are simple functions without input parameters and return value. The main program first initializes the peripheral devices, after the initialization the program calls the task functions in loop. Figure 2 illustrate the simplified flow chart of program based on multitask programming model.

Source code written in cooperative multitasking model is more transparent than the codes written in sequential method. The tasks can be easily separated, each task have different job. These tasks are in different functions, and these functions are located in different source files usually. If the task-functions are located in different source files

the program developers can be work together easily, because they do not interfere with each others work. Each developer has to modify only their own files, and don't need to change content of files created by other developers.

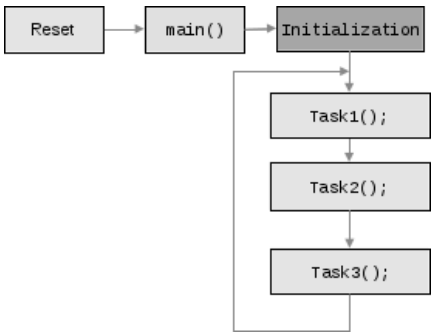


*Figure 2: Simplified flow chart of program based on cooperative multitask programming model*

Following piece of C-language source code represents the main loop responsible for calling the task functions.

```
int main ( void )
{
  vInitSystem();// Initialization of peripherals
  while(1)      // Infinitive function calling loop
  {
    vTask1();  // Calling task function named vTask1
    vTask2();  // Calling task function named vTask2
    vTask3();  // Calling task function named vTask3
  }
}
```

Developing source code in cooperative multitasking model required more software planning time than sequential solution. The designer has to divide the whole program-task to small individual working tasks in a first phase of development. Tasks are communicating with each other on global variables or with another name: via mailboxes. The cooperating task functions usually read its inputs values at the beginning and writing they output values at end of each running sequence. The program scans its inputs and updates its outputs values several times during a one circle in the main loop.

The task should complete own running sequence as soon as possible to got the shortest program response time. The tasks should not use blocking or waiting loops. Using blocking loops would drastic incise the response time of running system. Some blocking loops examples: Waiting for releasing a push button or waiting for an UART peripheral register flag. The tasks have to remember the current state of running and return back to the calling function in case when a resource is not available.

The task functions should be structured using state machine model due to lack of a blocking waits. In state machine model the functions are using static local variables to store them next states. The backbone of each task function is a switch-case structure. The task first examines the value of the state description variable, and then jumps to the program code of the state. Following piece of C-language source code illustrates the body of task function based on state machine model.

```
void vTask( void )
{
  /* State description variable. Initial state is:
     INIT_STATE */

  static enum { INIT_STATE, STATE1, STATE2, STATE3 }
  xState = INIT_STATE;

  /* Selection of sub-task based on the value of state
     variable */
  switch ( xState )
  {
    case INIT_STATE:  // Initialization tasks
         /* ... */
         xState = STATE1; // Selection of next state
         break;           // End of actual running

    case STATE1:        // First task
         /* ... */
         xState = STATE2; // Selection of next state
         break;           // End of actual running
    /* ... */
    default:         // Protection state:
         // Normally the program never gets here.
         xState = INIT_STATE; // Re-initialization of
                              // task-function
   }
}
```

The advantage of cooperative multitasking model is the possibility of creation quasi-parallel multitask system without using pre-emptive multitask operation system. The disadvantage of cooperative multitasking model is the pretension of good developer programming skills. The response time of program is depends on the tasks execution time. The execution time of task is not a constant value, because every task state has other execution time. The response time of program will be swinging, but is possible to calculate the fastest and slowest reaction time of system. The shortest reaction time of system is the sum of fastest running time of tasks, and the longest response is the sum of slowest running time of tasks.

Another disadvantage of the cooperative multitasking is that the program is not able to manage energy consumption of the processor. The processor runs the code always, it can not go to energy-efficient mode (sleep or idle), this means the processor will be have maximum energy consumption.

## 5. Timed cooperative multitasking

The traditional cooperative multitasking model do not deal with time, it means if somebody would like to create timed functions or events then the programmer must to create own timer to measure the elapsed time. In timed cooperative multitasking model the tasks do not run always like in classical cooperative multitasking model, only when they blocking or waiting time has expired.

If somebody would like to implement timed cooperative multitasking model, then he must create own lightweight kernel to manage the task functions. There is some known implementation of cooperative multitasking, with other name co-rutins, like FreeRTOS. FreeRTOS is an open source operating system for embedded systems written in C language.[2] The implemented kernels working with time, but the time is not the basic element of they kernel model, therefore we design a own lightweight cooperative multitask kernel.

To demonstrate the difference between classical cooperative multitasking and the timed cooperative multitasking we made an example program. In our program are two

tasks. The tasks are running quasi-parallel. The mission of each task is very simple: Invert value of one output pin. Next code example written is C language shows the implementation of these tasks.

```
/* Task function of task #1*/
void vTask1 ( void )
{
    mTurnOnLED( 3 );          // The task starts here
    mToggleLED( 1 );          // Toggle LED #1
    mTurnOffLED( 3 );         // The task stops here
}

/* Task function of task #2*/
void vTask2 ( void )
{
    mTurnOnLED( 0 );          // The task starts here
    mToggleLED( 2 );          // Toggle LED #2
    mTurnOffLED( 0 );         // The task stops here
}
```

Our initial kernel is very simple. Next code example shows our initial, not timed kernel.

```
/* endless loop */
while (1)
{
          vTask1(); // Call Task1 function
          vTask2(); // Call Task2 function
}
```

The Figure 3 illustrate the result of program running is simulator. In picture you can find 4 lines. The line with label "Task #1" is in high level when the task #1 is running, and is in low level when the task is in "not running" state. The line with label "Task #2" demonstrates the actual state of the task #2 (the conditions of high and low level is similar like in previously described line). Line with label "PIN #1" and line with label "PIN #2" shows the output of Task #1 and Task #2 (toggle LED on output pin). We can see in the figure that the both tasks are running always in circa half of the processors time.

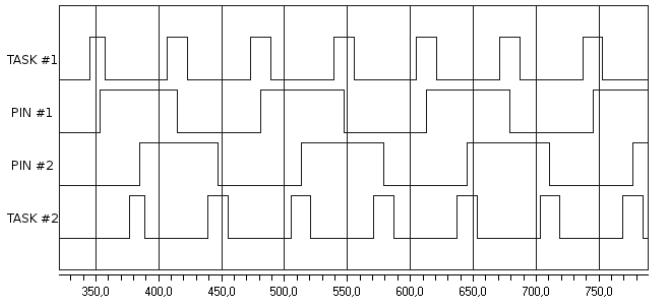


*Figure 3: Result of running program write in traditional cooperative multitask model*

To create a timed task calling we need one global timer, which measure the continuous global time in tick. Operating system usually measure the time in tick. The tick counter is 16 or 32 bit long unsigned variable, but it can be an 8 bit counter in very small systems. We are using 16 bit wide architecture to test our kernel; therefore our tick counter is 16 wide too. In this example the timer increase the value of tick counter in every one millisecond.

We need an array list too. The array list contains the task descriptors. One element of array is a structure, which represents one task. The descriptor structure has three fields:

the pointer of task function, the recall interval in tick and the time stamp of last call. Next code example shows the declaration of task descriptor structure.

```
/* Type define: Task Entry structure */
typedef struct
{
  void (*pvTaskPointer) ( void );//Pointer of task func.
  TICK_TYPE tickRecallInterval;  //Recall interval
  TICK_TYPE tickLastTimeStamp; //Time stamp of last call
} TASK_ENTRY;
```

Next piece of code shows the description list of tasks. The list must be closed with predefined closing entry where the value of function pointer is NULL. When the array is closed with closing entry, the programmer do not need to predefine the size of array list, because the parser part of the program could determinate the size of given array.

```
static TASK_ENTRY xTaskList[] =
{
    {vTask1, 3, 0},
    {vTask2, 6, 0},
    {NULL, 0, 0}  // End of Task List (closing entry)
};
```

The kernel first calculates the difference of current time and the time stamp of last call, and when this value is greater than or equal to tasks recall time then calls the task function. Next piece of code shows the implementation of kernel.

```
/* Local variables */
TICK_TYPE tickCurrentTime;
HTASK_ENTRY hTask;
UBASE_TYPE uxTaskIndex = 0;

/*  endless loop*/
while (1)
{
  hTask = &xTaskList[uxTaskIndex++];//Get handle of task
  if( hTask->pvTaskPointer != NULL )
  { /* If task entry is not closing entry: */
    tickCurrentTime = tickGetCurrentTime();
    if ( (tickCurrentTime - hTask->tickLastTimeStamp)
          >= hTask->tickRecallInterval )
    {/* If task time was expired */
      hTask->pvTaskPointer(); // Call task function
      hTask->tickLastTimeStamp = tickCurrentTime;
    }
  }
  else
  {
    uxTaskIndex = 0;  // Restart loop counter
  }
}
```

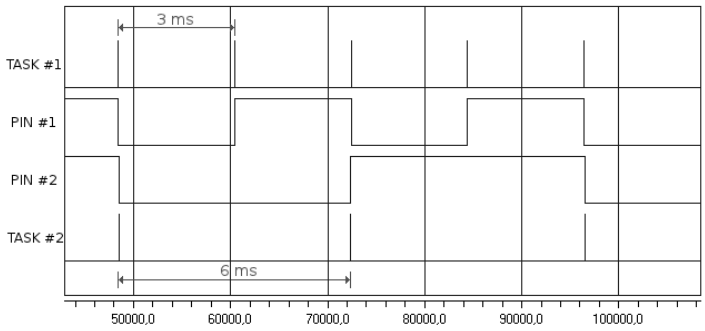


*Figure 4: Result of timed cooperated multitasking*

The Figure 4 illustrates the result of program running in simulator. In picture you can find 4 lines. The meanings of the lines are same like in Figure 3. You can see in the figure, that the both tasks are running only when they blocking time has expired.

## 6. Event-driven programming model

Before analyzing the event-driven programming model let's look at the concept of the event. The event is an occurrence (incidence), which may change the status an object [3]. The events are signals from the outside of world in generally. Events are describing dynamic changes of inputs. Events can be external -hardware- events such as a button press or a tank becomes full or internal – software – events such as queue is full or semaphore was taken.

The objects are informed about events through messages. The message in complex, distributed system can be objects too, such as a communications packet (MODBUS message or TCP/IP packet). In single-processor systems we are using a simple function calls to transmit the messages.

In traditional event-driven model based programs are only passive objects. The objects recalculates they output values do the effect of change they input values. The event-driven program runs only when the input values are changing. The response time of program depend on the number of changing input values in same time, and do not depend on the controlled network complexity.

The traditional event-driven system consists the following actors:

*Interrupt service routines (ISR)* – The processors interrupt periphery calls the interrupt service routines in case of external or internal interrupt event. Hardware interrupt can be a change of the value of input pin (Interrupt On Change), incoming data on communication port or end of data transmission. Internal hardware event can be a timer overflow or end of analog-digital conversion. The interrupt service routines create event-telegrams, which are posted to event queues by ISRs.

*Event-telegraphs* – The event-data structures consist of a minimum of two parts: The signal of the event conveys the type of the occurrence, and event parameters convey the quantitative information about the occurrence [4]. Following piece of C-language source code illustrates example for event-telegraph structure.

```
typedef struct EventTag
{
  unsigned int uiEventID;  // Event ID
  unsigned int uiParam;    // Event parameter
} Event;
```

*Event queue* – Event queue is a list (first in first out type list) of event telegraphs. The interrupt service routines put the event telegraphs to the end of queue and the event handler loop gets events from queue. Care should be taken when implementing the event queue because is shared resource. The event telegraphs arrive to the queue asynchronously. All operation with event queue should be made in critical section; exclude multiple writes, or read and write, in queue in same time.

*Event message processing loop* – The event message processing loop located in the main program. The event message processing loop is an infinite loop. The loop first tries to get message for event queue. If there is a waiting message in the queue, then the

loop process it based on message ID and message parameters. If there is no message waiting to be processed, then the loop puts the processor to the power saving mode. The interrupts will be wake up the processor from power-saving mode.

Not only the interrupt service routines can put events to the queue, but the event processing loop too. It can be happens the actual event processing ends with generation of new event. In such cases, the generated event is added to the end of the queue of events. Figure 5 illustrates the traditional event-driven program structure.

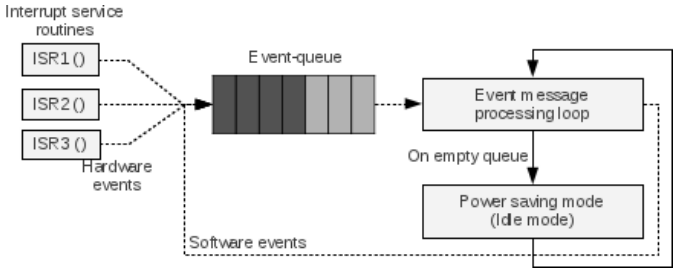


*Figure 5: Traditional event-driven program structure*

Event-driven systems require a distinctly different way of thinking than traditional sequential programs [4]. The event-driver program do not wait for an external event, the program react to events [5]. The program must be designed in if-then conditions, for example: if the set pin of set-reset flip-flop change to true, then the output of flip-flop must be set to true; if the reset pin of set-reset flip-flop change to true, then the output of flip-flop must be set to false.[6]

The structure of event processing loop is similar to the functions developed basis on state-machine model. The core of loop is an switch-case structure. The switch tag jumps to the selected function description based on incoming event ID. Following piece of C-language sample code illustrates the body of event processing loop.

```
while(1)
{
  /* Getting event from event queue */
  if( xQueueReceive( xEventQueue, &xReceivedEvent, 0 )
      == pdPASS )
  { // On successful reception:
    /* Jump to selected task based on  message ID */
    switch ( xReceivedEvent.uiEventID )
    {
      case BUTTON:   // The button has bean sent
           /* ... */ // the message
           break;       // End of message processing

      case TIMER:       // The timer has bean sent
           /* ... */ // the message
           break;       // End of message processing
    }
    else  // There is no event waiting to be processed:
    {
      Idle(); // The processor goes to power saving mode
    }
}
```

The advantage of program based on traditional event-driven model is that the model includes the automatic control of processor power consumption. If the message comes when the event queue is empty the response time of program is the message processing plus the answer generation time. The disadvantage is that the program can not rank events based on their importance and is not suitable to create modular program.

## 7. Conclusions

All programming models presented here have their own reason for existence. For smaller tasks may be useful to use design models presented at the beginning of the article, for complex systems are better solutions described in the second half of the article. Complex models are using more processor for administrative tasks instead of real problem, thereby reducing the effectiveness of the processor. On battery powered solutions should be used solution where the models automatically manage the processors energy consumption.

## References

[1] Bruce Powel Douglass: *Real-Time UML: developing efficient objects for embedded systems*, 1998.
[2] Richard Barry: *Using The FreeRTOS Real Time Kernel*, 2009.
[3] Angster Erzsébet: *Az Objektumorientált tervezés és programozás alapjai*, 1997.
[4] Miro Samek: *Practical UML Statecharts in C/C++*, Second Edition, 2009.
[5] Dr. Kondorosi Károly, Dr. László Zoltán, Dr. Szirmay-Kalos László: *Objektum-Orientált Szoftverfejlesztés*, 2003.
[6] József Kopják, Dr. János Kovács: *Event-driven control program models running on embedded systems*, 2011.

# Computation Techniques in a High Performance Parallel Simulation of Gas Dynamics in a Combustion Chamber

**L. Környei**

**Széchenyi István University, H-9026, Győr, Egyetem tér 1.**
**Phone: +36-96-503-400/3150**
**e-mail: leslie@sze.hu**

Abstract: The article describes several techniques utilized in the author's study of gas flow in a combustion chamber. Various models of Compressible Fluid Dynamics (CFD) are used in conjunction with the Finite Volume Method (FVM). Piston and valve movement is introduced with the grid snapping method.

Several methods are investigated and implemented in order to prepare the simulation software for high performance computing environments. Some of these methods (MPI, OpenMP, and their hybrid), and their feasibility is discussed below. It proves, that when starting the proper number of MPI processes, and the adequate number of threads for each process – these are determined by the hardware environment – the MPI-OpenMP hybrid method is scalable for the underlying problem for up to 200 processor cores, with a speedup of 60.

Two other delicate problems are also hand-picked, that rarely surface in static space simulations: vertex-matching in neighboring meshes, and the transformation of local physical values with interpolation during the change of space discretization, especially when swapping the mesh. Appropriate algorithms are presented for both. These need considerably smaller resources in memory and processor time, which make them applicable even runtime.

*Keywords: CFD, FVM, moving boundary, MPI, OpenMP*

## 1. Introduction

There is a particular type of physical phenomena, where the actual extents of the space investigated is changing, deforming, or moving in a predefined way [1]. Special care is required to describe the dynamics of gases, even with conventional CFD models, to handle piston and valve movement in finite volume discretization [2]. Apart from the physical and mathematical exercises, the computational tasks are also challenging. This article is hand-picked from the later.

During the simulations, the k-component Euler equations [3] are solved, where the local state is described by k components of partial density, $\rho_k$, three dimensions of

impulse density, $\rho v_X$, and an energy density scalar, $e$. The governing equations are as follows:

$$\begin{matrix}\rho_k \\ \rho v_X \\ e\end{matrix} + \nabla_Y \begin{matrix}\rho_k v_Y \\ \rho_k v_X v_Y + \delta_{XY} p \\ v_Y\ e + p\end{matrix} = 0. \quad (1)$$

Boundary and initial conditions are additional, furthermore an equation of state is also needed to complete the model. In this work basic no-slip boundary conditions are applied on the chamber walls, and isobar conditions on the inlet and outlet ports. This way gas flow is induced by the piston movement solely. Time advancement is calculated with the first order explicit Euler method [3]. Space discretization is done using FVM. Several parts of the engine are split into subdomains of structured and unstructured meshes. The first order Euler method is based on a first-neighbor stencil.

*Figure 1. Combustion chamber during the intake phase. The intake valve is at the bottom position. The freshly drawn gas is depicted as the dark range, showing where its relative density reaches 50%. The outlet valve is closed, and the corresponding cells are rendered inactive, thus are invisible here.*

There are several methods to handle piston movement, where additional neighboring regions are present. The multi-component method decomposes the meshes in a way that only one part is moving with the piston and is deforming in a time-dependent fashion. Additional equations are solved for each cell and time step, to obey mass-conservation [4]. Another method is using an overlapping grid, one of which is always moving in front of the piston. This requires a constant interpolation of the local state values, although deals with degenerate cells [5]. The final method, which is used in this study, is called snapper. A special structured grid is generated, and the last line of vertices is moved with the piston, until the cell layer reaches its half height. Then this cell layer is set inactive, and the next one is stretched to one and half of its height. Local data is recalculated with interpolation only in these layers. This action is referred to as "snapping" [6].

It is undoubtedly useful to use simulations capable of calculating the gas dynamics in a high performance computing environment. In the first part of the article a hybrid approach of parallelization is presented within the simulation on topic. It is shown, that the proper mixture of MPI [7] and OpenMP [8] techniques is capable of vastly benefit from the hardware used.

The next chapter is dealing with the challenging task of fitting multiple structured and unstructured meshes together. As most unstructured meshes are made manually using HyperMESH [9], there is the inevitable scatter, introduced by human error. Two neighboring meshes, that seem to have a common surface, may have unnoticeable scatter in their vertex coordinates. This error introduces unphysical anomalies in the simulation even in short runs. As these scatters are much smaller than the grid size, a proper pairing algorithm, one of which is presented here, can eliminate the problem.

As interpolating data is one of the major issues in this simulation, the last part will address methods, that are fast enough to handle local data transformation conveniently. Data transformation is not only required by the snapper algorithm of the piston motion, but also the more complex geometry of the valves. They have a less constricted shape, which introduces several problems in discretization. A basic type interpolation algorithm is shown, that is fast enough to use runtime.

## 2. Methods of parallelization

Both methods discussed in this part are in fact programming standards, which have been known for a long time now: MPI dates 1994, and OpenMP 1997. A few years later there were successful trials on combining these, resulting in a “mixed” or “hybrid” method [11]. The basic idea comes from combining independent accelerator methods for shared memory and distributed memory system. As for inter-node communications MPI is used, along with the additional burden of domain decomposition of the data, the leftover in-memory calculations are freely boostable with OpenMP, CUDA, or even a new layer of MPI, depending on the architecture of the computation units.

It is well known, that the achievable speedup on these methods heavily depends on the type of the problem. Is it possible to reach high performance in this special case? In this case the present local resources are investigated. Two many-CPU-core systems are available:

1. **MEMO** is an SMP NUMA system with 8 pieces of Intel Xeon X7560 processors @2.27GHz. These have 8 cores and 24 MByte of shared L3 cache each, connected with QPI, and additional 1 TByte of RAM.
2. **PLEXI** is a cluster system with 20 nodes. Each node is a NUMA system with 2 pieces of Intel Xeon X5650 processors @2.67GHz. These have 6 cores and 12 MByte of L3 cache each. Nodes are interconnected with quad-speed Infiniband and have 48 GByte of RAM.

As MEMO can handle up to 64 threads for one process, this machine will be used for OpenMP benchmarks. All other measurements are issued on PLEXI. The software environment includes GCC version 4.1.2 as C++ compiler with libgomp version 3.0 for OpenMP support, and OpenMPI 1.4.2 for MPI support.

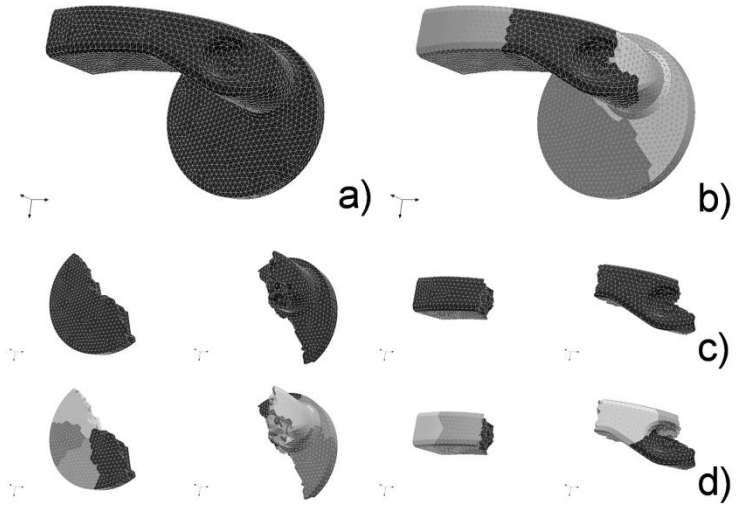


*Figure 2. Visualization of various methods of parallelization. Single process, single thread, serial (a); single process multiple threads, OpenMP (b); multiple processes, one thread each, MPI (c); multiple processes, multiple threads each, Hybrid (d)*

There are several issues in the simulation at hand, which makes parallelization a challenging task. Most of the vital issues, listed below, have been addressed, there are however several others, that need further attention.

- There are multiple types of meshes, each requiring unique treatment. This messes up domain decomposition. However, the support of handling multiple domains within one process, not just one, ensures manageability.
- There are interaction surfaces with more than two meshes connecting. However at a given time there are only two active cells on the opposing sides. Introducing an additional step, that synchronizes active cells only will prevent invalid data to be used.

Some of the non vital issues to be addressed presently are as follows:

- Inactivating, ergo skipping certain cells in the calculations induces tip over in the load balance. This is particularly present in a combustion chamber of high compressibility. Presently this is handled with special domain decomposition: the structured cylinder is split up along the axis of the piston motion. This ensures the nearly equal distribution of the computations. However communication costs are far from optimal.
- Special structured meshes, that require a wide stencil interpolation while snapping do not support decomposition within the stencil. This is considered a minor problem, as these meshes have few cells, the number of cells scales slower than linear, as the resolution gets finer.

The implementation is extensively tested to ensure the transparency of the MPI layer. Benchmarks are run for a quarter cycle, with the piston moving from the topmost to the bottommost position. Computation time is measured for each 200-loop-period, these are

treated as measured points. Speedup is calculated from this value by dividing the time cost of the serial code by that. Results for MPI, OpenMP and Hybrid measurements are shown on Figure 3, left.

Additional measurements are conducted with simpler, auto-generated meshes, in order to test scaling on the number of cells. Only one piston-like mesh is deforming in this model. Results on the strong scaling is shown on Figure 3, right.

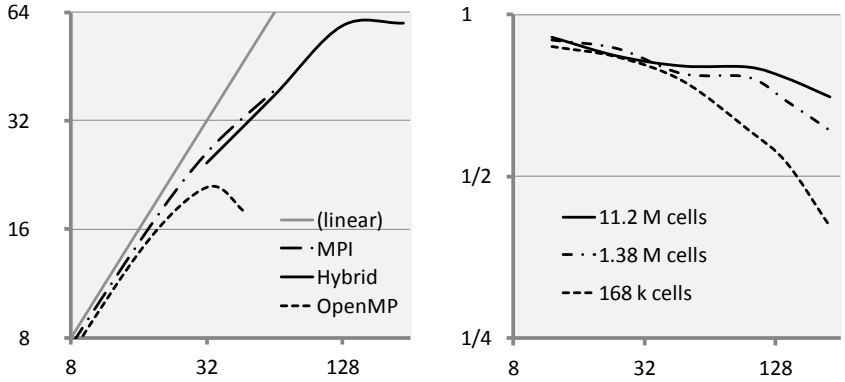


*Figure 3. Achieved speedup values for the simulated combustion chamber with moving piston and valves is shown on the (left). The speedup is plot against the number of computing cores on log-log scale for the methods investigated. The strong scaling of the hybrid method is shown for generated systems with various cell counts (right). The speedup to number of cores ratio is plot against the number of cores on log-log scale.*

It is observable, that the asymmetry resulting from the NUMA architecture does impair OpenMP implementation, that can be only improved by decomposition-like data aggregation. MPI scales very well up to a few processes per node, however fragmenting a not-so-large mesh to even smaller pieces will reveal a large surface to communicate. Also this lowers the available RAM per one process, which can inhibit the simulation from running. The MPI-OpenMP hybrid configuration with one process per processor (not node!) proves to achieve the best speedups. Running with above 128 cores, a speedup of around 60 is achievable, although there is still room for improvement.

We can also observe that the scaling is better with larger system size. This is naturally expected, as the communication cost proportionally lower with more cells to process. It can be stated, that this implementation is feasible for simulations of the presented kind with a cell count beyond one million up to ~200 processor cores.

## 3. Assembling multiple meshes

A rare case of challenge is presented in this part. For most FVM simulations mesh data is treated as one, partitioning and decomposition is done by extracting parts from the same mesh. In our case, however, there are special structured meshes, which are generated on the fly, from specific, marked surfaces of particular meshes. As most parts of the combustion chamber is deforming (the chamber itself, and meshes around all

valves as well), it must be ensured, that common surfaces of generated and unstructured meshes fit.

There are two problems, that make this fit harder. For once, mesh geometry data are stored in NASTRAN files [12], and the current PARMOD system supports only short field formats of 8 characters. This format may cut precision at even $10^{-4}$, which is much cruder than the float precision of $10^{-7}$. Additional scatter is introduced by human error. It is impossible to edit three dimensional data precisely as a machine.

Fitting the naïve way would require checking the distance of each pair of vertices. If we have *n* points on the surface, so *2n* points to be paired, time cost would be $O\ n^2$ . Provided we have point pairs with coordinates that match exactly, ordering both set of coordinated lexicographically will place pairs in the same position.

The scatter in the coordinates renders this ordering unusable. A small change in the first coordinate can warp away the point to a far position. This is an optimization problem referred to as nearest neighbor search [13]. Usual solutions include space partitioning methods, like the k-d tree [14], and the local sensitive hashing, or "bucketing" [15]. The later one is implemented, and discussed here.

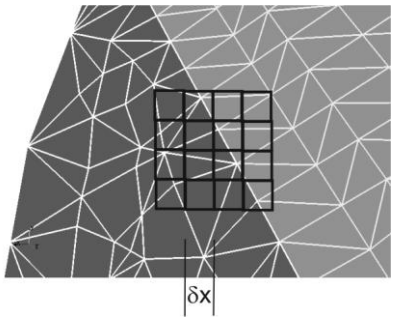


*Figure 4. The joining surface of two meshes (structured on the left, unstructured on the right). The vertices of both meshes are "hashed" into buckets of linear size dx, and the shape of a cube. (8 different hashing are required for proper matching in three dimensions)*

Using local sensitive hashing, each vertex is thrown in a cube form bucket of appropriate size, as shown on Figure 4. Two vertices in the same bucket can be considered coinciding. There is the possibility however, that two points sufficiently close to each other are not considered, as they sit in two separate, adjacent buckets. To avoid this, seven more bucketing is also conducted, and coincidence is approved, if any of the eight hashing gets two vertices in the same bucket.

The bucket has the actual size of the matching tolerance. This value has to be chosen carefully. Examining the spectrum of the inter-mesh vertex-to-vertex distance, there is a big gap below the minimum of the intra-mesh grid size. Human error will introduce a far smaller scatter, than this value. If the matching tolerance is chosen not far below that, the mesh joining will be successful. This will reduce matching time to $O(2^d n \log n)$. This method still slows down exponentially with the increasing of the dimensions. This is called the curse of dimensionality.

## 4. Mesh swap

Within the simulation at hand, there are several events, which require the change of discretization within the simulation space. First of them is the snapping in the simple deforming structured mesh, like the combustion chamber deformed by the moving piston. In this case, data in one or two cell layers gets interpolated. The next event is also snapping, now in the interface mesh, shown on Figure 5. This mesh handles interaction between two regions, where the surfaces are sliding on each other. During snapping, almost the entire mesh data is recalculated with interpolation.

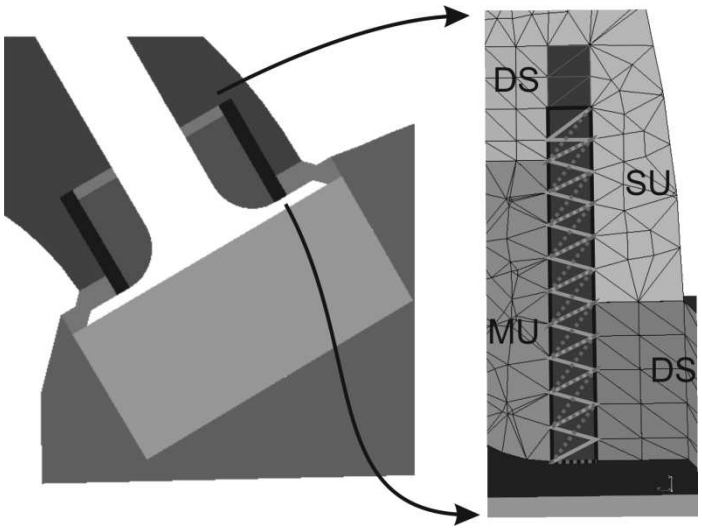


*Figure 5. The mesh structure of the valve is shown on the (left). It consists of a moving unstructured (MU), three deforming structured (DS), and a special slipping interface mesh. It is engulfed by two static unstructured (SU) meshes on the top and bottom. The snapping of the interface mesh is shown on the (right). The discretization within the black frame changes from the continuous to the dotted, if the valve is closing (or vice versa, if it is opening).*

The last case of mesh swap is in the case of the piston motion overlapping the path of the valves. This requires heavy data transformation with interpolation between multiple large meshes from different types. The parallel implementation of the later is also complicated, and yet to be done.

Interpolation must be implemented in a way, which is appropriate for the system simulated. It must preserve the corresponding physical properties:

- As all state variables are intensive, the weighed average must not change for any of the variables. A change in these variables will faultily create material, energy, or impulse.
- The local physical structure is to be conserved. Changing the mesh structure too often or with a too wide stencil will smear and degrade fine scale information.

In the sense of the above, data transformation is done in a way, where the new cell value is a weighed average of the data from the old cells that intersect with the new one. Weights are proportional to the relative common volume of the cells.

The first step is to calculate the sparse matrix with relative weights, showing the proportional volume coming from the intersection of the $i^{th}$ and $j^{th}$ cell to the space of the $i^{th}$ cell in row *i*, column *j*.

The naïve algorithm for the calculation of the interpolation constants would require $O(nm)$ time. However, provided having convex cells, the old cells intersecting the new one will form a closed cluster. Thus using a breadth-first search on the neighbour structure, and junking non-intersecting old cells will yield a algorithm with a time cost proportional to the number of vertices: $O(\max(n, m))$.

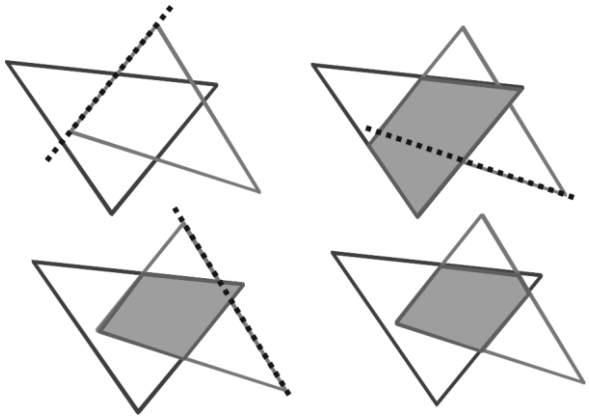

*Figure 6. Step-by-step calculation of the intersection shape issuing one cutting plane at a time.*

There is an algorithm to determine the volume of the intersection. The volume, *V*, of the intersection is calculated from the area, $A_i$, of the faces with the following formula:

$$V = \frac{1}{3} \quad _{face\ i}\, x_i n_i\, A_i, \tag{2}$$

where $x_i$ is any point on the face, and $n_i$ is the corresponding normal vector. Assuming the vertices within a face are on one plane, and they are indexed in order, the area, *A*, can be calculated as follows:

$$A = \frac{1}{2} \quad _i\ v_i - v_0\ \times (v_{i+1} - v_0)\ , \tag{3}$$

where $v_\iota$ is a vector of vertex coordinates.

The proper sorting approach will make interpolation time cost linear, making this approach ripe for runtime implementation.

## 5. Conclusion

It is apparent, that advanced computational techniques are required to handle sheer situations in this simulation, which can be especially strenuous for the average physicist.

It was also shown, that the proper use of these techniques can immensely aid the investigation of the physical phenomena. The speedup of 60 can reduce simulation time from five days to two hours. This allows for broader spectra of tests, or the investigation of a system that has almost four times the cell count.

Runtime usage of the mesh assembly and the interpolation procedures will greatly decrease manual work time on preparation. This also forecasts a more user-friendly like environment, hopefully usable by a wider range of users, like engineers.

There are still several challenging issues to be addressed. These include higher order, or implicit solution of the Euler equation within this setting. Also it would be most rewarding to implement acceleration for the graphics card with CUDA. The exhaustive study of moving mesh decomposition strategies and scaling would also prove invaluable.

These ideas will be realized next.

## Acknowledgements

This work is done in conjunction with the project Simulation and Optimization on the Széchenyi István University, which is funded by the project TÁMOP-4.2.2-08/1-2008-0021 of the European Union. Major part of the software is based on previous works of András Horváth and Zoltán Horváth [10]. The simulation is using the PARMOD software system, primarily developed by Gábor Takács. Most meshes are created and generated by Tamás Morauszki, Péter Mándli and their team. To these people goes my sincere thanks. Special thanks to Gundolf Haase and Zoltán Horváth for the invaluable discussion on the topic.

## References

[1] see e.g.: M. Lesoinne, C. Farhat: *Geometric conservation laws for flow problems with moving boundaries and deformable meshes, and their impact on aeroelastic computations*, Computer Methods in Applied Mechanics and Engineering **134,** 1996, pp 71-90.

[2] A. Jameson, W. Schmidt: *Numerical Solution of the Euler Equations by Finite Volume Methods Using Runge-Kutta Time-Stepping Schemes*, AIAA **M,** 1981, pp 1-19.

[3] see e.g.: C. B. Laney: *Computational Gas Dynamics*, Cambridge University Press, 1998.

[4] P. H. Epstein et al.: *Computations of a Two-Stroke Engine Cylinder and port Scavenging Flow.* SAE 910672.

[5] J. Steger: *On the Use of Composite Grid Schemes in Computational Aerodynamics.* Computer Methods in Applied Mechanics and Engineering **64,** 1987, pp 301-320.

[6] A. A. Amsden et al.: *Comparisons of Computed and Measured Three-Dimensional Velocity Fields in a Motored Two-Stroke Engine.* SAE 920418.

[7] for the official version of the MPI standard see: http://www.mpi-forum.org/docs/docs.html

[8] for the official version of the OpenMP standard see: http://openmp.org/wp/openmp-specifications/
[9] for product description see: http://www.altairhyperworks.com/
[10] Z. Horváth, A. Horváth: *Numerical Simulation of Compressible Fluid Flow in 3D Domains with Translating Boundaries Proceedings in Applied Mathematics and Mechanics Vol. 4.* Issue 1., 2004, pp 422-423.
[11] L. Smith, M. Bull: *Development of mixed mode MPI / OpenMP applications*, Journal of Scientific Programming Vol. 9**.** Issue 2,3 2001.
[12] for extensive information on the file format, see: http://www.openchannelfoundation.org/projects/NASTRAN
[13] see e.g.: D. Knuth: *The Art of Computer Programming Vol. 3.* 1973.
[14] J. L. Bentley: *Multidimensional binary search trees used for associative searching, Communications of the ACM Vol. 18.* Issue 9. 1975.
[15] P. Indyk, R. Motwani: *Approximate nearest neighbors: towards removing the curse of dimensionality Proceedings of the thirtieth annual ACM symposium on Theory of computing* 604-613 1998.

# GPS Based Data Acquisition System for Mobile Applications

**D. Covaciu, I. Preda, Gh. Ciolan**

**Transilvania University of Brasov, Romania**
**e-mail: dinu.covaciu@unitbv.ro, pion@unitbv.ro, cgicu@unitbv.ro**

Abstract: The Global Navigation Satellite Systems allow an accurate determination of the position in a geocentric reference system, using the signals from the artificial satellites network, received with dedicated devices. The GPS devices are well known and used by many people, especially for navigation. These are commercial GPS devices, which can be found at decent prices. Professional devices also exist for geodesic applications, and even for dynamic data acquisition. These are much more precise devices, but more expensive. This paper presents an acquisition system developed by the authors, using a high performance GPS device, available on the market, a portable mini-computer and dedicated software. The GPS sensor is one oriented to OEM users, for machine operation and guiding and agricultural applications. The sensitivity is very high and the registration rate is 5 Hz. It is connected to a computer through serial interface. The software application developed for this system takes the information from the GPS sensor using the sentences defined by the NMEA messages standard. Information about position, velocity and acceleration are displayed in real time on the computer screen and all useful data acquired are saved in a text file. These data are imported then in a special CAD application, for post-processing. The system was used in various studies regarding vehicle dynamics or efficiency and in traffic or noise analysis.

*Keywords: data acquisition, instrumented vehicle, GPS, programming*

## 1. Introduction

Navstar-GPS is the Global Navigation Satellite System developed by US Department of Defense, originally for military applications but with significant benefits for civil users. As all the existent satellite navigation systems (including Galileo and Glonass), GPS is composed by three segments: the space segment, the control segment and the user segment. The space segment consists in the satellites transmitting information about their position. The ground control segment transmits the location parameters, controls the paths and the data transmitted and changes the satellite orbits. The user segment consists in all the GPS devices that receive simultaneously the signal from the visible satellites and calculates the solution of the navigation equation, PVT (Position, Velocity and Time). The signals from at least four satellites are needed to obtain the solution.

Based on the satellites navigation parameters it is possible to calculate the distances between each satellite and the GPS receiver [8].

Using a GPS receiver installed on a rigid body (like an automobile) it is possible to ascertain his position on Earth. Having two or three receivers (or a dedicated receiver with two or three antennas) on the same rigid body, it is possible to ascertain the orientation, on a plan or in 3D space.

The determination of position using GPS can be affected by some errors, like: orbital errors (also known as ephemeris errors, these are inaccuracies of the satellite's reported location), ionosphere and troposphere delays, signal multipath (occurring when the GPS signal is reflected off objects such as tall buildings or large rock surfaces), receiver clock errors (a receiver's built-in clock is not as accurate as the atomic clocks onboard the GPS satellites), errors caused by reduced or changing number of satellites, satellite geometry/shading (this refers to the relative position of the satellites at any given time).

Because of these errors, the absolute coordinates on the ground are calculated with an accuracy given in meters. However, it is possible to obtain high accuracy (centimetres or millimetres) in relative coordinates (using two receivers) or by receiving a correction (differential) signal from a fixed station (DGPS).

## 2. GPS receivers

The block diagram of a GPS receiver [4] is shown in figure 1.

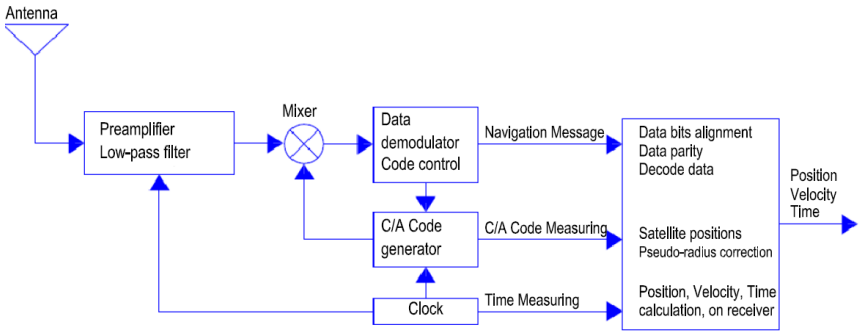


*Figure 1. Simplified block diagram of a GPS receiver*

Basically, the signal received by antenna is taken by a preamplifier with a low-pass filter, to reduce the higher frequency noise and to amplify the useful signal, with a carrier frequency over 1 GHz. The signal is then mixed with the *C/A* code generated locally and introduced in a demodulator for extracting the navigation data.

The GPS satellites transmit signals on two carrier frequencies, offering two levels of service: SPS and PPS. The SPS (*Standard Positioning Service*) signal is received by most of the commercial devices. The quality of the SPS signal may be altered intentionally by the US *DoD* (*Department of Defense*). The SPS signal is transmitted on the $f_1$ frequency, which is 1575.42 MHz. The PPS (*Precise Positioning Service*) signal offers higher accuracy and it was initially reserved for military and special applications.

The signal is transmitted on the $f_2$ frequency, which is 1227.60 MHz, and it is used for ionosphere and troposphere delays measurement.

The two carrier frequencies are phase modulated using three binary code signals:

- The *C/A* (*Coarse Acquisition*) code modulates the phase of the $f_1$ carrier;
- The *P* (*Precise*) code modulates both carriers, $f_1$ and $f_2$;

The navigation message modulates also the $f_1$ carrier signal. The navigation message is a 50 Hz signal consisting in data bits describing the GPS satellite orbits, the time corrections and other system parameters.

At reception, based on the three signals, the PVT (Position, Velocity, Time) information is calculated and sent further to the navigation device, using NMEA or similar protocols.

The GPS receivers can store data in their own non-volatile memory (like *SD* cards or *CompactFlash*), in text files using a *txt* or *gpx* format, or they can send data to other devices using RS232 or USB interfaces and a certain transfer protocol.

The most known transfer protocol used for transmitting GPS data is the standard recommended by NMEA (National Marine Electronics Associations). The NMEA 0183 standard [7] defines the requirements for the electric signal and for the data transmission protocol, and also the specific instructions format for a serial data bus of 4800 baud rate. For higher transmission rates (up to 38.4 kBd) it was defined an extension of the protocol, NMEA 0183-HS (High Speed). The NMEA standard is not intended only for communication with the GPS devices, but also for other electronic devices used in marine applications.

A NMEA sequence consists in a character string composed by a type identifier and more data fields, comma separated. The type identifier is used at reception for establishing the type and format of the data sequence that is to be read. The number and length of data fields depends by the sequence type.

Data taken from GPS include the geographic coordinates (longitude and latitude) and the altitude, used to position the receiver on the earth surface. The geographic coordinates must be converted in rectangular coordinates (x, y, z), in order to use them in the automotive kinematics studies. This operation can be done using dedicated software.

## 3. Use of GPS devices for data acquisition

GPS position relies on precise measurements of the distance from the receiver to the satellite and is affected by numerous effects which can reduce the quality of the signal, like atmospheric conditions or reflections from nearby objects such as buildings which introduce multipath, again adding to the length of the signal. The speed calculated as changes of the position in time will give a “noisy” result, as in Figure 2, left side. Interpolation of the values obtained this way will affect the accuracy which is very important when testing the vehicle's performances.

However, GPS velocity can be measured using a different method which measures the change of the signal from satellite, or Doppler Effect. By measuring this change, the

errors which normally affect GPS have very little influence over the quality of the signal, and the velocity measurement is phenomenally accurate. Another great aspect of GPS is that all satellites have atomic clocks on-board, and by utilising this signal, the timing remains stable to within less than a millionth of a second [10].

Therefore, instead of using position to measure distance, the accurate Doppler derived velocity is integrated using the precise time signal to derive distance. The result of the combination of these two is an extraordinarily accurate distance measurement. An example result is in Figure 2, right side.

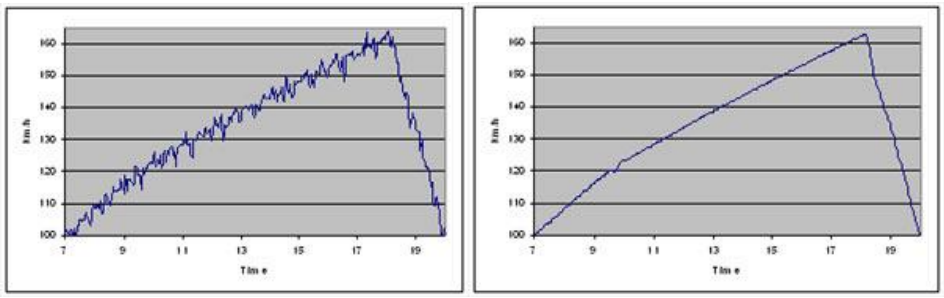

*Figure 2. Velocity calculated from position and time information (left), and using the Doppler Effect (right) (source: http://www.racelogic.co.uk)*

It is preferred to read the velocity directly from the GPS receiver, whenever is possible (e.g. by reading NMEA sequences), instead of calculating the velocity based on successive positions.

To measure the dynamic performances of a vehicle, no matter what instruments or tools are used, it is required to install these instruments on the vehicle and to collect data on the move. The traffic data can be also collected either by using instruments installed on moving vehicles (*instrumented vehicle* or *chase vehicle*) [1].

The process of data acquisition and processing is shown schematically in Figure 3. Data collection phase is contained in two blocks in the first column and consists in the instrumented vehicle method.

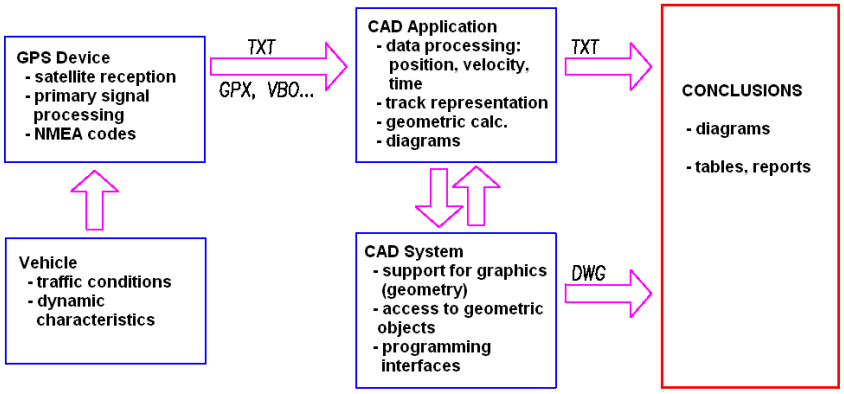


*Figure 3. Flow diagram of data acquisition and processing*

The instrumented vehicle is a vehicle with data acquisition equipment installed. When using GPS devices as data acquisition equipment, only those data related to that vehicle behaviour will be recorded.

Some of the advantages of the instrumented vehicle method are as follows:

- There is not necessary equipment installed on various places on the route (radar, inductive loop, video camera);
- Speed is recorded for the entire route length, not only in a single point (like when using external speed sensors);
- It can be ascertained also the acceleration, since the record is continuous in time;
- The time needed to collect data on different routes is shorter;
- It can be obtained an accurate velocity field on the travelled routes.

The preparation of instrumented vehicle consists in installation of data acquisition equipment. In the case of GPS devices, depending by their type, the most complex installation procedure consists in placing the external antenna on the vehicle roof, connecting the computer and starting the devices and software applications.

The use of GPS devices for data acquisition has some important advantages:

- Collect real data for the vehicle on which the device is installed;
- Simultaneously obtain time and grade information;
- Possibility to associate the collected data to a certain area, based on the digital maps, and automatically associate data with the density of population;
- Possibility to record many points on various tracks;
- Easiness of devices' use and installation, on any vehicle.

Some disadvantages of using GPS data acquisition are:

- Areas without satellite signal (canyons, tunnels);
- The GPS devices accuracy depends by a third-party technology (selective availability, controlled by DoD, the need for terrestrial station to have differential signal).

## 4. The new data acquisition system (DS-5)

Based on the Garmin GPS 18x-5Hz receiver [6], it was developed an original tool for vehicle dynamic behaviour analysis (called DS-5) [2], [9]. The system has two main components: hardware and software. The hardware part (figure 4) consists in the GPS receiver, a minicomputer and the connecting interface, usually a RS232-USB adapter. The software part is a stand-alone computer program developed by the authors in Delphi programming language. The program is used for data acquisition and for storing that data as text files on the computer.

### 4.1. DS-5 Hardware

The system is composed by the GPS receiver, the interface and the minicomputer. Depending on the chosen minicomputer, sometimes may be necessary to use also an inverter, for plugging the computer to the vehicle 12 V outlet.

The receiver's power supply is not the vehicle's 12V outlet (this can be used as power supply for the computer). Instead, it is used one of the computer USB connectors as a 5 volts power supply. The advantage of using the computer's USB interface is that the computer battery is also a power back-up for the GPS receiver. Since the minicomputers (tables PCs) does not have an RS232 interface, it must be used an adapter cable between the computer USB connector and the device connector.

The GPS receiver is the Garmin GPS 18x-5Hz device. This device has a connecting cable terminated as bare wires and it has to be connected to a RS232 interface.

*Figure 4. GPS 18x-5Hz and the DS-5 data acquisition system*

GPS 18x-5Hz (Figure 4) is a GPS sensor used especially for machinery operation and guiding, and for different agricultural applications, where are required very precise position and velocity information [6].

GPS 18x-5Hz has 12 parallel channels (is able to process simultaneously the signals received from 12 satellites), it is WAAS enabled (can process the differential radio signal when available) and has an integrated magnetic base. It has a permanent memory for storing the configuration information, an internal clock (independent by the satellite signal) and measured raw data, for high precision and dynamic applications.

The receiver sensitivity is –185 dBm. It is also available a function for generating an output pulse signal (*Measurement Pulse Output*) of 5 Hz, with the superior limit aligned with offsets of 0 ms, 200 ms, 400 ms, 600 ms and 800 ms from the signal front that mark the UTC seconds, in 1 microsecond interval, for all cases when the GPS receiver reports a valid and accurate positioning in a period of at least 4 seconds.

The GPS 18x-5Hz device does not work independently; it must be connected to a computer.

Of high importance is the transfer rate through the serial interface, because this influences directly the data acquisition rate from the GPS device. To ensure reception of all information at intervals of 0.2 seconds, the transfer rate should be 19200 bauds. There are not needed all the NMEA data sequences that the GPS receiver is able to send, because the acquisition rate of 5 Hz may be affected (will be reduced to 2.5 Hz).

The device configuration influences the volume of received data in a measure given by the results of the simple relation below (1).

$$\text{Length of received sequence} = \frac{(\text{number of transmitted characters})}{(\text{characters transmitted per second})} \quad (1)$$

Ascertaining the required transfer rate (bauds) can be done using the above relation and the data given in Table 1 and Table 2.

*Table 1 – Characters per second transmitted at various transfer rates*

| Transfer rate (bauds) | Characters per second |
|---|---|
| 300 | 30 |
| 600 | 60 |
| 1200 | 120 |
| 2400 | 240 |
| 4800 | 480 |
| 9600 | 960 |
| 19200 | 1920 |
| 38400 | 3840 |

*Table 2 – Transfer rate and sequence length for NMEA 0183*

| Sequence | Transfer rate | Max. characters |
|---|---|---|
| GPRMC | One / record | 74 |
| GPGGA | One / record | 82 |
| GPGSA | One / record | 66 |
| GPGSV | One / record | 70 |
| PGRME | One / record | 35 |
| GPGLL | One / record | 44 |
| GPVTG | One / record | 42 |
| PGRMV | One / record | 32 |
| PGRMF | One / record | 82 |
| PGRMB | One / record | 40 |
| PGRMT | One / minute | 50 |

The useful NMEA sequences that should be taken from the GPS receiver are: *$GPRMC* (includes position data, speed in knots, time), *$GPGGA* (3D position and accuracy – quality of the signal, number of satellites) and *$GPVTG* (heading and ground speed in knots and km/h) [7], [2], [3].

Maximum number of characters to be transmitted is: 74 + 82 + 42 = 194.

In this case a baud rate of 2400 bauds is needed to transmit one record per second, and for 5 records per second (5 × 194 = 970 characters) is required a rate of 19200 bauds.

The useful data taken from receiver are: time (with a rate of 0.2 seconds and the accuracy given by satellite), latitude, longitude (both in degrees, with 7 decimals accuracy), altitude (accuracy of 0.1 meters) and velocity (accuracy: 0.01 km/h).

Additionally, as coordinates accuracy information, there are known: the satellites number (in good receiving condition there are 8-10 satellites visible) and *HDOP* (*Horizontal Dilution of Precision*) – usually less than 1.5 (with differential signal: < 1).

### 4.2. DS-5 – Software

For the acquisition, primary processing and saving of received data with *DS-5* (based on GPS 18x-5Hz) it was developed a dedicated software application using Delphi programming language. It was chosen this programming environment because it features dedicated objects for creating flexible and easy to use user interfaces. In addition, libraries are available with predefined functions dedicated to various kinds of applications, including serial port programming (RS-232). So it was possible to write the user interface shown in Figure 5.

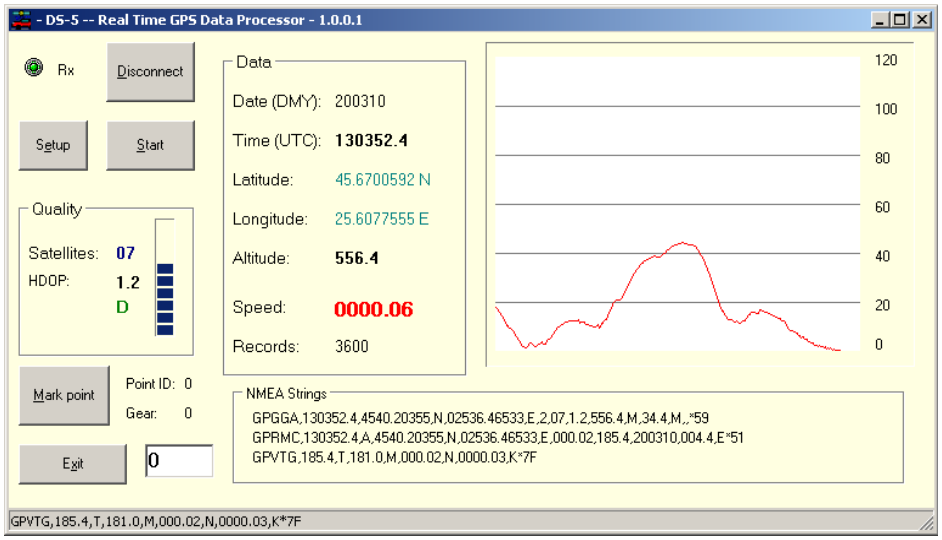


*Figure 5. User interface of the GPS data acquisition software*

The main areas in the user interface (the main screen of the program) are:

- *Data* – display in real time the information received from the GPS sensor; when the satellite signal is not available (not enough visible satellites), the coordinates displayed in this field are taken from the internal memory of the device;
- *Quality* – information about quality of the signal, like the number of visible satellites and *HDOP* (*Horizontal Dilution of Precision*); when differential signal is available, a „D" appear also in this area;
- *NMEA Strings* – the NMEA sequences received from the GPS sensor; these strings are displayed in order to have an additional control of the data received, especially in the software development phase;
- The graphic area (white area on the right side of the screen) – here is displayed, in real time, the speed versus time diagram, when data logging is enabled;
- Marking area (bottom-left) – includes the „*Mark point*" button; by clicking on this button the current position is recorded and also the edit box „*GEAR*", where it can be entered the current transmission gear (numeric keys, from 0 to 6);
- The control area (upper-left) – in this area are placed the buttons for configuration, connecting to the GPS device and start/stop the recording; the buttons are big enough for easy use with a Tablet-PC with touchscreen.

## 5. Performances of the DS-5 data acquisition system

In order to check the influence of the measurement errors on the collected data, numerous tests were made. These tests can be grouped as follows:

- Measurements with GPS receivers stationary for a long time (minutes);
- Recording the same track with the same receiver at different times (in the same day or different days);
- Simultaneous recording of the same track with two GPS receivers, of same or different models;
- Simultaneous recording of the same track with the GPS receiver and other type of measuring device.

The influence of atmospheric condition and obstacles may be revealed by recording the position of a stationary receiver. The results measured with a stationary *GPS 18x-5 Hz receiver* are shown in Figure 6. Both records were taken in the same position, for 30 seconds and 100 seconds, respectively. The number of satellites was 8 for the first measurement, and 7-8 for the second measurement. The accuracy reported by the receiver through *NMEA* sequences (*HDOP – Horizontal Dilution Of Precision*) was 0.9 – 1.2, values which generally indicate a good accuracy. According to Figure 6, with these measurements it was obtained a positioning precision of 0.342-0.475 meters.

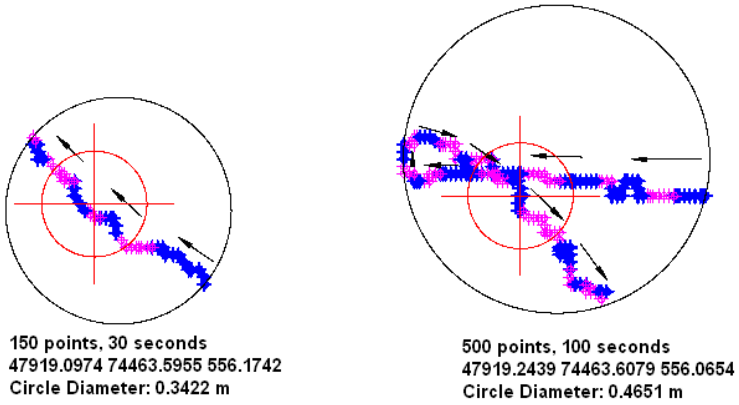


*Figure 6. Measurements with the GPS receiver stationary [2]*

For testing the *DS-5* system on a moving vehicle, the vehicle having the new system activated simultaneously with a GPSmap 60CSx system [5] was driven on a short track, with a total length of 500 metres, Figure 7.

In Figure 8 is presented the speed versus time diagram for the same track (Figure 7) recorded with both devices. As it can be seen in this diagram, the two signals are not perfectly synchronized (the GPSmap signal is delayed with one second). The difference is caused by the internal processing of the GPS signal by the microcontroller embedded in the GPS device, which also make a filtration of the position.

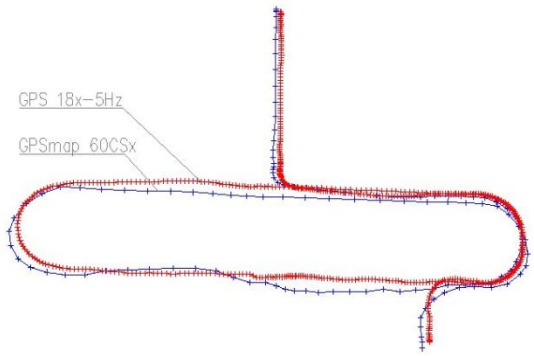


*Figure 7. 500 m track recorded with two different devices: GPSmap and DS-5*

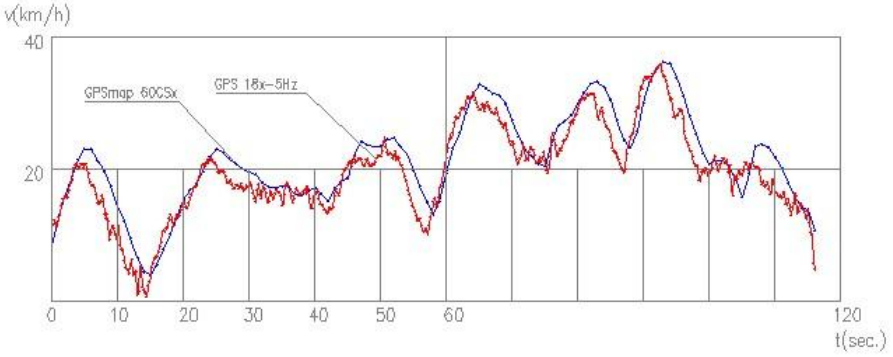


*Figure 8. Time/Speed diagram for two different devices: GPSmap and DS-5*

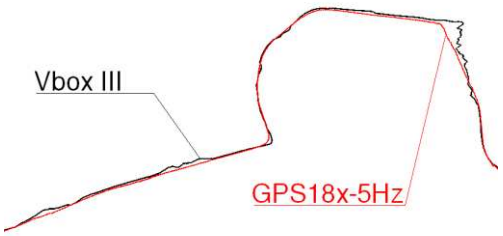


*Figure 9. Part of a track recorded with Vbox and DS-5, simultaneously*

The speed computation was based on the successive positions recorded at the time interval allowed by each device: 1 s (GPSmap) and 0.2 s (GPS 18x), respectively. The noise (signal discontinuity) in the diagram of speed recorded with GPS18x in Figure 8 (the red curve) will not appear if the speed is read from the device, using the NMEA codes.

Another comparison was made between DS-5 and Vbox III, a professional data acquisition system made by Racelogic [10]. Figure 9 presents a part of a track, recorded

with both devices. It is obvious a pretty high deviation from the route of the track recorded with Vbox, device which was expected to be more accurate than GPS 18x, in similar conditions. The speeds versus time diagram, and also speed versus distance, are shown in Figure 10.

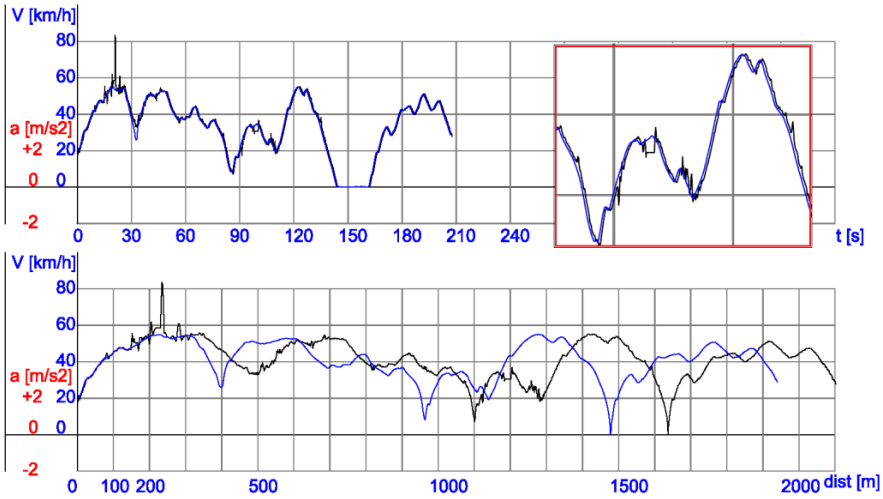


*Figure 10. Time/Speed diagram (top) and Distance/Speed diagram (bottom), measured with Vbox (black) and DS-5 (blue)*

The deviation from the route of the track recorded with Vbox does not seem too big and it would not be a problem if the objective would be guiding the driver, based on a digital map. But the speed versus distance diagram reveals important differences. In Figure 10 the speed recorded with Vbox is represented in black, and the speed recorded with GPS 18x (DS-5) is presented in blue. In both cases the speed is read directly from the receiver, not calculated from successive positions and time. First, the time/speed diagram shows the records' synchronization, but the Vbox records present some unrealistic deviations. These deviations do not seem to be just a recording noise, as in Figure 2. In the distance/speed diagram the differences are too high (more than 5% difference between the two records, for the total length of the track – Figure 10), and are caused probably by the positioning errors – the distance between successive points is ascertained based on the recorded positions.

The source of the positioning errors of the *Vbox* system seems to be the reduced number of visible satellites; *Vbox* has received signals from 5-6 satellites, since *GPS 18x* has received signals from 7-8 satellites. The test was made inside a city, on a "*canion*" road, with high buildings on both sides. The errors given by Vbox is explainable, but in the same time the quality of signal reception of *GPS 18x* is remarkable.

## 6. Conclusions

DS-5 is a low cost data acquisition system, based on GPS technology. The performances are good enough for analysis of vehicle dynamic behaviour, but can be used also for collecting traffic data [1].

The DS-5 system has two components: the hardware equipment and the software application. The hardware is realized by putting together elements available on the commercial market: a high precision GPS sensor and a small size computer. The software component is an original application developed by authors [2], [3].

The precision given by the GPS device (GPS 18x-5Hz) is as high as 7 decimals for longitude and latitude, 0.1 meter for altitude and 0.01 km/h for speed. The data sequences are transferred from the GPS device at a rate of 5 samples per second (0.2 seconds time period); the time accuracy is given by satellites. The accuracy of recorded data is indicated by the number of satellites (8-10 satellites are available in good weather conditions) and by the *HDOP* parameter. *HDOP* is usually less than 1.5 and can be even less than 1 when differential signal is available [3].

Although the positioning accuracy is increasing continuously, the errors remain an important problem, quite difficult to control, especially in reduced satellites visibility. However, a proper use in correlation with quality processing-algorithms permits to the GPS systems to provide a precision of speed and acceleration measurements at least as good as other measuring systems used in experimental research.

## References

[1] Covaciu, D., Florea, D., Preda, I., Timar, J.: *Using GPS Devices for Collecting Traffic Data*, SMAT 2008 International Conference, Craiova, 2008.
[2] Covaciu, D. *Study of the dynamic and in-traffic vehicle behaviour using GPS and CAD applications*, Ph.D. Thesis, Transilvania University of Brasov, 2010.
[3] Covaciu, D., Preda, I., Ciolan, Gh., Câmpian, O.V.: *Data acquisition system based on GPS technology, for vehicle dynamics analysis*, The XI-th International Congress on Automotive and Transport Engineering CONAT 2010, Volume 5, paper 4006, Brasov, Transilvania University Press, 2010, , pp.31–36.
[4] Dana, Peter H.; *Global Positioning System Overview*. The Geographer's Craft Project, University of Colorado, 2000. http://www.colorado.edu/geography/gcraft/notes/gps/
[5] Garmin Intl.: *GPSMap 60CSx Technical Specifications*, http://www.garmin.com.
[6] Garmin Intl.: *GPS 18x Technical Specifications. Revision B*, 2008. http://www.garmin.com.
[7] Garmin Intl.: *Garmin Proprietary NMEA 0183 Sentence Technical Specification*, (2006). http://www.garmin.com.
[8] National Instruments Corp.: *Tutorial on GPS Receiver Testing*, http://www.ni.com/automatedtest/gps.htm.
[9] Preda, I., Ciolan, Gh., Covaciu, D.: *Systems Based on GPS Devices Used for Vehicles Dynamic-Behaviour Study*, Intelligent Transportation Systems ITS-Romania-2009 International Conference, Bucharest, 2009.
[10] Racelogic: *VBOXTools Software Manual*, Ver. 1.4.

# Processing GPS Data in CAD Environment for the Study of Vehicles' Dynamics

**I. Preda, D. Covaciu, Gh. Ciolan**

**Transilvania University of Brasov, Romania**
**e-mail: pion@unitbv.ro, dinu.covaciu@unitbv.ro, cgicu@unitbv.ro**

Abstract: The GPS technology is more and more widespread between common users, mainly for navigation applications. To date, the improved performances of the GPS devices permit using them as reliable tools in the research activities. The price and easiness of use make this type of devices extremely interesting to experimentally study the dynamics of any vehicle type. This paper shows some possibilities to process GPS data in order to obtain useful information about the vehicle dynamic behaviour. Also, there are presented and compared the data obtained from various GPS devices. The authors realised a computer program that run in AutoCAD environment, taking benefits from its graphical and list processing features. The data can be imported from different GPS devices using standard or proprietary file formats. Based on position and time information, the speed, acceleration or slope can be ascertained and the moving resistance forces or the power delivered by the engine can be estimated. These results were plotted in different ways, for easy interpretation.

*Keywords: vehicle dynamics, GPS, data acquisition and processing, CAD programming*

## 1. Introduction

In the last years, the GPS technology became common and popular. On the market are offered various applications, especially for navigation and for recording of the route travelled by different vehicles (aircraft, ships, cars) or pedestrians (on city or on mountain trails). Combining position information obtained from GPS with detailed digital maps, it can find the desired destinations and the optimum routes to follow.

The diminishment of electronic-devices price and the increase of the precision offered by the GPS, even for commercial applications, encourage the apparition of more and more new applications.

This paper presents possibilities, designed and experienced by the authors, to use GPS devices for the assessment of the vehicles dynamic behaviour by measuring and estimating. Some results of the performed tests are also presented.

## 2. GPS devices used for the study

For the vehicle dynamics study, some different GPS devices with tracking possibilities were used. These are presented in figure 1:

- *Holux M-241*, a GPS data logger, able to store a sample at every 5 seconds;
- *Garmin GPSMap 60CSx* [4], a handy and light-weight commercial device (1 sample per second recording rate, able to compute speed);
- *Garmin GPS 18x-5Hz* [5], a precise very small device (5 sample per second recording rate); connecting this to a notebook (figure 1, right) and realising an original software for real-time communication, data storing and primary processing (speed calculation, data filtering and trajectory graphical representation), the authors realised a valuable, affordable and easy to use GPS data logger;
- *Racelogic VBox 100* [11], a professional device (with the recording rate up to 100 sample per second, able to compute speed and acceleration and to graphical represent the gathered data in real-time).

*Figure 1. The GPS devices used in measurements (from left to right): Holux M-241; Garmin GPSMap 60CSx; GPS 18x-5Hz; Racelogic VBox (the blue case) and the previous two devices*

During the last five years, the authors made a lot of tests with these devices aiming to verify theirs precision or for research purposes.

Compared with other measuring devices used for the vehicle kinematics study, as the "*fifth wheel*" or *Correvit optical device*, the actual commercial GPS-systems present some important advantages: small packaging, reasonable prices, augmented performances, short time for vehicle instrumentation, easiness of use, simple connectivity with computers and ability to store large amount of data. Furthermore, any study of vehicle dynamics is based on reliable information about travelling time, acceleration, velocity and distance, which means exactly the processing results offered by common GPS receivers.

The recording of the altitude and geographical coordinates, also available, make GPS devices more attractive for the experimental study of vehicle dynamics, because the 3D profile of a track or a route can be easily obtained on a digital map, figure 2. Because each data sample is well identifiable in time, GPS information can be perfectly synchronized with test data provided by other measuring devices. The GPS tools can be

used by day or by night, in on- and off-road applications, conditions in which other measuring instruments for vehicle kinematics can have difficulties to work.

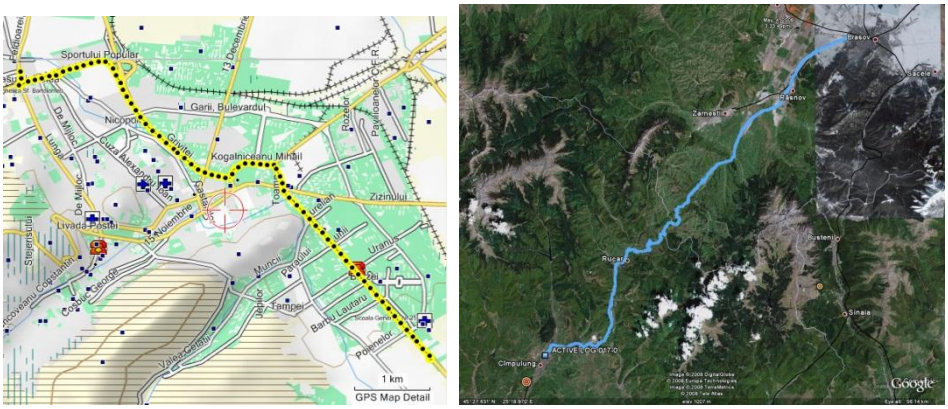


*Figure 2. Tracks viewed in Garmin's MapSource software (left) and on Google Earth*

Exterior mounting of small GPS antennae will not impede the vehicle's manoeuvrability or change its aerodynamics. If wonted, these can be even placed inside cabin, near the windshield. Also, simple data processing and plotting can be done in real-time, permitting very quick displaying of useful information.

## 3. Base algorithm to obtain vehicle kinematics from GPS data

The primary data, which one disposes after GPS tracking, are the time, longitude, latitude and altitude. The algorithm imagined and implemented by the authors starts with the transformation of that *global positioning data* in local x,y,z coordinates, according to the track mean position on the Earth [1], [2]. As a result, the vehicle path is obtained as a series of three-dimensional points well related to the time, figure 3, left. Sorting these series of coordinates according to the time increase, a passing direction will be associated with the track, figure 5, left.

For the programming of the algorithm it was choose the Autodesk Autocad software for its capabilities in handling graphical objects and for the ability to process lists of its Autolisp programming language. This ensures to the researcher freedom and easiness in processing large amount of data.

All the information (time, geographical coordinates and CAD coordinates) is stored as a list of *point properties*. Another list will be made with *line properties* to store information referring to the intervals between consecutive points. New other information can be easily aided to these lists after new processing stages.

Based on the time and 3D coordinates of the points, for each pair of two neighbouring points, a time interval $\Delta t$ and a distance $\Delta s$ are calculated. Then, from these distances and time intervals, the mean vehicle velocities between points $v_{med}$ are computed. This data is stored in the second list that contains the interval properties. Each of the two ordered lists (with point properties and with interval properties) can be used according with the aim of data processing or visualization.

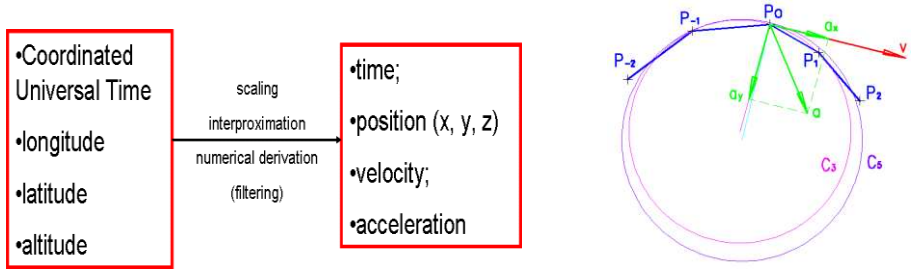


*Figure 3. Schematic of GPS data processing (left) and schematic of velocity and acceleration derivation from coordinates and time (right)*

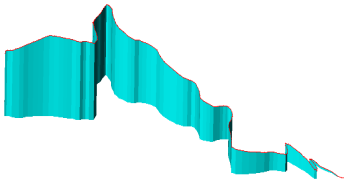

*Figure 4. Three-dimensional representation of the trajectory (road's path and height)*

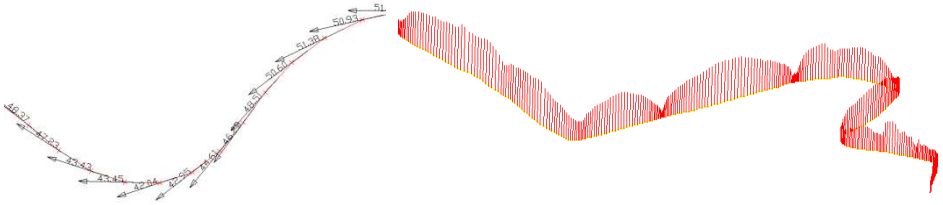

*Figure 5. Modalities to represent speed evolutions on the trajectory left – speed as vertical lines; right – speed as vectors with magnitude and orientation*

To estimate GPS-point *velocities*, the both lists can be used. One method can use an odd number (usually 3) of GPS-point time-space pairs ($t_p$,$s_p$), first to find by interpolation or interproximation a function $s = f(t)$ and then to obtain the point velocity $v$ as a derivative of this function, figure 3, right. The other method can use an even number (usually 2) of interval mean-velocities $v_{med}$ to reach, by interpolation or interproximation, the point velocity $v$. Both methods were tested and the results are quite similar if ones compare with the velocities furnished by the GPS receivers. Based on that, the second method is normally preferred because is faster.

A similar approach was used to obtain the path *slope*. First a mean slope value $\alpha_{med}$ was calculated from the interval variations of the altitude and horizontal distances, then the GPS-point slop was reached by interpolation.

Due to the graphical capabilities of the computer program, numerous types of visualisations can be used and automatically realised. As example, figure 4 shows a possibility to visualise the vehicle trajectory, permitting to observe the path as a 3D shape, with the option to mark local valleys and peaks or to graphically indicating certain levels of height. Figure 5 presents the plot of the vehicle velocity in the GPS-points. As can be seen, in the left side of the figure the vectorial representation indicates

both the magnitude and the orientation of the velocity and in the right side the speed is represented as successive verticals to the path, allowing to view the vehicle stops or speed changes.

To obtain the *orientation* of the speed vectors, as shown in the figure 5, left, it was necessary to realize first an approximation of the vehicle *trajectory* and then to represent the vector tangent to that, pointing in the travelling direction.

The simplest way to approximate a curved trajectory was to use a circle passing through three points: current, previous and next, figure 3, right. If the angle of the two line segments connecting the three vicinal points is too small, a straight-line trajectory was assumed (a curvature radius approaching infinity). For the other cases, the velocity vector orientation is perpendicular to the circle radius in the current point.

Of course, there are also other methods to approximate a trajectory when ones know its points. For example, the radius of curvature can be obtained using cubic spline interpolation or interproximation and then applying the second-order derivative function. The *radius of curvature R* was used also to calculate the *lateral (centripetal) component of the vehicle acceleration*:

$$a_y = v^2 \quad R \tag{1}$$

The other component, the *longitudinal (tangential) acceleration* $a_x$ obtains as the first-order derivative of the function $v_p = f(t)$ that estimate the magnitude of the vehicle speed.

Figure 6 shows the lateral and longitudinal components of vehicle acceleration. In the left side, the green and magenta vectors indicate left-hand, respectively right-hand turn. The vectors tangent to the trajectory mean braking, if are pointing rearwards (before turns), and gearing-up, if are pointing forward (after turns).

The *total acceleration* of the vehicle can now be calculated by a vectorial summation of the lateral and longitudinal components. The magnitude is:

$$a = (a_x{}^2 + a_y{}^2)^{0.5} \tag{1}$$

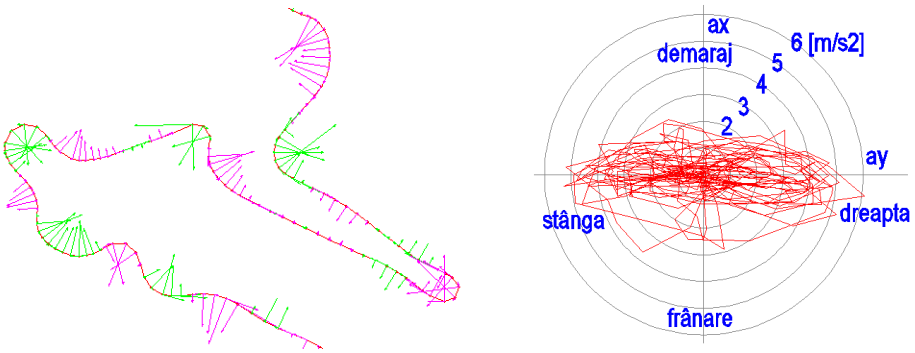


*Figure 6. Graphical presentation of the acceleration's lateral and longitudinal components: as vectors on the track (left-side); as radar plot or g-g plot, showing the handling ability of the driver-car pair (right-side)*

The magnitude and the orientation of the total acceleration with respect to the vehicle coordinate system can be presented as polar plot in a so called g-g plot (radar plot), figure 6, right. Such a polar representation gives us an idea about the vehicle-driver system's performances or about the mean stress and grip of the vehicle tyres.

One major advantage of the program is represented by the possibility to maintain a biunique link (one-to-one correspondence) between the global positioning data and the calculus results. So, a certain point of a results plot (for example a pick of the speed or acceleration) can be identified on the map, or vice-versa, it can be found on the map a certain position where the vehicle behaves with specific kinematic or dynamic parameters. If necessary, the time information can be maintained also for any analyse.

The open data-structure and the experience obtained by the authors facilitate the program improvement by the development of new procedures allowing managing large amounts of GPS or other-source data. Some of these are:

- a graphical user interface (GUI);
- different possibilities to filter the numerical data;
- two-dimensional graphical representations having as abscissa any primary data or processed result;
- tree-dimensional graphical representations, with changing height or colour;
- new software procedures, which permit to select only part of data or to retrieve and further process geometric and kinematic information directly accessing already-existent graphical-objects, as plots, lines or points; for example, starting from an existent speed plot it is possibly to directly obtain histograms or new curves with filtered values, mathematical derivative (acceleration) and integral (distance).

Also, some data-import and -export types are already implemented (TXT, XLS).

## 4. Aspects regarding the measuring precision of GPS devices

Since the functioning of the GPS relies on receiving high-frequency radio signals, the data precision or even the usability can be affected by obstacles interposing between the satellites and GPS receivers [6], [2]. That means the GPS-based measuring techniques are not suitable in lab research or on routes passing tunnels, canyons or forests.

The main causes of GPS-receiver *errors* are: receiver imprecision (clock, gain); multipath and reflection (up to 0.5 m); atmospheric effects (up to 10 m); reduced visibility (at least four visible satellites needed); selective availability (intentionally induced); human's wrong device-operation or data-interpretation. Also, the measuring error for the altitude is bigger than the latitude- or longitude-error. Fortunately, for small distances (metres) and short time intervals (seconds), the position will be not affected too much, which means the relative position error between neighbouring points will normally be in acceptable limits.

The errors introduced by the derivative functions, needed to obtain speed and acceleration from position information, are relatively easy to control by numerical filtering procedures.

In time, the authors made numerous and systematic tests [1], [2] to verify if sensitivity, position accuracy and position repeatability of the available GPS devices are good enough to be used in researches [8], [9], [2], [10], [3]. To put in evidence different kind of errors, different test types were performed:

- measurements kipping immobile the GPS receiver for a longer period of time;
- recording simultaneously the same track with more GPS receivers of the same or different types;
- recording the same point or track with one receiver at different moments of time (in the same day or in different days);
- using GPS receiver and other measuring tools for simultaneously recording and comparing values of speed and acceleration (for example the speed supplied by a Garmin GPSmap system was compared with the same information computed by the ABS controller and obtained by logging on the vehicle CAN, via an OBD II software).

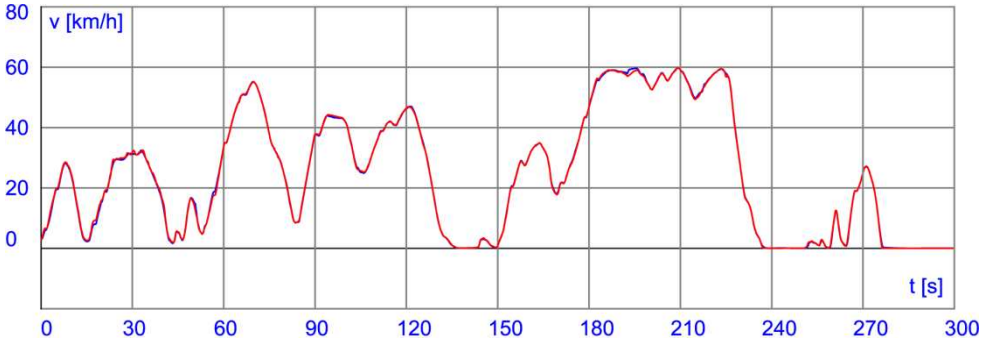


*Figure 7. Plots of simultaneous speed records obtained with two similar GPS devices (Garmin GPS 18x-5Hz) placed very close one to other*

An example of such comparative test can be seen in the figure 7: the unfiltered speed information, obtained with the presented algorithm from the primary global-position data, is almost identical for two similar GPS devices that were placed very close one to other.

The conclusion was: the modern global positioning systems offer good precision in the majority of studies and are suitable for researches implying vehicle kinematics and dynamics.

## 5. Vehicle dynamics results obtained by GPS data processing

The experimental data regarding the vehicle kinematics can be used as it is. Often simple representations versus time (figure 8 and figure 9, up-middle) or versus travelled distance (figure 9, down-middle) are sufficient. For example, figure 8 shows the maximal acceleration and braking performances recorded in straight-line motion. In the left side ones can see evolutions of speed and acceleration during a vehicle take-off, followed immediately by a hard braking. The data was recorded and plotted with the VBox system. Due to the logging rate of 20 samples per second, rapid phenomenon can be observed clearly, as gear changes, clutch engaging shocks or ABS cycles.

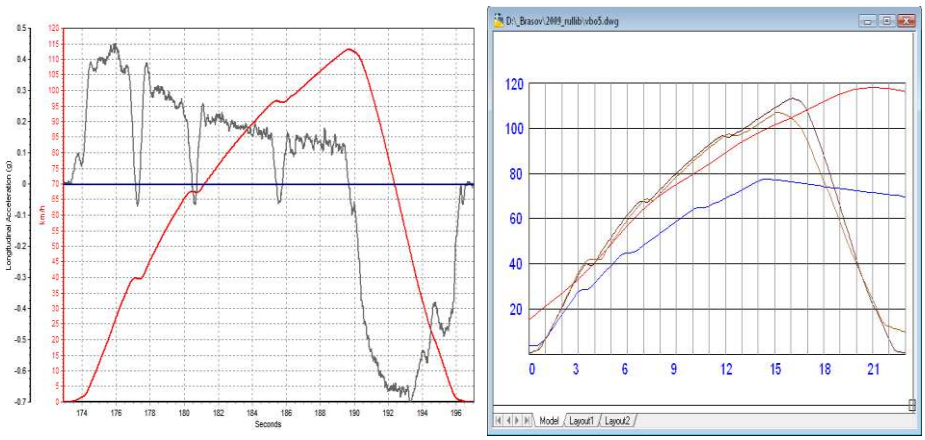

*Figure 8. Example records of starting – braking tests*

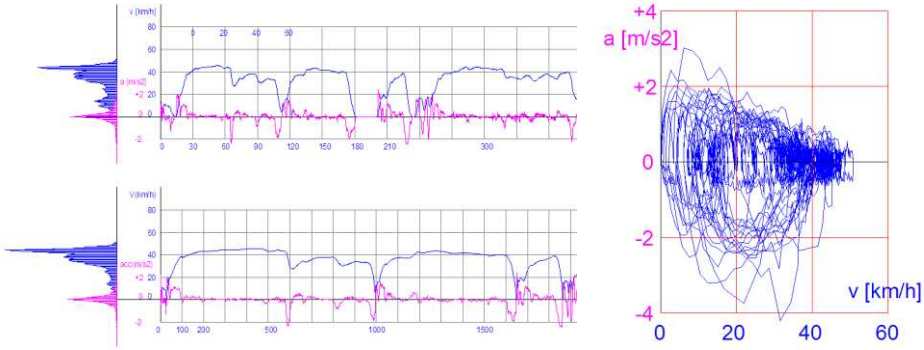


*Figure 9. Speed and acceleration representations (urban conditions): left – histograms; middle – fragments from plots vs. time (up) and vs. distance (down); right – city driving cycles*

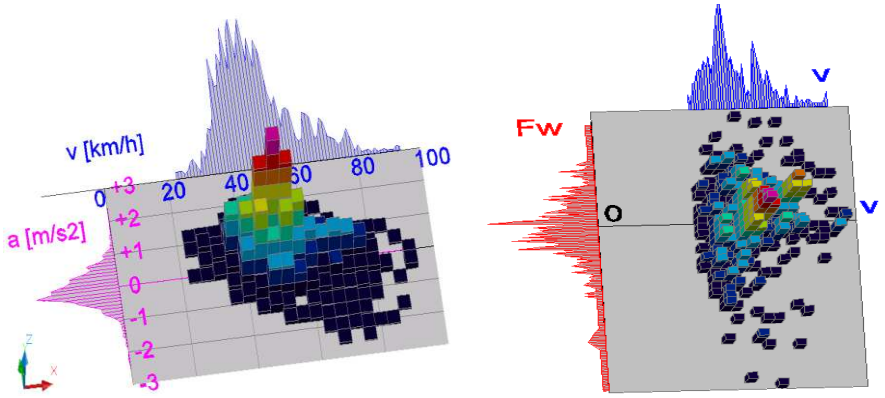


*Figure 10. Mono- and bi-parametric probability density functions for mountain route left – speed and acceleration vs. time; right – speed and traction/braking force vs. dist.*

In the right side of the figure 8, the VBox data of the left side was imported in Autocad and plotted with the described program in order to compare four records: two obtained with the same car in successive tests and the others obtained with other two cars. One can observe that the first vehicle starts from rest almost identically and its pulling performances are superior to the other cars (red and blue curves).

Figure 9 shows a way to take the time- or distance-related information of vehicle speed and acceleration (presented as a fragment in the middle area of the figure) and to represent it (the right side) or statistically process (the left side) so that to obtain a good perception of the vehicle dynamic behaviour in given conditions. Such graphical representations, as presented in figures 9 and 10, give the possibility to know what speed or acceleration regimes are more probable (are found more often) during driving.

First dynamic evolutions that may interest are the vehicle's *total resistance force* and his components: the rolling resistance, the grade (slope) resistance and the aerodynamic drag. In this case, the measurements will include the determination of the vehicle total mass and its repartition on each wheel, the vehicle frontal area (for example, using a scaled vehicle picture) and an estimation of the rolling drag coefficient measured on a roller dynamometer or obtained by coast-down (free-rolling) tests [7], [10]. Other operations, as the measurement and regulation of the tyre inflation pressures or the readings of atmospheric temperature and pressure, may be very useful for results comparisons or interpretations.

Starting from experimental kinematics and using such supplementary measurements or even assuming some vehicle parameters, it is possible to estimate very important dynamic values as motion resistance forces, traction/braking-force or -power [8]. The right-side of the figure 10 presents statistical information regarding the uni- and bi-parametric probability to drive a car on an un-congested mountain road with certain speed and force applied to the wheel (traction or braking force). This histogram is related to the travelled distance, while the histogram from the left side is related to the travelling time.

The experiments' importance can be further increased if one can pass from the vehicle kinematics (distance, speed, acceleration) to the dynamics (forces, torques). Thereby, to obtain valuable results about vehicle dynamics, supplementary experimental determinations must be performed immediately before or after the GPS-data recording. The number of these laboratory measurements depends of study's aim and complexity.

The combination of the acquired kinematic data with other information types can be realised easily with the presented computer program due to the open structure of data, to the possibility to extract sub-sets of data and to the graphic capabilities. Figures 11 and 12 are examples of how the data obtained by GPS and by other sources (marks manually introduced, on-board computer or instrumented sensors) can be mixed to obtain extremely helpful results.

Figure 11 shows a processed plot of the vehicle speed in urban driving. Manual marks (permitted by the receiver Garmin GPSMap 60CSx, memorising the time and the coordinates) were added to indicate the gear changes. These permitted to obtain the statistics of the gear use, as is presented in the right-side of the figure. Assuming zero wheel slip and knowing the transmission ratios and the tyres' dimensions, the engine

speed can be computed in any moment. Also, if the driving force and the efficiency of the drivetrain are estimated, the approximation of the engine torque is also possible.

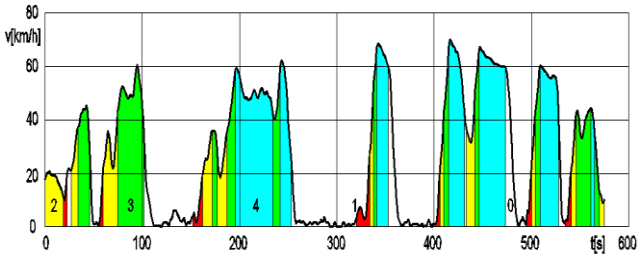


| Gear | Time [%] | Dist [%] | Vm [km/h] |
|---|---|---|---|
| 0 | 36.3 | 8.7 | 6.6 |
| 1 | 8.5 | 2.7 | 8.9 |
| 2 | 15.8 | 15.1 | 26.4 |
| 3 | 17.4 | 28.4 | 45.3 |
| 4 | 22.0 | 45.1 | 56.6 |
| | | | |
| Total | 100 | 100 | 27.7 |

*Figure 11. Car-speed evolution with gear indication in city route (speed vs. time plot and statistics)*

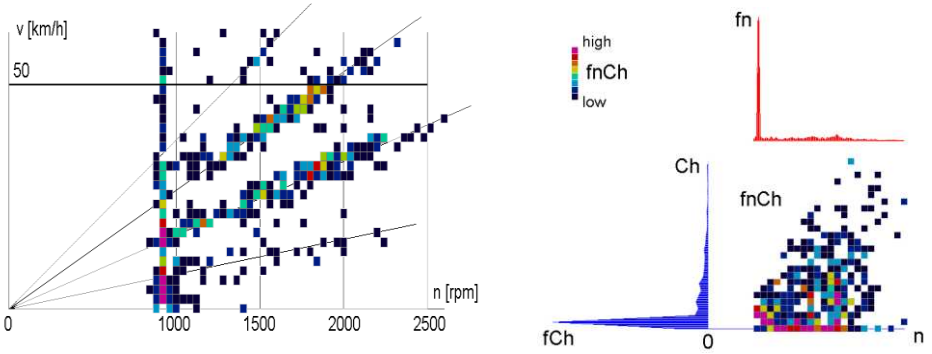


*Figure 12. Experimental mono- and bi-parametric probability density functions for city route: left – engine speed and road speed; right – engine speed and hourly fuel consumption*

OBD software permits today to access the vehicle communication network. The data furnished by the on-board sensors, through the vehicle computer and CAN interface, can be easily synchronised with the GPS data.

Figure 12, left, presents a histogram obtained by the combination of the engine speed read from CAN and the vehicle speed provided by GPS on city traffic. The engine idling and the engaged gear can be recognised, even the powertrain's vibrations or the clutch-slippage or -disengagement alter the measuring points alignment in straight-line. In the same manner, the right side of the figure presents the graphics of mono- and bi-parametric probability density functions for the engine's speed and hourly fuel consumption, obtained from the on-board computer data.

The methods for GPS-data processing imagined and implemented by the authors were also used to estimate the rolling resistance, the grade resistance and the aerodynamic drag of road vehicles [10] and also, in combination with supplementary data, to approximate the working regime of the engine and driving wheels [8].

The same GPS-based acquisition systems were used to statistically estimate the traffic intensity, the fuel consumption or the chemical and noise intensity in congested areas

[2], [9]. Based on an enormous amount of traffic data, a particular urban driving cycle was proposed for Brasov city [2], [3].

## 6. Conclusions

Professional GPS systems ensure global positioning records of high accuracy, allowing using them in precise studies aiming the vehicle behaviour on the path. The short time needed for instrumentation, the ease of use, the simplicity of connection to portable computers and the universal time information are key qualities that make them preferable in vehicle dynamics studies. To these elements one can add the rapid improvement of performance-price ratio, which currently allows utilising common-use commercial-receivers to carry out extensive and accurate researches.

Although the positioning accuracy is increasing continuously, the errors remain an important problem, quite difficult to control, especially in environments that detract or partly diminish the satellites visibility.

However, a proper use in correlation with quality processing-algorithms permit to the GPS systems to provide a precision of speed and acceleration measurements at least as good as other measuring systems used in experimental research. But comparing with other systems, the GPS devices have the advantage of very precise time measurement, perfect synchronization with other devices and recording of the 3-D motion trajectory.

The GPS-based method presented here proves to be accurate enough for vehicle kinematics measurements, in different on-road and off-road condition, including urban environment. With some precautions and less accuracy, it is also applicable to determine the road profile (altitude and slope).

Performing supplementary laboratory-measurements or adopting approximate values for different vehicle parameters, the method can be extended to assess the vehicle's resistances and dynamic behaviour, or more, to calculate in-traffic fuel consumption, to estimate the level of chemical and noise pollution, or even to conduct fatigue calculations (variable stresses) for different vehicle parts.

Biunique connections between the points on the diagrams and the geographical data permit the complete identification of each GPS-point and, as consequence, a better interpretation.

The method can be easily adapted to measure the kinematics and to estimate the dynamics of other vehicle types, as boats, ships, aircrafts or trains, as the better satellite-visibility is a premise for an even better measurement precision. As the authors intend to experiment further, combining the data of two or more GPS devices, used simultaneously, it is also possible to derive the vehicle rotation movements: roll, pitch and yaw. For large vessels, for example, this information may be used to estimate the dynamical stresses applied to the vessel hull or propulsion and steering systems.

Obtained by the processing of large amounts of data, such event- or statistical-information can be extremely useful for different types of studies.

As this work tried to prove, it is expected that the number of future uses of GPS systems to grow in the near future in a very large extent.

## References

[1] Covaciu, D., Florea, D., Preda, I., Timar, J.: *Using GPS Devices for Collecting Traffic Data,* SMAT 2008 International Conference, Craiova, 2008.
[2] Covaciu, D. *Study of the dynamic and in-traffic vehicle behaviour using GPS and CAD applications*, Ph.D. Thesis, Transilvania University of Brasov, 2010.
[3] Covaciu, D., Preda, I., Florea, D., Timar, J., Câmipan, O.V., Gomes, L.: *Development of a Particular Urban Driving Cycle,* Revista Inginerilor de Autovehicule – RIA (Magazine of the Romanian Automotive Engineers), No. 17, 2010, pp. 6–9.
[4] Garmin Intl.: *GPSMap 60cx Technical Specifications,* http://www.garmin.com.
[5] Garmin Intl.: *GPS 18x Technical Specifications. Revision B,* 2008. http://www.garmin.com.
[6] National Instruments Corp.: *Tutorial on GPS Receiver Testing,* http://www.ni.com/automatedtest/gps.htm.
[7] Preda, I., Untaru. M., Peres, Gh., Ciolan, Gh.: *Algorithm for computing space in free running,* Revista Inginerilor de Autovehicule – RIA (Magazine of the Romanian Automotive Engineers), No. 2, 1990, pp. 11–13.
[8] Preda, I., Covaciu, D., Ciolan, Gh., Dima, D.S.: *Vehicle Dynamic Behaviour Analysis Based on GPS Data,* SMAT 2008 International Conference, Craiova, 2008.
[9] Preda, I., Covaciu, D., Florea, D., Ciolan, Gh.: *Study of in-traffic vehicle behaviour, based on GPS and radar devices,* The 8th International Automotive Congress, ESFA 2009, Bucharest, 2009.
[10] Preda, I., Covaciu, D., Ciolan, Gh. *Coast-down test – theoretical and experimental approach,* The XI-th International Congress on Automotive and Transport Engineering CONAT 2010, Volume 5, paper 4030, Braşov, Transilvania University Press, 2010, pp.155–162.
[11] Racelogic: *VBOXTools Software Manual,* Ver. 1.4.

# Influence of the Office Electrical Equipment to the Indoor Environment and Comfort of the Occupants

**C. Bujdei, S. A. Moraru**

**Transilvania University of Brasov, Romania**
**Phone: +40 268 418836**
**e-mail: catalin.bujdei@unitbv.ro, smoraru@unitbv.ro**

Abstract: In the last period of time our work was based on monitoring and controlling the indoor environment conditions in office buildings. To ensure the comfort of the occupants is one of the main tasks to be accomplished. Their productivity depends directly on their comfort. The environment could be influenced by many internal and external factors, and the office electrical equipment (devices) could be one of them. This article presents the description of our work and the success of our results. At the beginning it is described the testing stand developed, and after a deep analyze, the selected sensors, which will be used for the monitoring process. Different types of electrical equipment have been tested and the information obtained has been graphically represented and processed.

*Keywords: office building, thermal comfort, equipment influence, work productivity, waste energy, sensors comparison*

## 1. Introduction

Nowadays there is not well known which is the real influence of the electrical equipment (devices) to the environment. It is known that all of them produce heat and the quantity of heat production depends on equipment efficaciousness. For heat production estimation have been proposed some equations [3], which are difficult to be resolved since not all the parameters values are always known. For some equipment there have been defined some standard values to be used as default, when calculating the total heat production for a space area, but all of them could be just estimated and more complicated to measure exactly [11, 12]. The heat is related on temperature and temperature is just one parameter which could be influenced by the electrical equipment. Other parameters describing the environment are humidity, noise, carbon monoxide, carbon dioxide, etc. Our research work presented in this paper proposes to determine approximately the influence of the office electrical equipment on the indoor environment and indirectly on the comfort of the occupants of an office space.

Some past experiments have been done, the most important of them supervised by Hosni and Wilkins, where they try to determine approximately the amount of heat loss of the electrical equipment [5, 6, 7, 14]. A correlation between the total power consumption presented on the nameplate of each electrical equipment and its heat loss

has been determined, but it is not valid in all cases. We try to do some similar experiments, by monitoring the temperature variation inside a closed space where the electrical equipment has been placed and turned on. According to the temperature variation, the head production could be estimated, and also the level of influence of the tested equipment. Together with the temperature, the relative humidity and noise level have been also monitored.

## 2. People's comfort in office buildings

In generally, the comfort of the occupants from office spaces could be described in the same way as the comfort from any type of buildings, but there are some differences which could influence the indoor environment and their comfort. These differences are determined by the functional systems from the building (e.g. heating, ventilation, air-conditioning), the existing furniture, the building materials, electrical equipment, etc.

People's comfort is directly related to the environment conditions. The comfort has been defined, by different researchers, like all existent conditions of a space for which a person will not prefer one with other conditions. It is a very complex concept that depends on setting of external and internal factors. Even if it could be literally described what the comfort represents, it is more complicated to define it into a mathematical format, which will be implemented into a software application for computing and analyze. Even so, many researchers have studied it and have provided solutions for making possible the estimation of the comfort conditions, but it does not include all existent possibilities [9, 10].

Taking into account that a person could feel comfortable from a point of view but uncomfortable from another point of view, the comfort has been divided in different areas, and the most important are:

1) *thermal*: described by temperature, humidity and air velocity parameters. It's one of the most important types of comfort with high impact to the human capacity to accomplish his activities.
2) *visual*: characterized by light intensity and other factors able to influence a person sight of view.
3) *acoustic*: described by the maximum level of noise or repeatable sounds which could start to disturb a person's activities.
4) *air quality*: described by the parameters which define the air conditions suitable for respiration and human health (e.g. oxygen level, pollution level).
5) *stability*: uncomfortable movements, vibrations or shocks should not be presented.
6) *security comfort*: each person should feel safe in the space where he accomplishes his activities.

It is not possible to ensure comfort for all people from a space (they could have different activities, metabolism, etc.), but it is important to ensure it for the most part of them and from as many points of view as possible. Not to forget that the productivity of people is dependent on their working conditions [2].

In what office spaces are concerned, one of the external factors which has influence to inside environment conditions is represented by the installed electrical equipment. The

electrical equipment could not transform electrical energy completely into their own specific functionalities without losing heat (waste energy). The produced heat could be easily felt by a person (as temperature difference) but we are interested to know which is the quantity of the produced heat and if there is other kind of influences to the environment.

## 3. Preparing for testing

For a more precise measurement of the influence it was necessary to make an isolation of the tested equipment from the external conditions. A closed box has been built as platform for testing. It has a wood frame and the walls have been made using specific isolation material. At a dimension of 71.5 cm × 71.5 cm × 71.5 cm (a total volume of 0.3655 $m^3$) it is enough space inside to put any of the most common office equipment. The box does not isolate completely but it is able to reduce a lot of the influence from the outside environment.

Inside the box, for each equipment, we were interested to verify which is the variation of the parameters temperature, humidity and noise level during its operating. From all these 3 parameters the temperature could be influenced more by the external temperature (the isolation layer is thin and with low thermal resistance). For this reason we have decided also to monitor the temperature variation outside the box and make a correlation with the variation from the inside. For the humidity and noise it was considered that the external influence will be minimum.

All the sensors used for monitoring are connected to an acquisition board (Arduino Duemilanove) and from there the information is sent to a computer. The computer stores the information into a database and from the database the information could be exported and processed when needed it. Figure 1 presents the architecture of the testing stand.

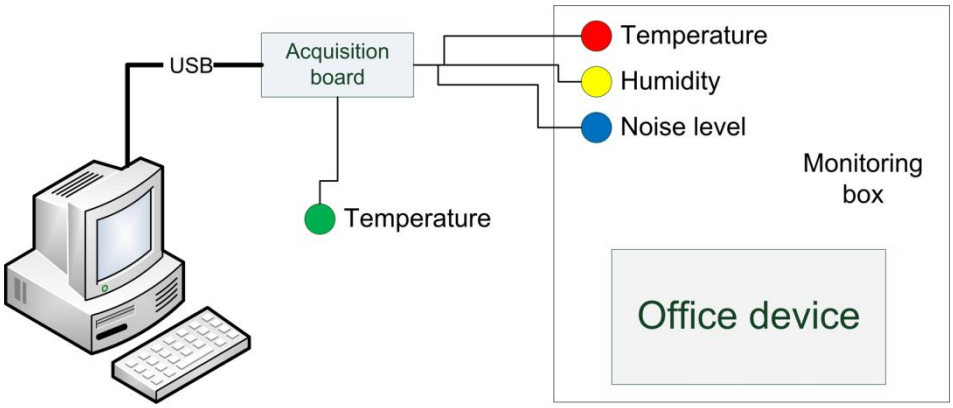


*Figure 1. Architecture of the testing stand*

## 4. Sensors to be used for monitoring

To measure the conditions inside the monitoring box we decided to use a Sensirion SHT11 sensor and an electret microphone sensor. The SHT11 is factory fully calibrated

and permits recording information about temperature and relative humidity. The typical accuracy for temperature is ±0.4 °C and for relative humidity is about ±3.0 %. It is a high precision sensor but quite expensive, which makes it not suitable for daily residential applications but for the applications where the correctness of the measurements is very important.

The electret microphone sensor is connected to an amplifier for obtaining a better signal gain and from there the measured parameter value is transformed into a digital format. This type of microphone sensor has a low quality and some tests have been necessary to be made before using it. The tests proved that it is difficult to measure the noise level with this sensor and the output could be just a digital value between 0 and 1023 (the analog-to-digital converter range). It was also established that for a very low noise space the digital value resulted is around 700. Since this was considered to be the minimum noise level, we decided to split the range (675 ... 1023) in 14 equal intervals, each interval identified with a number from 1 to 14. The highest the digital value is the highest the noise level.

For outside environment temperature monitoring another sensor was necessary. Since we did not have another Sensirion SHT11 sensor we decided to try other types of temperature sensors which we have, each one having other characteristics. The goal was to determine which has the best accuracy, even if the typical values are specified into their data sheets, and more appropriate to the SHT11 measurements. For this task an experimental test has been proposed and realized. Since the SHT11 sensor was considered to be the most precise calibrated, it was used as a reference sensor.

## 5. Performance comparison of temperature sensors

Our purpose was to connect 4 types of temperature sensors together (Sensirion SHT11 – digital, Twig – analog, LM35 – analog and LM75 – digital), on the same main board, and to record the registered temperature of each of them at the same time. Since they are placed in a small area with uniform environment conditions the registered temperature values should be the same. Normally the comparison should be made for the entire measurement range of the sensors but since we will use them to monitor values somewhere between 20 °C and 30 °C, a smaller range of values will have been used [8].

While the temperature value from the SHT11 could be provided in digital format on 14 bits, the resolution for LM75 sensor digital conversion is only 9 bits, much lower than in the first case. The value of temperature provided by the LM35 and Twig sensors, which have analog output signal, is converted into digital using the 10-bit ADC integrated into the main board. A better precision could be obtained if we had had the possibility to use a higher resolution digital converter. For our tests we are interested in having at least a precision for the first decimal of a degree C (0.1 °C); more precision is even better considering that we want to use these types of sensors also for monitoring the indoor environment conditions. In Table 1 there are presented the most important specifications for these sensors.

*Table 1. Temperature sensors specifications*

| *Sensor* | *Range* | *Accuracy (at 25 °C)* | *Resolution* | *Least Significant Bit* |
|---|---|---|---|---|
| SHT11 | – 40 ... 123.8 °C | ±0.4 °C | 14 bits (1 sign bit) | 0.01511 °C |
| LM75 | – 55 ... 125 °C | ±2.0 °C | 9 bits (1 sign bit) | 0.5 °C |
| Twig | – 40 ... 125 °C | ±1.5 °C | 10 bits | 0.16113 °C |
| LM35 | – 55 ... 150 °C | ±0.5 °C | 10 bits | 0.10742 °C |

For obtaining better results at the temperature sensors comparison we decided to record the information for a period of time of 16 hours. When we had all the information stored into the database we exported them into a CSV (Comma-separated values) text file. The text file was used as an input source for a Matlab application, developed for displaying the information into a single chart and making different analyses.

An initial performance comparison has been made taking into consideration the chart representation and then more mathematical computation have been done for obtaining better and more accurate results. Observations have been noted as well as during the monitoring process, visual following the variation of the information displayed on the computer application interface. Figure 2 contains the chart with graphical representation of the values evolution for all tested sensors. Having all the variations represented on the same chart makes it much easier to observe the differences between them.

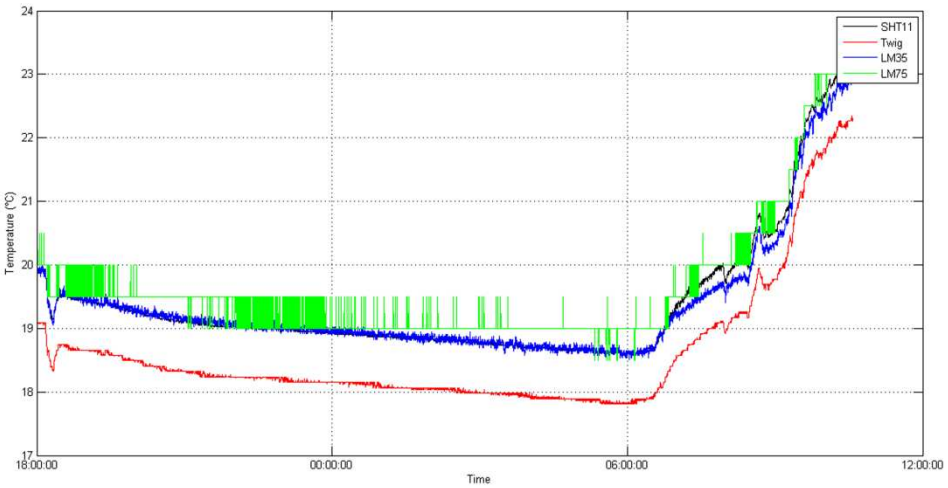


*Figure 2. Temperature value variation - recorded for 4 distinct sensors*

At the LM75 sensor, due to the low resolution at the digital conversion, it was observed a high and continuous variation of precision in a very short period of time (few seconds). In a second the precision could suffer a modification of about 0.5 °C (the LSB – Least Significant Bit – value is high and makes the evolution very instable). This kind of variation is not recommended when there are systems to be controlled at a better precision (decimal of degree Celsius). From the chart it could also be observed easily

this kind of variation, and even the measurements are appropriate enough to the measurements of the SHT11 sensor, the LM75 is considered not to be adequate for our purpose. It is the first one which is eliminated from the comparison competition.

From the chart it could be easily observed that the Twig sensor provides a variation of the measurements similar to the SHT11 sensor but there is a difference of about 1 °C between them. A more exact calculation proves having following differences: minimum = 0.65 °C, maximum = 0.98 °C and average = 0.7939 °C (which is quite higher for our purpose). The problem with this sensor seems to be an imprecise calibration. A solution is to make ourselves the calibration of the sensor by adding the average difference value obtained to all measured values. In this way we would obtain a maximum difference of about 0.2 °C. The solution is not optimum since other variation measurements could exist at other temperature ranges but should be taken into consideration.

The last sensor to be compared with SHT11 measurements was LM35. From the chart the measurements obtained with LM35 look very close to the measurements of the reference sensor. The minimum difference is 0 °C, the maximum is 0.44 °C and the average difference is 0.0313 °C. These are the best performances analyzed until now. A smooth variation of the recorded information was obtained from the LM35 sensor, which makes us consider it the best candidate for our further experiments and a veritable replacement of the SHT11 sensor, more expensive than LM35 sensor. With a bigger resolution ADC we would be able to obtain even a better precision from this sensor. Since LM35 sensor has an analog output it is very important to ensure that the external interferences are minimal. Our future work will propose to develop a small circuit board where the LM35 sensor will be attached and the conversion of the analog signal will be made in digital format at a higher resolution. In this way any possible external interference will be diminished.

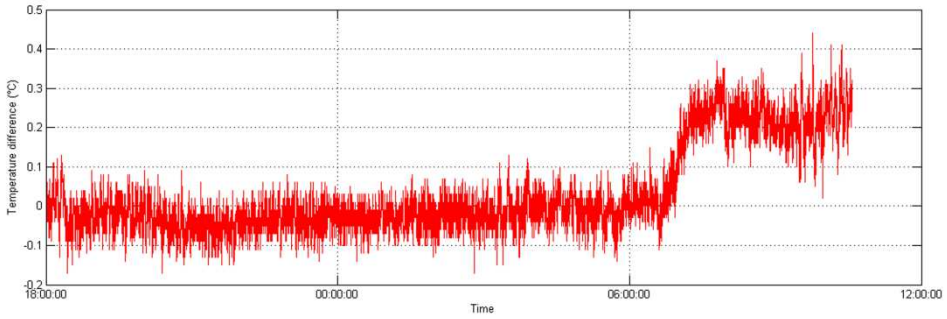


*Figure 3. Measured temperature difference variation - between SHT11 and LM35*

A decrease of the LM35 measurement precision was observed during the period of time when people occupied the nearby space where the test took place (somewhere after 7:00 AM, Figure 3). The phenomenon could be explained by the appearance of higher interferences in the wires which connect the sensor to the acquisition board. For this reason a second test was realized to be sure that the registered information is correct, and this time only with the sensors SHT11 and LM35, separately from any possible higher interference (the length of the connection wires has been also shorten). The

results obtained proved that it is possible to have an accuracy of about 0.1 °C between the measured values of the 2 types of sensors.

The final decision was to use the LM35 sensor together with the SHT11 sensor for our next tests, where we monitor the influence of the office equipment on the indoor environment (and indirectly to the comfort of the occupants).

## 6. Equipment to be monitored

Since there is a large variety of office equipment (device) type it is impossible to test all of them. We have decided firstly to select some main categories of equipment mostly used in office spaces. After that, we selected, from whose we had available, one or more types of devices, preferably with different characteristics and different influence type possibilities. In this way it is also possible to compare similar functionalities influences, accomplished by devices with different characteristics. Our main goal is to prove that there are cases when different equipment types could have enough influence to the environment to modify the existing conditions and that there are possibilities to reduce this influence, even reuse the influence for other useful purposes. It is known that each type of electrical equipment produces some heat, but it is also important to know approximately how much it is produced. This produced heat which is not useful is also called waste heat, secondary heat or low-grade heat.

The categories and the selected equipment for this research work are presented below, as:

1) *desk lamp*: 230 V, a single incandescent light bulb at 40 W;
2) *ceiling lamp*:
    a) one incandescent light bulb, 230 V, 100 W, ~1700 lm (luminous flux);
    b) one energy saving bulb (CFL - Compact Fluorescent Lamp), 230 V, 18 W (equivalent to 100 W incandescent light bulb, as the manufacturer specifies), ~1200 lm (luminous flux);
3) *display*:
    a) CRT (Cathode Ray Tube) display: AOC 7 klr, max. 600 W power consumption. Even if it is an old type of display it is still used for image/video processing, where the quality of image is very important. From the specifications it is observable that the power consumption is very high.
    b) LCD (Liquid Crystal Display) display: Samsung SyncMaster 740 N, max. 34 W power consumption. It is the most used type of display nowadays and the power consumption is very low comparing with the CRT display.
4) *computer processing unit*: Fujitsu Siemens (max. 660 W power consumption). The maximum power consumption is very high but the consumption depends on how much the functionalities of the computer are used (which software applications are executed and how much they use the existing hardware resources).

5) *laptop*: Sony Vaio VGN-NR21S (max. 90 W power consumption). Has a lower power consumption comparing with a personal desktop computer but the performances are also lower.
6) *multifunction printer*: Canon MP250 (max. 11 W power consumption). Usually the printers and scanners produce enough noise to disturb the persons which develop activities nearby. The level of noise depends on the printer type and the operation mode.

The list could be completed with even more types of devices to be tested, but for our research project we considered it to be sufficient. There is impossible for each device to detect the exact influence value to the environment but just an approximation of it. Any of them could be operated differently for distinct periods of time, so there will be variable influence to the environment. For our research work the influence will be described by the parameters which we proposed for monitoring: temperature, humidity and noise level. When we speak about the influence we are thinking of a negative influence, since there it could not be a positive influence to the environment from such kind of equipment (except from the equipment dedicated to air quality control, humidity regulation, etc.).

## 7. Equipment influence monitoring

After we decided which sensors to use for the monitoring tests, we assembled them on a main hardware platform for creating the necessary monitoring system, together with the dedicated software applications (for data gathering, processing and storage). Using the developed monitoring system each electrical equipment has been tested one by one.

It is well known that the electrical devices are not able to completely transform the electrical energy for executing their own tasks/functionalities (e.g. mechanical tasks), without losing a part of energy as heat. How much energy is lost as heat depends on the equipment type and characteristics and it is defined as equipment efficiency (lower the energy lost as heat is, higher the efficiency). The heat is the main factor which could influence the indoor environment in case of electrical equipment which don't work with chemical substances (pollution materials) - in special cases when other types of negative influences could appear and have a higher impact on the environment. During the winter days the produced heat may not be a big problem since the indoor building environment should be warmed at a proper temperature value, but in the summer days it should be eliminated, since usually, the temperature inside a building without air-conditioning system is higher than the accepted comfort value. Since it is not produced a constant amount of heat for a period of time, it is impossible to determine the exact value, but estimations could be made. The air-conditioning systems don't have a proper adjustment algorithm based on external factors influences but just to follow the variation of the temperature measured from some sensors. Knowing the approximate value of heat produced could allow deciding which the characteristics of necessary air-conditioning systems are. Another disadvantage of the produced heat by the electrical equipment is that it could be transmitted rapidly by radiation to the persons nearby and more slowly to the entire air from the indoor space, making more complicated to control the entire environment conditions. So, even the ambient air has a lower temperature, measured by the sensors, the persons nearby the electrical equipment could feel a higher temperature and be in thermal discomfort. Similar discomfort conditions could occur if there are

local space variations of the humidity and noise level. If it is possible to have uniform ambient conditions into the entire environment it would be much easier to control them. As we already said before our research work is to determine better which kind of influences could exist, their impact levels, to present some solutions to diminish the influences or even to use them as other sources of energy. Until now some research works have been made only on the heat produced by the equipment (in the most cases reporting to the industrial equipment) but without making a link with the thermal comfort or other types of comfort.

After monitoring the behaviour of each equipment, proposed from the beginning, we processed and analyzed the results, using some developed applications into the Matlab working environment. The temperature, the humidity and noise level variation have been analyzed and we tried to determine a correlation between each parameter variation and its influence to the ambient conditions. For a better representation of the results, suggestive charts have been generated.

The monitoring process was split in 3 different stages, each stage taking place in a variable period of time:

1) *the initial stage*: the parameters values are registered while the equipment is placed inside the monitoring box but not operating. These initial measured values would be used as references for comparing with the future values of the parameters. Even if the equipment is not operational it would be a temperature value difference between inside and outside of the monitoring box, since the external sensor could be influenced by some external parameters (e.g. the air movement), but limited external influences which don't disturb badly our testing results.
2) *the operating stage*: the time when the equipment is operating in different modes. This is the main stage when it could be observed the influence of the equipment on the environment conditions, but reported to the other stages.
3) *the final stage*: a period of time after the equipment is stopped from its operating mode, but the influence should be still present (it could not drop suddenly). The isolation material of the monitoring box will delay the moment of reaching the equilibrium between the internal and external conditions (energies equilibrium).

For each stage, the monitoring time, is not constant, but established during the monitoring process by analyzing directly the evolution of the monitored parameters.

### 7.1. Relationship between temperature and relative humidity

From the initial measurements we have noticed that there is a direct connection between the temperature and relative humidity: when the temperature increases the relative humidity value decreases. Since we did not know exactly which the connection between them was, we decided to start a short study about this phenomenon and find a proper explanation.

The humidity level from the air is an important factor for the human comfort and for the human body to function properly. In the summer days, when is very warm outside, the human body needs to cool down in order to keep a lower temperature. This is done

automatically by human body by producing perspiration. If the air is saturated with moisture it will be impossible for the perspiration to evaporate and it will be harder to keep the normal temperature of the human body.

But, the study shows us that we had a wrong concept about what relative humidity means. A better explanation for the relative humidity was found as its value is referring to the percent of the available energy, from a space area, which is necessary for the evaporation process to happen, for all moisture quantity. This explains why when the temperature increases, the available energy also increases and a lower percent from it is necessary to evaporation; considering that all the time the amount of water vapours from the air remains approximately the same. The concept of relative humidity still confuses many people and it is recommended to be used a better measuring parameter of the moisture: the dew point temperature. It represents the value of the temperature where the condensation process starts: the water molecules from the air cool, becoming slower in their movement and in this way they are able to stick to other water molecules. The dew point parameter is mostly used by meteorologists [4].

In Table 2 there are presented the levels of comfort percept by the human body according to the dew point and relative humidity, at an air temperature of 32 °C. The dew point is calculated based on the relative humidity and air temperature values.

*Table 2. Human body perception of air humidity*

| *Dew point* | *Relative humidity at 32 °C* | *Human perception* |
|---|---|---|
| > 26 °C | > 65% | severely high |
| 24 – 26 °C | 62 % | extremely uncomfortable |
| 21 – 24 °C | 52 – 60 % | very humid, quite uncomfortable |
| 18 – 21 °C | 44 – 52 % | somewhat uncomfortable |
| 16 – 18 °C | 37 – 46 % | a bit uncomfortable |
| 13 – 16 °C | 38 – 41 % | comfortable |
| 10 – 12 °C | 31 – 37 % | very comfortable |
| < 10 °C | 30 % | a bit dry for some people |

For calculating the dew point value it could be used a well-known approximation, Augut-Roche-Magnus, as presented in the Equations 1.

$$T_d = \frac{b \cdot \gamma\ T,RH}{a - \gamma\ T,RH}, \qquad \gamma\ T,RH\ = \frac{a \cdot T}{b + T} + \ln\ \frac{RH}{100} \tag{1}$$

where parameter $a$ = 17.271 and $b$ = 237.7 °C [13]. The approximation is valid when:

- 0 °C < $T$ < 60 °C (air temperature),
- 1 % < $RH$ < 100 % (relative humidity),
- and 0 °C < $T_d$ < 50 °C (dew point temperature).

Since the SHT11 sensor is able to measure both parameters, the temperature and relative humidity, it is easy to calculate the value of dew point using the Equations 1. Each time the temperature and relative humidity parameters are measured, the dew point is calculated by the software application and the resulted value is stored into the database. The relative humidity parameter could be used and compared with reference

values but the dew point parameter could be much easier understood. The conclusions obtained after this short research made us continue our main research study considering the temperature, dew point temperature and noise level as main parameters for analyzing the office equipment influence on the environment.

### 7.2. The heat produced by an electrical equipment

The temperature is one of the parameters related to the environment which could be easily detected by the human body (not its value, but an estimation correlated with the sensation felt by the human body). All electrical equipment produce an amount of heat during their operating. Since this waste energy remains unused, it is important to find applications for it, by converting it into other types of energy and in this way reducing the total amount of energy consumption (relating to an entire building or room space). Transforming it into other types of energy will also permit to control much easier the thermal comfort of the occupants.

For the electrical equipment there have been defined some mathematical equations to permit the heat production estimation, as in Equation 2, but there are not always known the parameters values necessary to resolve the equation.

$$H_{eq} = P_{eq} \cdot K_1 \cdot K_2 \tag{2}$$

where $H_{eq}$ is the heat transferred from electrical equipment (W), $P_{eq}$ is the electrical power consumption (W), $K_1$ is the load coefficient and $K_2$ is the running time coefficient.

The temperature and heat have correlated values. All molecules have kinetic energy (which is proportional with the speed of the molecules) and it is direct proportional with the temperature value. When the temperature increases the speed of the molecules also increases. For this reason the temperature is also defined also as a measure of the average kinetic energy of the molecules. If more heat is added to a substance the kinetic energy and temperature value will increase. To increase the temperature of a substance, more heat should be added, and to decrease the temperature, some heat should be removed. The heat also depends on the mass of the substance and the substance type. Each substance has a specific capacity of absorbing or releasing heat (specific heat). Specific heat represents the heat (calories) necessary to increase 1 gram of substance with 1 °C. Since the temperature could be measured using a thermometer, the heat could not be measured, but it could be calculated using temperature value. Heat as energy could be transmitted from one substance to another.

For calculating the heat gained or lost by a substance the Equation 3 could be used.

$$H_{gained\_lost} = M \cdot \Delta T \cdot S_h \tag{3}$$

where $H_{gained\_lost}$ is the heat gained or lost by the substance, $M$ is the mass of the substance, $\Delta T$ is the temperature difference which appears and $S_h$ is the specific heat. For air the specific heat is considered to be 0.25 cal/g · °C [1].

For our monitoring stage we consider that the monitoring box is filled only with air, at a density of 1.1839 kg/m$^3$ (corresponding to 25 °C temperature).

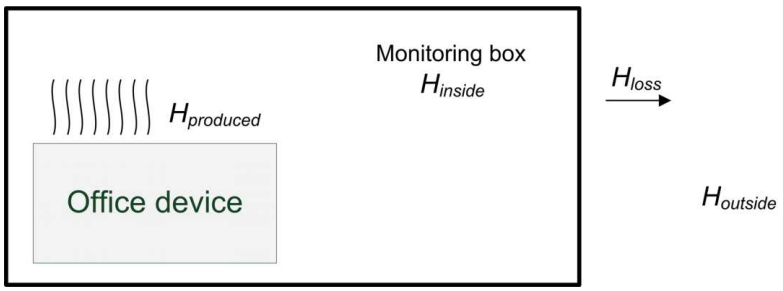


*Figure 4. Thermal energies in the testing conditions*

For the initial conditions (initial stage) of each monitoring test the Equation 4 should be accomplish. For simplifying the computing, $H_{outside\_original}$ in initial conditions has been considered to be 0 (in this case $H_{inside\_original}$ will represent the surplus of heat). And for the next 2 stages (operating and final) the Equation 5 has to be accomplished ($H_{outside}$ and $H_{inside}$ will represent the surplus of heat energy compared with the initial conditions). The equations have been established based on the energies (heats) equilibrium principle (Figure 4).

$$H_{inside\_original} = H_{outside\_original} + H_{aux} \tag{4}$$

$$H_{inside} = H_{outside} + H_{aux} + H_{produced} - H_{lost} \tag{5}$$

where:

- $H_{inside}$: the heat existent inside the monitoring box;
- $H_{outside}$: the heat *existent outside of the monitoring box (into a volume space equivalent with the box volume);*
- *Haux: the supplementary heat (energy), comparing with outside environment, which exists inside of the monitoring box, caused by the absence of some external conditions (e.g. air flow). Its value could be easily determined at the beginning of each test, when the equipment is not operational by measuring the difference of temperature between inside and outside. The value of Haux determined from Equation 4 will be used then in Equation 5.*
- *Hproduced: represents the heat produced by the equipment while it is functioning. Since the equipment does not have a uniform operating mode, the heat production will be also variable. The computing of the heat production will be made based on the measured* values of the parameters.
- $H_{lost}$: the heat lost from the inside environment to the outside environment. It is directly dependent on the thermal resistance of the insulation box walls.

The heat lost ($H_{lost}$) value could be calculated using the Equation 6.

$$H_{lost} = \frac{A \cdot \Delta T}{R_{insulator}} \tag{6}$$

where $A$ represents the surface area (the border between the inside and outside environments) equivalent with 0.715m x 0.715m x 6 = 3.067 $m^2$, $\Delta T$ is the difference of temperature between outside and inside environment and $R_{insulator}$ represents the thermal resistance of the insulator material. The value of the thermal resistance has been taken

from specification to be 0.07 $m^2 \cdot °C/(W \cdot cm)$. Knowing the volume of the monitoring box and the air density constant we determine the mass of the inside air to be 0.4327 kg.

An accurate estimation of the heat loss by electrical equipment would facilitate also the proper sizing of the cooling and ventilation systems required by buildings. The building systems will not be undersized with insufficient capacity or oversized with costly unused excess capability [3].

### 7.3. The tests performed

The first tested equipment was a desk lamp, with a single incandescent light bulb at 40 W power. The desk lamps are a very common device used in almost all office spaces where a separation of lighting from one office desk to another is necessary. The main role of them is to ensure the visual comfort in a small working place.

The results obtained are graphically presented in Figure 5. From the first chart it could be easily observed that the temperature inside the monitoring box started to increase when the lamp was turned on, until almost 4 °C higher than the temperature of the external environment. At the same time with the inside temperature increase the relative humidity level gets lower and increases back when the lamp was turned off. The dew point has an opposite variation comparing to the relative humidity, and increases while the temperature increases as well. The maximum dew point variation was 1.88 °C. After the lamp was turned off it took almost 1 hour for the monitoring environment to return to the approximately same initial conditions. The level of noise was minimal since the incandescent light bulb does not produce any external perceptible noise.

The second test was made on an incandescent light bulb, 220 V, at 100 W power. This type of devices is commonly used in any indoor building environment to ensure the lighting conditions. It is known that they produce a high amount of heat but it is important to know how much and if there is an influence also to the humidity variation. Figure 6 presents the variation of the parameters for the incandescent light bulb.

It could be easily observed that there is an increase of the temperature with almost 7 °C, which is quite high. Like in the previous case the relative humidity decreases, with more than 10%, while dew point increases with almost 3 °C.

During testing the incandescent light bulb we had the idea to test as well an energy saving bulb (economical bulb) and make a comparison between these 2 types of bulbs. It is known that the economical bulb will replace completely the old used incandescent light bulb. In some countries across Europe there are imposed regulations not to use anymore the old types of bulbs which are great consumers of energy with a low efficaciousness.

It is well known that the big advantage of the economical bulbs is the low power consumption for the same amount of lighting, comparing with the incandescent light bulbs. These types of bulbs are known also as CFL (Compact fluorescent lamp). They are in reality fluorescent tubes but at a lower scale and with different shapes. An energy saving bulb of 18 W, used for our tests, has a lighting power equivalent to 100 W incandescent light bulb, as it is written in its specifications, but normally the intensity light is lower than one from the incandescent light bulb (just 1200 lm).

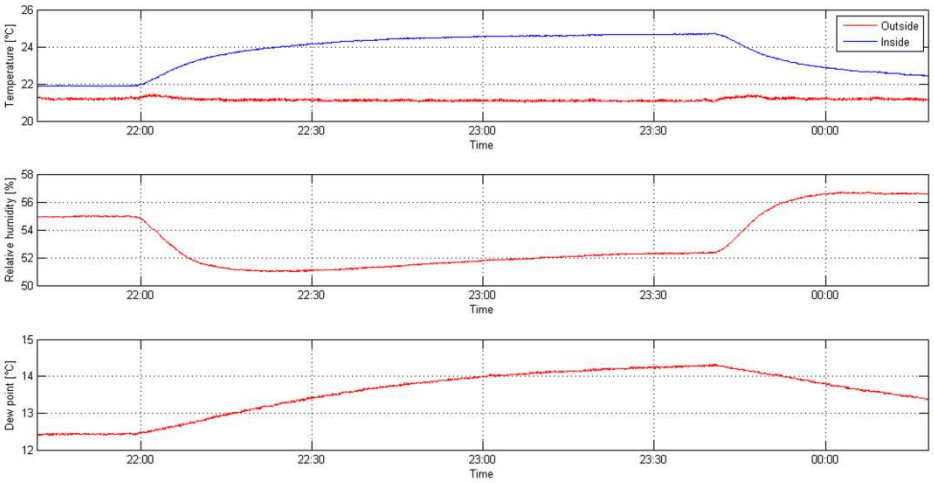


*Figure 5. Environment parameters variation - desk lamp, 220 V, 40 W*

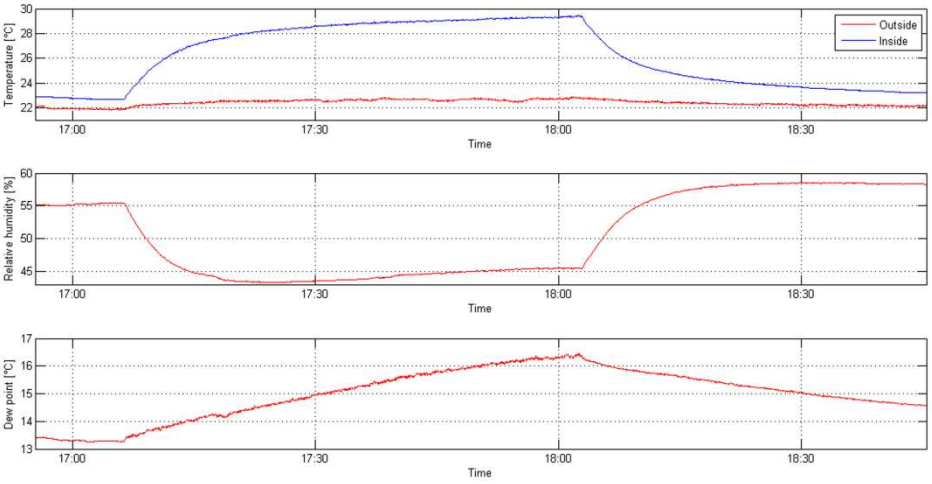


*Figure 6. Environment parameters variation - incandescent light bulb, 220 V, 100 W*

The results obtained, presented in Figure 7, are obvious. They are recommended to be used since they ensure low energy consumption and they produce minimum impact to the air quality (lowest heat transferred to the air). It produces an increase of the temperature with about 1 °C, a decrease of relative humidity of about 3% and a dew point variation of less than 1 °C.

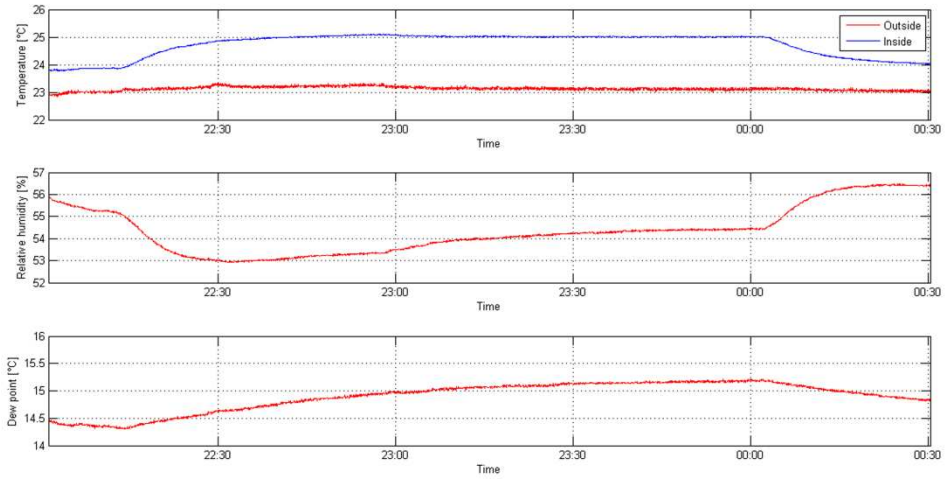


*Figure 7. Environment parameters variation - energy saving bulb, 220 V, 18 W*

Nowadays the CRT displays are seldom used, and especially in the activities where the image quality is very important (the main advantage of them). But the size and power consumption is too high for the today demands. Figure 8 shows a high increase of the temperature of the ambient air after the display has been turned on. There is a maximum increase of 6.8 °C comparing with to the initial value. The dew point temperature increases with 4.16 °C.

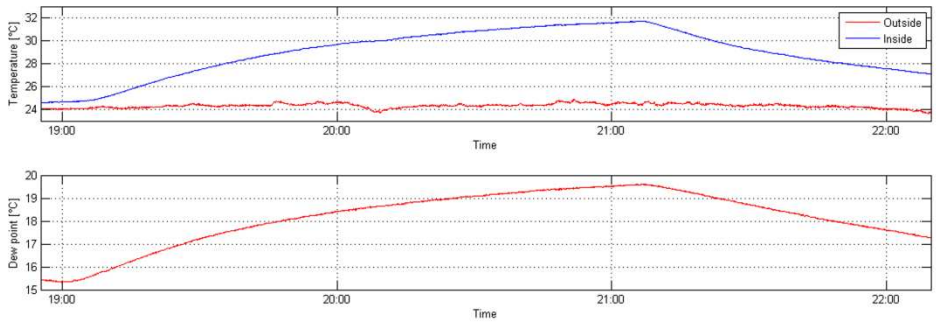


*Figure 8. Environment parameters variation - CRT display, AOC 7 klr*

The LCD display produces less influence to the environment, compared to the CRT display, and an increase of temperature of about 2 °C (Figure 9). It is recommended for its low power consumption and low heat production but the quality of the image could prove sometimes insufficient.

The computer processing unit has produced the biggest temperature increase (Figure 10) comparing to all other equipment tested until now, which could be directly related to the highest electrical energy consumption and a low efficiency. The dew point variation reaches easily 5 °C, comparable to the CRT display. Usually occupants are placed very close to their computer, which produces a transfer of the heat by radiation to

the human body. The environment is less influenced but the human body is much more exposed. This situation will cause an appreciable local discomfort.

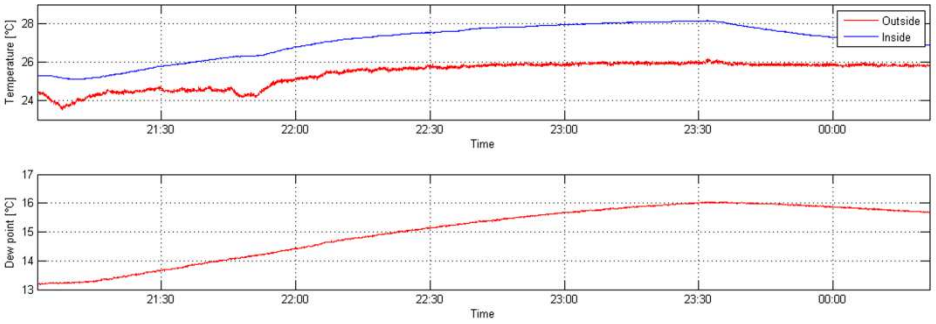


*Figure 9. Environment parameters variation – LCD display, Samsung SyncMaster 740 N*

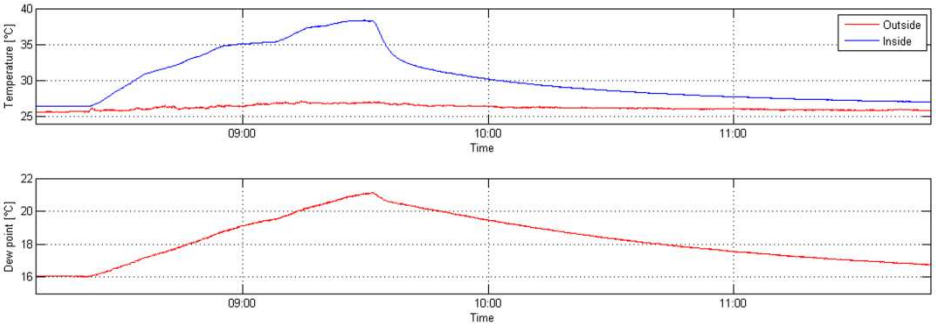


*Figure 10. Environment parameters variation – computer processing unit, Fujitsu Siemens*

As in case of the computer processing unit, the laptop could produce also a local discomfort, since the occupants are placed nearby. It could produce an increase of the air temperature with more than 5 °C (Figure 11).

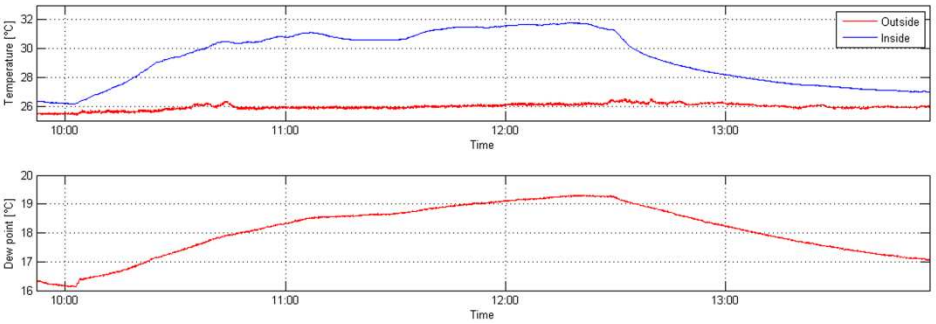


*Figure 11. Environment parameters variation – laptop, Sony Vaio VGN-NR21S*

The last tested equipment was the multifunctional printer. The temperature and relative humidity have been very low influenced during the printer operating but it was measured an increase of the noise level during printing pages or scanning documents. Figure 12 presents the noise level variation with a high increase of the level after the hour 8:35 (when the printing and scanning tasks are done).

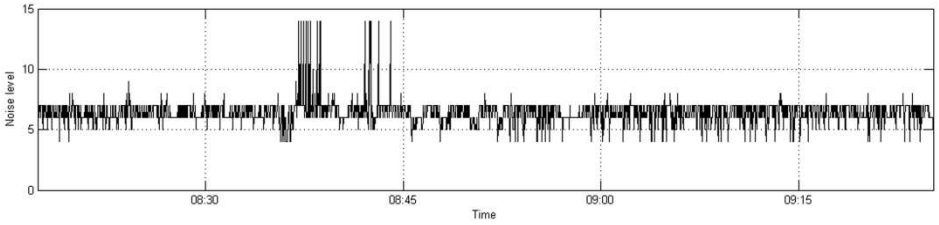


*Figure 12. Noise level variation – multifunction printer, Canon MP250*

### 7.4. The results of the tests

In Table 3 is presented the most important information of the results obtained after testing the office equipment. All maximum difference values have been calculated by comparing the parameter evolution with the value from the beginning of the test. A comparison could be easily done by following the values on each column. In this case it is evidently that the biggest influence, as heat production, is determined by the incandescent light bulbs, CRT displays and the computer processing units.

*Table 3. Results of the performed tests*

| *Equipment type* | *Initial temperature difference* | *Maximum temperature difference* | *Maximum relative humidity difference* | *Maximum dew point difference* | *Heat produced [W/hour (cal/hour)]* |
|---|---|---|---|---|---|
| Desk lamp, 40 W | 0.67 | 3.72 | 3.98 | 1.88 | 0.1433 (123.21) |
| Incandescent light bulb, 100 W | 0.73 | 6.82 | 11.86 | 3.09 | 0.2542 (218.56) |
| Energy saving bulb, 18 W | 0.88 | 1.98 | 2.94 | 0.76 | 0.082 (70.51) |
| CRT display, AOC 7 klr | 0.51 | 7.31 | 7.95 | 4.16 | 0.2645 (227.43) |
| LCD display, Samsung SyncMaster 740 N | 0.78 | 2.32 | 0.72 | 2.82 | 0.0922 (79.25) |
| Computer processing unit - Fujitsu Siemens, without display | 0.87 | 11.5 | 16.2 | 5.1 | 0.408 (350.86) |
| Laptop, Sony Vaio VGN-NR21S | 0.92 | 5.75 | 7.2 | 2.93 | 0.2172 (186.75) |
| Multifunction Printer, Canon MP250 | 0.64 | 0.82 | 0.96 | 0.52 | 0.0397 (34.14) |

Even if the dew point temperature value increases during the equipment functioning, its value tends to the initial value after the equipment was turned off. It is obvious that its variation was directly dependent on air temperature variation. The air temperature value is the main parameter which permits to a human body to distinguish between a more or a less humid air.

Analyzing the noise levels it was easy to determine that the printer is the single device, from all the equipment tested, which produces a very high level of noise during its functioning, being able to create acoustic discomfort to the occupants.

Knowing which types of equipment (devices) have the highest influence to the indoor environment makes it more easily to think at possible solutions for reducing their heat production or separate them from the occupants space. Do not forget that the heat is more easily transmitted to the human bodies placed close to the equipment.

### 7.5. Possible solution to reduce the influence to the environment

The highest influences generated by different types of equipment have been determined and solutions to reduce them must be found. The possibilities are many and are dependent on the working conditions and the necessary equipment to accomplish the office working activities. To establish all possible solutions will represent the work for another research project. Knowing the results of the tests and having the real life experience we could propose in this moment one solution which could be easily and successfully implemented. The technology from today permits the development of this solution and it will allow not only to reduce the influences of the equipment to the environment but also to minimize the amount of energy consumption. A short description of the solution is presented below:

- all processing units of the computers should be stored into a separated dedicated room or even replaced by a server computer, and thin clients will realize the interface between the server and the users displays. On the occupants desks should remain only the display, keyboard, mouse, any additional interface devices and maybe a low power thin client computer. The biggest heat production will be in this way isolated into a single space, from where it could be transferred to other systems (e.g. heating the necessary water by using heater exchangers) or eliminated to the outside environment (in this case it will be just waste energy).
- the noisy equipment, like printers which are often used, should also be placed into a separate room with phonic isolation but which can be easily accessible to the office occupants.
- the incandescent light bulbs will be replaced with energy saving bulbs.

The practical implementation of the solution into an office building will demonstrate its viability and efficaciousness and it will be high depended on the possibility to transfer the heat from one substance to another (e.g. from air to water) and on the possibilities of storing the heat (energy) for later use.

## 8. Real case scenario: heat production estimation for an office space

After all the scheduled tests have been accomplished we were also interested in making estimation for a real case scenario: an office space with multiple working desks where are many electric equipment installed. For this task it was selected as reference (example) one of the rooms from our University's building, with similar characteristics with what we need. Into this room there are installed the next equipment (devices):

- computer processing unit: 11 pieces;
- LCD displays: 11 pieces;
- incandescent light bulb 100W: 8 pieces;
- laptop: 1 piece;
- printer: 1 piece.

The office dimensions are 8.50 m (length), 5.00 m (width), 2.80 m (height) and the total volume is 119.00 $m^3$.

In these conditions, based on the results already obtained, the electrical equipment will produce about 6700 cal (7.79 W) heat energy every hour and the temperature will increase with 0.2 °C (in the conditions when the heat is transmitted directly to the air – no people inside the room). In 10 hours it will be a higher temperature with 2 °C, not a very big value, but even so, it represents a waste energy.

The heat produced by equipment will be transmitted more rapidly to the human body of the persons from nearby (the water from the human body has a much better conductance of the heat than air) and local discomfort would appear. This phenomenon should be also taken into consideration when electrical equipment is installed. In case of the office spaces are occupied with people, the measurements showed a quick growing of the temperature in a short time, higher than in the case when there were no people inside (the human body also produces heat by thermo regulation process).

A solution based on moving the main heat producers into a separate room, as presented into the previous section, will allow a better control of the temperature inside and possibility to reuse the waste energy. With this solution implemented it should be obtained a lower value of the heat production into the office space, of just about 1655 cal (1.92 W).

## 9. Conclusions

The influence of the electrical equipment to the indoor environment conditions have not been so much analyzed until today, and to make only mathematical estimations without testing, about the heat produced by each equipment, could be a very hard and long work. By our research work, presented in this paper, we have succeeded to obtain proper results and the possibility to estimate which equipment produces the most heat or noise and which should be separated into another room space, where the possibility of heat recovery exists. Too much heat inside a room produces thermal discomfort, too much noise produces acoustic discomfort. A main problem is that usually the main goal when designing a building is to ensure as low as possible the energy consumption, and the occupants comfort which influences directly their productivity, is less analyzed.

Even for a large space office the heat production could be considered low (as it was presented in the real case scenario estimation), it is possible to exist local discomfort for the occupants, and since the heat produced is lost energy why not to use it in other existent systems. The results obtained permit us to continue the research work with the designing of the necessary systems which accomplish the task of recovering the heat and store it for later use.

Also as future work would be interesting to verify if there are other types of influences to the environment from the electrical equipment (e.g. carbon monoxide or carbon dioxide variation - other important parameters for describing the air quality).

## Acknowledgements

This paper is supported by the Sectoral Operational Programme Human Resources Development (SOP HRD) financed from the European Social Fund and by the Romanian Government under the project number POSDRU/89/1.5/S/59323.

## References

[1] Bickford, J.: *Temperature and heat*, web: http://www.bickfordscience.com, 2009.
[2] Bujdei, C., Moraru, S. A.: *Ensuring comfort in office buildings – Designing a KNX monitoring and control system*, The 7th International Conference on Intelligent Environments, Conference Publishing Services, 2011, pp. 222–229.
[3] Crombie, M.: *Calculating the heat loss*, web: http://www.engineeringtoolbox.com, 2006.
[4] Hortsmeyer, S. L.: *Relative humidity ... Relative to what? The dew point temperature ... a better approach*, web: http://www.shorstmeyer.com/wxfaqs/humidity/humidity.html, 2008.
[5] Hosni, M. H., Beck, B. T.: *Update to measurements of office equipment heat gain data*, final report, ASHRAE Research Project 1482-RP, 2009.
[6] Hosni, M. H., Jones, B. W., Sipes, J. M., Xu, Y.: *Test method for measuring the heat gain and radiant/convective split from equipment in buildings*, final report, ASHRAE Research Project 822-RP, 1996.
[7] Hosni, M. H., Jones, B. W., Xu, H.: *Experimental results for heat gain and radiant/convective split from equipment in buildings*, document proposed for discussions, for including in Ashrae 1999, 1999.
[8] Mohamed, A. S.: *Performance of different temperature sensors in standard fire resistance test furnaces*, Fire Technology, Springer Netherlands, Vol. 46, No. 4, 2010, pp. 853–881.
[9] Santamouris, M., Asimakopoulos, D.: *Passive Cooling of Buildings*, Earthscan / James and James Science Publishers, 1996, ISBN: 1-873936-47-8.
[10] Sarbu, I. and Ceausescu, I.: *Methods for evaluation of the buildings thermal comfort (Modele de evaluare a confortului termic in cladiri)*, Installations technic (Tehnica instalatiilor), No. 2, 2007, pp. 20–24.
[11] White, W. N., Pahwa, A., Cruz, C.: *Heat loss from electrical and control equipment in industrial plants: part I - methods and scope*, ASHRAE Transactions, Vol. 110, 2004, pp. 842–851.

[12] White, W. N., Pahwa, A., Cruz, C.: *Heat loss from electrical and control equipment in industrial plants: part II - results and comparisons*, ASHRAE Transactions, Vol. 110, 2004, pp. 852–870.
[13] Wikipedia: *Dew point*, web: http://en.wikipedia.org/wiki/Dew_point, 2011.
[14] Wilkins, C., Hosni, M. H.: *Heat Gain From Office Equipment*, Heat Gain From Office Equipment, Vol. 42, 2000, pp. 33–39.

# Calculation of Bridge Structure according to Different Norms (EC2 and MSZ)

**A. Várdai**

**H-1114 Budapest, Vásárhelyi Pál utca 9. 4. em. 3**
**Phone: +3620 576 86 55**
**e-mail: attila.vardai@gmail.com**

Abstract: In this paper results of a structural design based on EC2 are compared with the findings gained by the application of the traditional Hungarian Standards (MSZ). Having introduced the loads (forces, bending moments) that affect the structure stresses in serviceability limit state at the critical section are analysed. The main conclusion is that previous designs in some cases are not acceptable according to the new regulation. The difference originates from the effects and not from sectional properties.

*Keywords: pre-stressed concrete, EC2, MSZ*

## 1. Introduction

In the beginning of 2011 a new era has started in the field of structural design. The traditional Hungarian Standards (MSZ) were recalled and replaced by Eurocodes (EC); which raised many questions. For instance, how big are the differences at the loads, stresses and, most importantly, at the safety of a structure? Some answers were clarified by a limited number of case studies for some types of structures, but many issues are still open to further discussion.

The subject of investigation presented in this paper is a highway bridge made of pre-cast, pre-stressed (pre-tensioned) concrete beams and an in-situ concrete slab. The bridge is statically determinate until an in situ slab is casted above the beams. The beams and the deck work together and create a composite structure. This type has been very common at the recent motorway constructions in Hungary.

The calculation was carried out by hand and checked with the Hungarian FEM program, AXIS VM 9.

## 2. Loads

### 2.1. Permanent loads

First permanent loads are calculated. Because of the unique statical behaviour of the bridge, dead loads effect at different times, when statical model has changed.

Self weight of the beam ($g_1$), the concrete deck ($g_2$), the sideways and asphalt surface ($g_3$) are taken into account. As long term effects, shrinkage and creep of concrete could cause extra stresses in the elements.

Because the pre-cast beam is constructed earlier than the in-situ deck (and as the beam belongs to a higher concrete class and also has different geometry), there will be differences between the shrinkage of the two parts, which will cause additional stresses ($\Delta\sigma_{cs}$). The method used by the MSZ to calculate this effect is much less detailed than that of the EC; however, the Hungarian Standards presents pre-calculated tables for engineers, which are very easy to use. The simplification used by MSZ was reasonable at the past, where there were only normal performance concrete materials.

On the contrary, in EC2, total shrinkage ($\varepsilon_{cs}$) is calculated as the sum of autogenous ($\varepsilon_a$) and drying shrinkage ($\varepsilon_d$).The proportion of autogenous shrinkage increases with concrete class (see Figure 1 for example). $\varepsilon_a$ occurs within a short period, so by the time of construction the shortening of the beams becomes greater according to EC than it was assumed in MSZ. To sum up, the MSZ simplification is not acceptable for high-performance concretes.

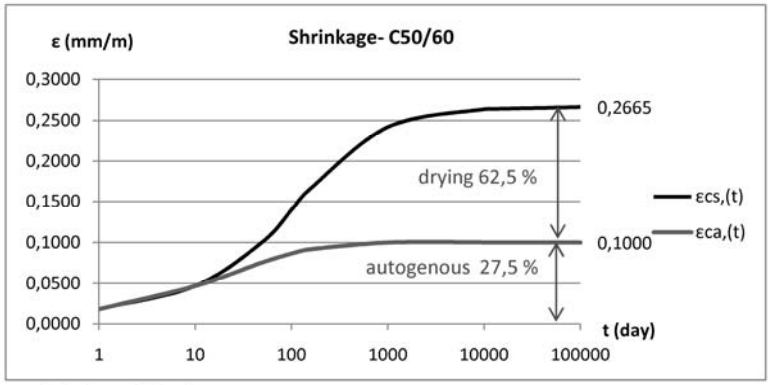


a., shrinkage of the beam

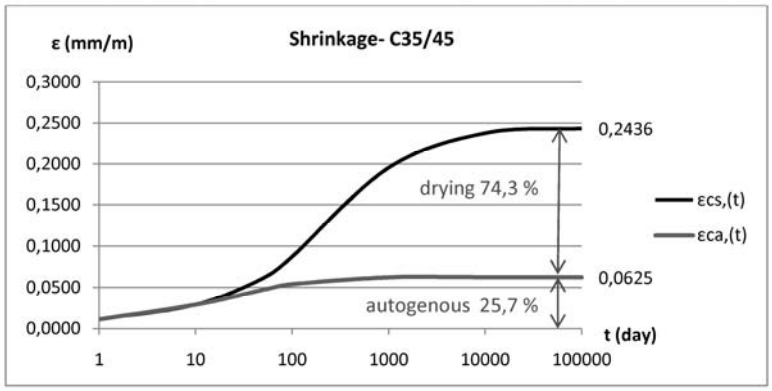


b., shrinkage of the deck

*Figure 1. Shrinkage of concrete- a., beam b., deck*

At the construction phase, which is about 100 days after casting, shrinkage is twice as great according to EC2 as it is forecasted in MSZ; but later, at the final state, it is the lower value. (Table 1.) Consequently, in the final state, the loss of pre-tensioning force is smaller in EC2, so the pre-stressing is more efficient (as shrinkage causes the loss of pre-stress).

*Table 1. Difference in shrinkage*

| | EC | | | MSZ | | $\Delta\sigma_{cs}$ (N/mm$^2$) | |
|---|---|---|---|---|---|---|---|
| ε (mm/m) | $\varepsilon_{ca}$ | $\varepsilon_{cd}$ | $\varepsilon_{cs}$ | $\varepsilon_{zs}$ | difference (%) | EC | MSZ |
| t=100 days | 0,086 | 0,065 | **0,151** | **0,077** | **96,1** | 29,5 | 15,0 |
| t=∞ | 0,100 | 0,180 | **0,280** | **0,321** | **-12,8** | 54,1 | 62,7 |

The creep of concrete has a very complex effect during the further calculations. Its value (the creep coefficient, $\varphi_{(t)}$) modifies the effective modulus of elasticity of concrete ($E_{c,eff(t)}$). $E_{c,eff(t)}$is a basic parameter to create the idealized cross-section ($A_{id}=A_c+\alpha*A_s$, $W_{id}$; where $\alpha=E_s/E_{c,eff(t),}$ values are presented in Table 3) for the stress limitation calculations. In our case, because of the great compression deriving from pre-stressing, non-linearity of creep coefficient must be considered.

*Table 2. Difference in Creep*

| | t=100 | | | t=∞ | | |
|---|---|---|---|---|---|---|
| | EC | MSZ | difference (%) | EC | MSZ | difference (%) |
| $f_{(t)}$ | 0,9350 | 1,1991 | **-22,0** | 1,4112 | 2,7576 | **-48,8** |
| $E_{(t)}$ (N/mm$^2$) | 19210 | 16722,1 | **14,9** | 13914,7 | 9786,4 | **42,2** |

As Table 2 shows, the difference in the creep coefficient of the two norms increases with time; the MSZ value at the final state is twice as great as the EC one.

*Table 3. Difference in sectional properties*

| | | Sectional properties | | | | | | | | |
|---|---|---|---|---|---|---|---|---|---|---|
| t (days) | | 0 | | | 100 | | | ∞ | | |
| | | EC | MSZ | difference (%) | EC | MSZ | difference (%) | EC | MSZ | difference (%) |
| **FPT beam (beam only- for loads on single span structure)** | | | | | | | | | | |
| $A_i$ | mm2 | 350314 | 350434 | **0,0** | 368373 | 373961 | **-1,5** | 382666 | 404539 | **-5,4** |
| $W_{il}$ | mm3 | 5,21E+07 | 5,22E+07 | **-0,1** | 5,75E+07 | 5,92E+07 | **-2,8** | 6,17E+07 | 6,78E+07 | **-9,0** |
| $W_{iu}$ | mm3 | 6,69E+07 | 6,70E+07 | **0,0** | 6,88E+07 | 6,93E+07 | **-0,7** | 7,00E+07 | 7,17E+07 | **-2,3** |
| **Composite cross section (beam and deck together- ED, for loads on multispna structure)** | | | | | | | | | | |
| | | for short term loads | | | for long term loads | | | | | |
| $A_{i,ED}$ | mm2 | 507973 | 505716 | **0,4** | 526032 | 529243 | **-0,6** | | | |
| $Wi^{l}_{,ED,deck}$ | mm3 | 1,28E+08 | 1,29E+08 | **-1,0** | 1,33E+08 | 1,35E+08 | **-1,8** | | | |
| $Wi^{u}_{,ED,deck}$ | mm3 | 7,51E+07 | 7,60E+07 | **-1,1** | 7,92E+07 | 8,13E+07 | **-2,5** | | | |
| $Wi^{l}_{,ED,beam}$ | mm3 | 6,04E+07 | 6,03E+07 | **0,1** | 6,70E+07 | 6,89E+07 | **-2,8** | | | |
| $Wi^{u}_{,ED,beam}$ | mm3 | 1,18E+08 | 1,17E+08 | **0,6** | 1,22E+08 | 1,22E+08 | **-0,3** | | | |

Table 3 displays the properties of the investigated section. According to EC, the (lower) sectional modulus of the beam for single span loads decreases more with time, compared to the MSZ result. It means that greater stresses originates from the beam's dead weight and pre-stress. Because in this case stresses from pre-tensioning are much greater than dead loads, pre-stressing is more effective than it is in MSZ.

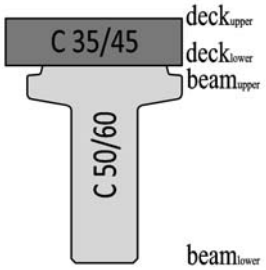


*Figure 2. Cross-section of the beam*

### 2.2. Traffic loads

Traffic loads as imposed loads are the dominant factors among the effects, especially in case of highway structures. These types of loads are crucial because they generate the greatest difference between the two norms.

To place the loads at the most unfavourable positions for each pre-cast beam the Guyon-Massonet method has been applied, using influence lines to get the worst load position at longitudinal direction.

In the calculations of EC1 the whole width of the carriageway has to be divided into notional lanes with lane number 1 to be at the worst position and so on. The uniformly distributed loads (UDL) and concentrated loads (or tandem system, TS) have different values for each lanes (Table 4). $Q_k$ and $q_k$ are the characteristic values of the loads from vehicles modified by the adjustment factors ($\alpha_Q$, $\alpha_q$). Adjustment factors depend on the load class of the bridge. For highway bridges, which are subjected to heavy traffic, their values are equal to 1.00.

*Table 4. Traffic load in EC*

| Lanes | $Q_{ik}$ | $q_{ik}(q_{rk})$ |
|---|---|---|
| 1. | 300 kN | 9,00 kN/m2 |
| 2. | 200 kN | 2,50 kN/m2 |
| 3. | 100 kN | 2,50 kN/m2 |
| remaining | 0 kN | 2,50 kN/m2 |

EC traffic load values include the dynamic amplification. The proportion of effect of each load ($K\alpha$, in concordance with the Guyon-Massonet method) is shown in Figure 3.

For the presented bridge, traffic load of the third lane ($Q_{3,k}$; $q_{3,k}$; $q_{r,k}$) can be neglected since its value is almost equal to zero (and it has even an advantageous effect on the beam).

If the whole width of the carriageway is loaded, the values do not change relevantly; however, other structural geometries could be more problematic. That is why influence lines are necessary, not just in longitudinal but in cross directions as well.

The MSZ method calculates traffic loads in a simpler way. There is only one vehicle and a UDL system. Base values have to be modified by dynamic factors, which depend on the length of the longest span of the bridge. Table 5 shows the values of the

concentrated loads (TS), the importance of them at the most unfavourable position (Kα, see also Figure 3) and the bending moments (M) they caused.

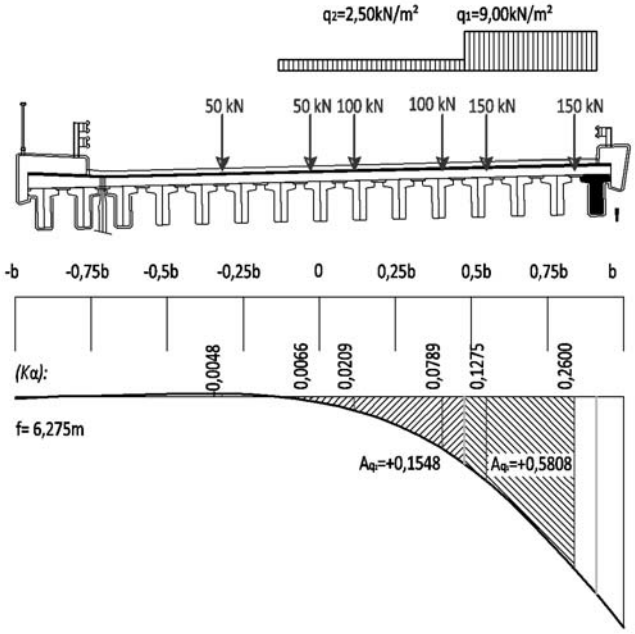


*Figure 3. Worst load positions for the right edge beam*

*Table 5. Difference in TS loads*

| | TS (kN) | | ($K\alpha_i$) | avg. (Kα) | M (kNm) | |
|---|---|---|---|---|---|---|
| EC | $Q_1$ | 150,00 | 0,2600 | 0,1937 | 627,63 | |
| | | 150,00 | 0,1275 | | | |
| | $Q_2$ | 100,00 | 0,0789 | 0,0499 | 107,82 | |
| | | 100,00 | 0,0209 | | | |
| | $Q_3$ | 50,00 | 0,0066 | 0,0009 | 0,94 | |
| | | 50,00 | -0,0048 | | | |
| | **∑EC=** | | | | **736,38** | **kNm** |
| MSZ | $P_{,traff}$ | 111,51 | 0,1156 | 0,1156 | **525,89** | **kNm** |
| | | 111,51 | 0,1156 | | | |
| | | | | | **difference=+** | **40,0 %** |

Table 6 shows the same for uniformly distributed traffic loads, where UDL is the characteristic value of the load (kN/m$^2$; it has to be modified by the dynamic factor in MSZ). A is the area under the Guyon-Massonet graph (diagonally hatched parts in Figure 3), q is the load projected to the investigated beam, M is the bending moment from the loads.

Because these are the dominant load types for the structure, the differences displayed above are very notable.

*Table 6. Difference in UDL loads*

| | UDL | A | q (kN/m) | M (kNm) |
|---|---|---|---|---|
| $q_1$ | 9,00 | 0,5808 | 5,23 | 339,08 |
| $q_2$ | 2,50 | 0,1548 | 0,39 | 25,10 |
| $p_{traff}$ | 4,24 | 0,7582 | 3,21 | 208,53 |
| | | **Σ EC=** | **5,61** | **364,18** |
| | | **Σ MSZ=** | **3,21** | **208,53** |
| | | **difference:** | + 74,6 % | |

## 3. Load combinations

Pre-stressed concrete structures first has to be calculated in serviceability limit state, about which the first requirement is decompression. It means that the whole cross-section has to be compressed (no tensile stress is allowed). For this calculation, EC uses frequent load combination (with five different load cases for bridges):

$$\sum_{j\geq 1} G_{kj} + P_k + \begin{Bmatrix} (\psi_{1,TS} * TS + \psi_{1,UDL} * UDL + \psi_{1,UDL} * qfk) + \psi_{2,T} * T_k \\ \psi_{1,gr1b} * gr_{1b} \\ \psi_{1,gr4} * gr_4 \\ \psi_{1,T} * T_k \\ \psi_{1,w} * F_{wk} \end{Bmatrix}$$

The next prerequisite for bridges to fulfil the criterion of deflection. According to EC, the characteristic load combination has to be used:

$$\sum_{j\geq 1} G_{kj} + P_k + \begin{Bmatrix} gr_1 + \psi_{0,w} * F_{wk} \\ gr_{ii\ =\ 2,3,4,5} \\ LM2 \\ T_k + (\psi_{0,TS} * TS + \psi_{0,UDL} * UDL + \psi_{0,UDL} * qfk \\ F_w * \end{Bmatrix}$$

In these expressions G stands for the permanent effects, P is pre-stressing force, Q is imposed loads and ψ is the factor for each combination, which represents the proportions of the loads affecting together.

The MSZ uses the load combination for serviceability state for both cases; there are no further separations like in EC:

$$F_{ser} = \sum_{i=1}^{m} G_i + Q_1 + \sum_{i=2}^{n} \psi_i * Q_i$$

Ultimate limit state conditions are not described here.

## 4. Decompression

Table 7 shows the stresses at the bottom of the beam, where tensile stress appears according to EC. Effects of each load type are shown.

*Table 7. Stresses in frequent combination*

| | pre- tension | $g_1$ | $g_2$ | $g_3$ | shrinkage | $Q_{ser}$ | $q_{ser}$ | Σ | |
|---|---|---|---|---|---|---|---|---|---|
| $\sigma_{Ed}^{MSZ}$ | -27,01 | 7,94 | 4,69 | 6,41 | 1,40 | 4,70 | 0,98 | -0,89 | $< 0,0$ N/mm$^2$ |
| $\sigma_{Ed}^{EC}$ | -30,18 | 8,70 | 4,83 | 6,60 | 1,02 | 9,32 | 2,42 | 2,71 | $> 0,0$ N/mm$^2$ |
| difference | -11,7 | + 9,6 | + 3,0 | + 3,0 | -27,1 | + 98,3 | + 146,9 | | |

Greater tensile stresses occur in EC from the imposed loads. Because the sectional properties for the actions of traffic are almost the same in EC and MSZ (see Table 3, column t=0), the difference must follow only from the values of the loads. By applying factor ψ, MSZ reduces the TS loads to 37% and the $UDL^{traffic}$ loads to 29% of their characteristic value. Meanwhile, the same reduction in EC for frequent combination is only to 75% for TS and to 40% for UDL loads (and characteristic values have relevant differences as well, see Tables 5 and 6).

Because $\sigma_{Ed}>0,0$ N/mm$^2$ (the bottom of the cross-section is not compressed), more tendons (for more initial pre-stressing force), or a cross-section with greater dimensions are necessary.

On the other hand, the bottom is still compressed with MSZ; so all the chosen properties provide enough resistance for the cross-section, according to the "Old Standard".

## 5. Further consequences

The tendency that EC has smaller resistance than MSZ, is very common. A reason for that could be that EUROCODE takes the maintenance purposes into consideration. It categorizes the structural elements into environmental (exposure) classes and uses strict regulations to protect them against corrosion. Nevertheless, safety of the structures increases less than the related initial costs (however, such great differences are not expected regarding the overall costs).

*Table 8. Reduced factors*

a., Case 'A'- recommended values by EUROCODE

| | Notional lane | | | frequent combination | |
|---|---|---|---|---|---|
| | 1 | 2 | 3 | | |
| $\alpha_{Qi}$= | 1,00 | 1,00 | 1,00 | $\Psi_{1,TS}$= | 0,75 |
| $\alpha_{qi}$= | 1,00 | 1,00 | 1,00 | $\Psi_{1,UDL}$= | 0,40 |

b., Case 'B'- recommended values by HEC

| | Notional lane | | | | |
|---|---|---|---|---|---|
| | 1 | 2 | 3 | | |
| $\alpha_{Qi}$= | 1,00 | 0,80 | 0,00 | $\Psi_{1,TS}$= | 0,60 |
| $\alpha_{qi}$= | 0,80 | 1,00 | 1,00 | $\Psi_{1,UDL}$= | 0,30 |

The above-mentioned reasons convinced Hungarian authorities to harmonize MSZ values with the load values of EC (via the changes of adjustment factors $\alpha_Q$, $\alpha_q$). α factors may be specified in the National Annexes of EC.

Table 8 compares the original EC factors with the reduced ones recommended by the Hungarian EUROCODE Committee, HEC.

I investigated the structure with the reduced adjustment and partial safety factors of Case 'B'. This change is enough to satisfy decompression criteria, to provide compression at the bottom (Table 9).

*Table 9. Reduced factors*

| load | Case 'A' | Case 'B' |
|---|---|---|
| p | -30,18 | |
| $g_1$ | 8,70 | |
| $g_2$ | 4,83 | |
| $g_3$ | 6,60 | |
| cs | 1,02 | |
| TS | 9,32 | 7,23 |
| UDL | 2,42 | 1,48 |
| ∑= | **2,71** | **-0,32** |

In the future these (or similar) reduction factors should appear in National Annexes to fulfil the requirements of limit state design at the same level as did the late MSZ.

However, besides the criteria of load bearing structures resistance, economic aspects of designs should be considered as well. In the view of overall costs, the increase of load level in EC could be reasonable, because frequency of repairing and maintenance costs may decrease this way.

To find the optimal balance between costs and safety is a next problem to solve.

## Acknowledgement

The author appreciates the comments and support given by Z. Teiter (UVATERV) and P. Scharle (Széchenyi István University) during the completion of the research and preparation of this paper.

## References

[1] Klatsmányi, T.: *Reinforced concrete structures (in Hungarian-Vasbetonszerkezetek)*, Tankönyvkiadó, 1988.
[2] Szlukovényi, I.: *Bridge building (in Hungarian – Hídépítés),* Tankönyvkiadó, 1979.
[3] Farkas, Gy., Huszár, Zs., Kovács, T.: *Concrete design according to Eurocode (in Hungarian – Betonszerkezetek méretezése az Eurocode alapján )*, TERC, 2006.
[4] Németh, F.: *Optimal design of reinforcing bars of bended shell structures (in Hungaian – Hajlított héj acélbetéteinek optimális méretezése)*, Vasbetonépítés, 2007/4, pp.117-124.
[5] Mosley, B.: *Reinforced concrete design to Eurocode 2*, Palgrave Macmillan, 2007.

# Contactless Torque Sensor Development

**F. Hajdu, P. Horváth**

**Széchenyi István University**
**Department of Mechatronics and Machine Construction**
**9026 Győr, Egyetem tér 1.**
**e-mail: h12flora@t-online.hu, horvathp@sze.hu**

Abstract: This paper presents the development of a contactless torque sensor, which operates on a new principle. The used method is based on the birefringence effect of optically anisotropic materials. Experiments made are similar to the reflective photoelasticity. Instead of conventional photoelastic coating a Perspex tube of thin wall thickness was used. When torque was applied, stress had arisen in the tube, which could be measured optically. The main goal of this study was to create a torque sensor, which could be used in industry too. The paper deals with the theoretical basics, it gives an overview of the development up to now, presents measurement results, shows possible practical realizations for small and large torques, and also proposes possibilities for further developments.

*Keywords: optical torque sensor, photoelasticity, birefringence*

## 1. Introduction

Torque sensors are used in many fields, such as research, testing, production and education. The commonly used force and torque sensors apply indirect measuring principle, which means they measure the deformation of an elastic element due to the applied torque. The most common sensing element is strain gauge. This method has some problems, for example it is difficult to pick the signal from the rotating shaft and the friction loss of the slip rings can result in inaccurate measurement. When small torque is to be measured, due to the small dimensions of the elastic element, there can be 20% strain difference between the two ends of the gauge [10].

There are contactless torque sensors too, which operate on optical or magnetic principle. In the commonly used industrial optical torque sensors there are two plates with radial slots between a detector and a LED. One of the plates is mounted to the input shaft, the other one to the output shaft. Applying torque the shafts rotate relative to each other and the gaps will be overlapped. The overlapping is proportional to the applied torque. These sensors are used in vehicles to aid braking and steering [5]. The sensor described in [8] and several rotary optical sensors and transducers [9] operate with similar principle.

Other possibility is described in [1]. Here polar filters are attached to the two ends of the shaft between a detector and a LED. Applied torque changes the angle of polarization between the filters, which changes the intensity of light entering the receiver.

The operational principle of the developed torque sensor is based on the birefringence effect of optically anisotropic materials.

## 2. Physical principles

When polarized light beam enters into a birefringent material (like glass or several plastics) it splits into two perpendicular beams. The directions of beams are identical to the ones of principal stresses arising in the material due to loading. Since the birefringent materials have different refractive indexes in the principal directions, the velocity of the two light beams will be different, so one will be delayed. This delay is called retardation [2].

At photoelastic experiments the sample to be tested is placed between two polar filters. Assuming that the birefringent sample's width is $b$, strains in the direction of the principal stresses are $\varepsilon_{b1}$ and $\varepsilon_{b2}$, retardation $R$ can be written in form of

$$R = bK(\varepsilon_{b1} - \varepsilon_{b2}) \tag{1}$$

where $K$ is material specific, strain-optical coefficient.

It is experienced that in case of elastic deformation the optical and the mechanical principal directions are the same, on the other hand the phase shift between the two light beams is proportional to the difference between the principal stresses in the birefringent material. This proportionality can be expressed with stress optical coefficient:

$$\mathrm{R} = \frac{\lambda \mathrm{b}}{S}(\sigma_{b1} - \sigma_{b2}). \tag{2}$$

Sometimes it is more convenient to use relative retardation $m$ [2]:

$$m = \frac{\mathrm{b}}{\mathrm{S}}(\sigma_{b1} - \sigma_{b2}) = \frac{\mathrm{bE_b}}{\mathrm{S}}(\varepsilon_{b1} - \varepsilon_{b2}). \tag{3}$$

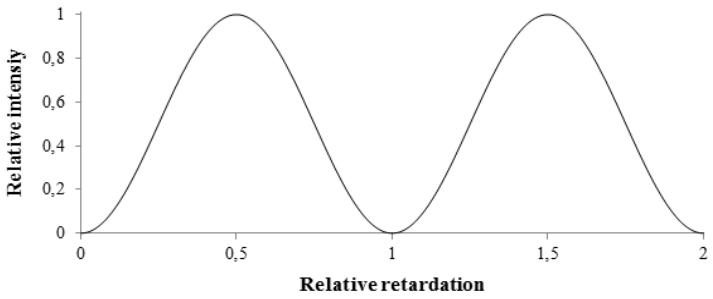


*Figure 1. Relative intensity vs. relative retardation*

When the birefringent sample is loaded steadily, retardation will change. If this material is examined between perpendicularly polarized polariser and analyser plates, then the image sometimes enlightens, sometimes darkens. The relationship between the relative retardation proportional to the loading and the intensity of light can be expressed with the following equation assuming 45° angle between the plain of polarisation of the polarizer and the first principal optical axis [7] (see in Figure 1).

$$\mathrm{I} = \mathrm{I_0^2 sin^2(m\pi)} \tag{4}$$

## 3. Contactless torque sensor development

### 3.1. Test equipment and basic calculations

Our test equipment is based on reflective photoelasticity. The shaft to be measured was coated by a photoelastic layer that deformed together with the shaft. When torque was applied to the shaft, stress could be measured by a reflective optical sensor. As photoelastic coating was not available, thin perspex and polyurethane tube was used. Polarizing filters available on the market are too expensive, so the polarizer and the analyzer were taken out of an old calculator display. The sketch of the test equipment is shown in Figure 2.

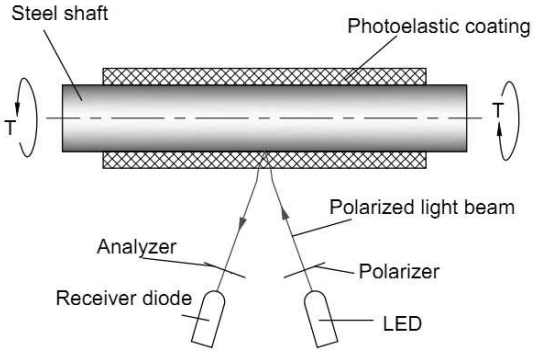


*Figure 2. Test equipment*

At first the range of measurement of the sensor was calculated using relative retardation. Equation (4) shows how the sample darkens and enlightens due to relative retardation. The function has its maximum at m=0.5, where the first enlightenment occurs.

In case of pure torsion of a shaft of outer radius R, the difference of the principal stresses equals to the diameter of Mohr's circle [4]:

$$\sigma_1 - \sigma_2 = 2\frac{T}{I_p}R \tag{5}$$

The difference of principal strains at the outer radius is [3]:

$$\varepsilon_1 - \varepsilon_2 = 2\frac{T}{I_p E}R \tag{6}$$

The light passes through the coating of width *b* twice, so the relative retardation is:

$$m = \frac{2bE_b}{S}(\varepsilon_{b1} - \varepsilon_{b2}) \tag{7}$$

Assuming that a thin coating does not contribute to torque transmission and adheres perfectly to the shaft, strain at the outer radius of the shaft is equal to that of in the coating. This assumption leads to

$$m = \frac{4bRE_b}{SI_pE} T \tag{8}$$

expression. From equation (8) the maximal torque can be calculated at different relative retardations.

### 3.2. Test equipment for measuring large scale torque

For measuring large torque Perspex tube as coating was used. The realized test equipment is shown in Figure 3.

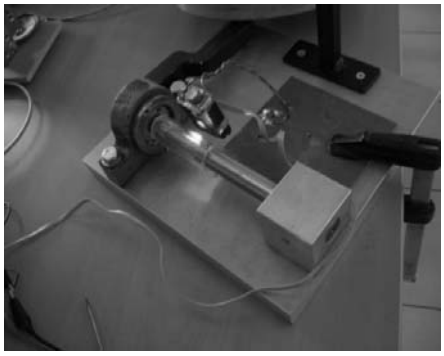

*Figure 3. Realized test equipment*

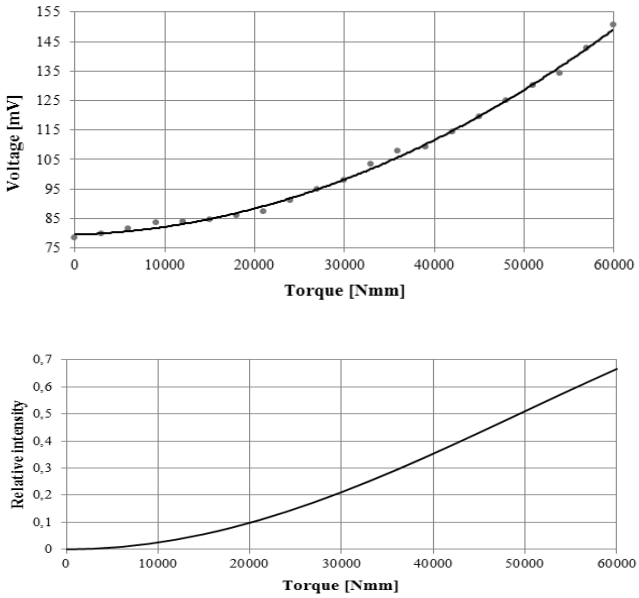


*Figure 4: Measured data (up), theoretical diagram (down)*

Several experiments were performed. Measured data and the theoretical calculated diagram are shown in Figure 4.

Comparing measured data with the theoretical diagram it can be seen, that the curves are very similar, so the theory was confirmed. Small deviations are due to the disturbing effect of ambient light and the residual stresses in the tube after production.

### 3.3. Test equipment for measuring small torque

For measuring small torque the metal shaft of high rigidity was omitted and only an elastic tube was used as a measuring and coupling element all in one, as it can be seen in Figure 5 [6].

Several optically active materials were tested. The first experiments were performed with Perspex tube, but it was not suitable for measuring small torque because of its high stress-optical coefficient. Later a Polyurethane tube was used and the experiment proved to be more successful. When torque was changed the output voltage also changed.

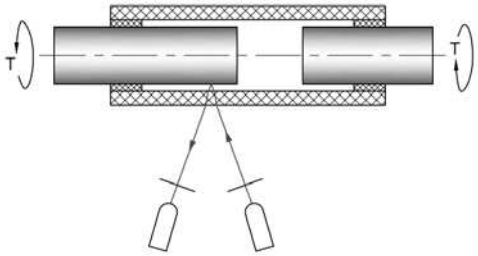


*Figure 5. Test equipment for measuring small torque*

## 4. Conclusions and further development

This paper presented a torque sensor operating on a brand new principle based on the birefringence effect of optically anisotropic materials. The experiments confirmed the physical theory and that it can be used for torque measurement. A working test equipment was created. Further investigations are needed to make the sensor more accurate. These developments include using thinner coating, eliminating ambient light with covering or modulation and keeping the optical part in a fixed position with fine mounting. Additionally new experiments are necessary to examine the usability of the principle during high speed rotation and setting a favourable operational point with preload to be able to sense torque direction too.

## References

[1] Anderson P. M: *Optical torque sensor utilizing single polarizing area filters and mechanical amplifier*, US patent No. 5389780, 1995
[2] Csiszár S.: *Photoelasticity (in Hungarian)*, Technical College of Budapest (BMF)
[3] Égert J.: *Finite Element Mechanical Modeling Opportunities in Machine Design*, Acta Technica Jaurinensis, Vol 1. No. 1, 2008, pp. 47-50

[4] Égert J., Jezsó K.: *Mechanics of materials (in Hungarian)*, Széchenyi István University, Győr, 2006
[5] Hazelden R. J.: *Optical torque sensors and steering systems for vehicles incorporating them,* US patent No. 5369583, 1994
[6] Horváth P., Nagy A.: *Optical torque sensor development*, Proceedings of Mechatronics Conference, Luhacovice, 2009, pp. 52-56
[7] Nagy S.: Experimental and numerical stress analysis (in Hungarian), University of Miskolc, 1999, pp.18-35.
[8] Puzio D.: *Optical torque sensor,* US patent No. 7591195B2, 2009
[9] Sensor technology: *E200 Optical Rotary Torque Series*, 2011 http://www.sensors.co.uk/torqsense/E200-ORT/
[10] Varsányi P.: *Dynamic force and torque measurement (in Hungarian),* http://www.tesla.hu/varsanyi/nyomatek.htm